Summer 2019

Semiconductor Nanowire Doping: Controlling Magnetic and Electronic Properties of Colloidal Nanowares

Preecha Kittikhunnatham

SEMICONDUCTOR NANOWIRE DOPING: CONTROLLING MAGNETIC AND ELECTRONIC PROPERTIES OF COLLOIDAL NANOWIRES

by

Preecha Kittikhunnatham

Bachelor of Science
Chulalongkorn University, 2012

Master of Science
University of South Carolina, 2017

Submitted in Partial Fulfillment of the Requirements

For the Degree of Doctor of Philosophy in

Chemistry

College of Arts and Sciences

University of South Carolina

2019

Accepted by:

Andrew B. Greytak, Major Professor

Michael L. Myrick, Committee Member

Morgan Stefik, Committee Member

Thomas M. Crawford, Committee Member

Cheryl L. Addy, Vice Provost and Dean of the Graduate School

DEDICATION

This dissertation is dedicated to my family, friends, and loved ones.

ACKNOWLEDGEMENT

I would like to thank to my advisor, Dr. Andrew B. Greytak, for his guidance and supports, which help me achieve a successful graduate student path. In addition, I would like to thank all of my research collaborators including, Fiaz Ahmed, Christian A. Juillerat, and Dr. Andrew B. Greytak, to help me complete the work described in this dissertation. Additionally, I would like to thank my PhD committee members, Dr. Michael L. Myrick, Dr. Morgan Stefik, and Dr. Thomas M. Crawford for the suggestions and help in reviewing this dissertation. Moreover, I would like to thank Dr. Linda S. Shimizu and Dr. Vitaly Rassolov for the help and support to complete my works during my master's degree study. Also, I would like to thank my coworkers from the Greytak's lab, Pravin Paudel, Rui Tan, Yi Chen, Megan Gee, Bobby Barker, Adam Roberge, Stephen Roberts, John Dunlap, Matthew Kelly, Fiaz Ahmed, Sakiru Abiodun, Colin Johnson, Paolo Milan, Abigail Loszko, Cole Love-Baker, Raeven Flake, and Garrett Harbin, for all the help and support during the time that I work in the lab. Furthermore, I would like to thank people who work in department of chemistry, University of South Carolina for help and support since the first day I started my graduate study here. Finally, I would like to acknowledge a Development and Promotion of Science and Technology Talents Project graduate fellowship from the Royal Government of Thailand for financial support throughout my graduate study.

ABSTRACT

Electronic devices have been utilized in a wide range of applications, such as computing, data storage, sensors, lightings, energy production, and energy storage; they are building blocks of computer processors, solid state data storage devices, image sensors in digital cameras, LEDs, and solar cells, etc. These electronic devices operate based on properties of semiconductors, which are their essential components. Not only being fundamental components of electronic devices, semiconductors can be crucial materials for other applications, such as catalysts, battery electrodes, etc. One of the primary current quest on semiconductor research is to develop semiconducting materials that are more compact and more efficient than existing materials. Science and technology for nanoscale materials has been applied to develop nanoscale semiconducting materials to complete the quest. One of the promising nanoscale semiconducting materials is semiconductor nanowire; its geometry and properties allow for several advantages. One of the challenges preventing semiconductor nanowire from practical usage is the insufficient technology to control its properties. This dissertation presents novel practical approaches to control magnetic and electronic properties of semiconductor nanowires via doping. First, preparation method of Mn(II) doped CdSe nanowires via nanocrystal diffusion doping mechanism and the effect of manganese doping as well as ligand exchange on magnetic property of Mn(II) doped CdSe nanowires are discussed. Moreover, indium doping on CdSe nanowires via sequential nanocrystal diffusion doping and cation exchange and its effect on electronic property of CdSe nanowires are demonstrated. Finally, an effort to use

photochemical doping method to control electronic property of CdSe nanowires is presented here.

TABLE OF CONTENTS

LIST OF TABLES

LIST OF FIGURES

CHAPTER 1

INTRODUCTION

Semiconductors were understood in the last century. Since then, a tremendous amount of research has been conducted in an effort to better understand and control their properties and invent semiconductor devices resulting in great benefits to humankind. One of the primary current quest on semiconductor research is to develop semiconducting materials that are more compact and more efficient than existing materials. Science and technology for nanoscale materials has been applied to develop nanoscale semiconducting materials to complete the quest. One of the promising nanoscale semiconducting materials is semiconductor nanowire; its geometry and properties allow for several advantages. One of the challenges preventing semiconductor nanowire from practical usage is the insufficient technology to control its properties. This dissertation presents practical approaches to control magnetic and electronic properties of semiconductor nanowire via doping.

This chapter will provide general context and the significance of the work presented in this dissertation. The first section will discuss about the significance, properties, and fundamental physics of semiconductor. The following section will explain the characteristic of semiconductor nanowires and properties of semiconductor nanowires and will highlight the potential applications of semiconductor nanowires. Finally, the significance of doping process on semiconductor and the challenge of doping process on semiconductor nanowire will be discussed.

1.1 SEMICONDUCTOR AND ITS SIGNIFICANCE

Development of electronic devices enabled modern technology. Electronic devices have been utilized in a wide range of applications, such as computing, data storage, sensors, lightings, energy production, and energy storage; they are building blocks of computer processors, solid state data storage devices, image sensors in digital cameras, LEDs, and solar cells, etc. Prominent examples of electronic devices are diodes and transistors. These electronic devices operate based on properties of semiconductors, which are their essential components. Not only being fundamental components of electronic devices, semiconductors are crucial materials for other applications, such as catalysts, battery electrodes, etc. Semiconductors have electrical conductivity in the range between those of metal and insulator, and they are sensitive to heat, light, and external electric field. This fundamental property of semiconductors leads it to be useful materials in many applications, which can be visualized by energy band diagrams of a semiconductor, electronically allowed states of a semiconductor as a function of energy, illustrated in Figure 1.1. An inorganic semiconductor are formed by group of atoms connected through covalence bonds. This connection forms two bands of electronically allowed states: the upper band is called conduction band and the lower state is called valence band. These bands are divided by the forbidden gap, so called band gap. At absolute zero, all electrons in a semiconductor reside in the lowest energy state. Therefore, the valence band are completely filled with electrons while the conduction are empty, thus all electrons are localized in the valence band allowing no current to flow through the semiconductor. The electrons in the valence band can be excited by heat or energy from photons (illumination) and move to the conduction band. The thermal excitation or the illumination generates

delocalized electrons in the conduction band and delocalized empty states in the valance band called holes. The delocalized electrons and holes induce the flow of current through the semiconductor, and thus increase electrical conductivity of the semiconductor.

1.2 SEMICONDUCTOR NANOWIRES

Traditional electronic devices were made of bulk semiconductor. Due to the improvement of nanotechnology, size of the electronic devices is reduced while the efficiency of electronic devices is improved. Modern electronic devices are primarily made of thin film semiconductor, which allows for compact size and high efficiency. Thin film morphology has a confined thickness in nanometer to micrometer range. To obtain more compact electronic devices, more dimensions of a semiconducting material need to be confined. Two-dimensional confinement to nanometer scale results in nanowire geometry. A semiconductor nanowire is a quasi-cylindrical shape semiconducting material with diameter in nanoscale and length ranging from micron to millimeters. This geometry allows for unique characteristics, which has potential for many applications. First, the high aspect ratio geometry allows for being integrated into a micro-/nanoscale electronic device as well as superior charge separation and light absorption properties as compared to bulk semiconductors. Moreover, the large surface-to-volume ratio of nanowire increases the sensitivity to surface interaction as well as chemical reactivity. Additionally, the radial dimension of the nanowire is in or below the range of many characteristic length scales, such as Bohr radius, sub-bandgap wavelength, and exciton diffusion length, and magnetic domain. These unique characteristics cause semiconductor nanowires to have different properties form their bulk counterparts, and lead semiconductor nanowires as a promising

material for many applications, such as micro-/nanoscale electronic devices, nanosensors, nanophotonics, themoelectrics, photovoltaics, catalysis, and battery.[1,2]

1.3 SEMICONDUCTOR DOPING

Electronic property of a semiconductor has to be tuned before being used as a component in electronic devices. This property tuning process is done by adding a small quantity of impurity atoms into a pure or intrinsic semiconductor crystal, so called doping. The electronic property can be controlled by type and quantity of the impurity atoms, so called dopants. Higher concentration of a dopant in a semiconductor crystal leads to higher charge carrier concentration in the semiconductor, increasing conductivity of the semiconductor. As mention above, there are two type of charge carriers: delocalized electrons, which are negative charge carriers, and delocalized holes, which are positive charge carriers. Adding dopants which introduces delocalized electrons to a semiconductor creates an n-type semiconductor while adding dopants which introduce delocalized holes to a semiconductor creates a p-type semiconductor. This can also be explained by energy band diagrams of intrinsic and doped semiconductors (Figure 1.2). Typically, n-type doping introduces filled electronic states narrowly below the conduction band of a semiconductor while p-type doping introduces empty electronic states narrowly above the valence band of a semiconductor. For example, adding phosphorus atoms to silicon crystal generates n-type semiconductor while adding boron atoms to silicon crystal generates p-type semiconductor. Electronic devices, such as diodes, bipolar junction transistor, and field-effect transistors, are fabricated by assembling n-type semiconductor(s) and p-type semiconductor(s) into specific configurations as shown in Figure 1.3.

Beside electronic property, doping can also control magnetic properties of semiconductor. This is done by introducing magnetic impurity atoms, such as manganese (Mn), iron (Fe), and cobalt (Co), into a semiconductor crystal. Introducing low concentration of the magnetic impurities into a semiconductor crystal generates dilute magnetic semiconductor, which has a promising candidate for spintronic application.

Doping in bulk semiconductors can be accomplished by several techniques; the prevalent techniques are diffusion doping and ion implantation. Diffusion doping process is done by coating a layer of impurity atoms, e.g. impurity atoms dispersed in polymeric medium, on a surface of a semiconductor crystals. Then heat is used to diffuse the impurity atoms from the surface to the semiconductor parent crystal. In ion implantation process, a semiconducting parent crystal is bombarded with dopant ions embedding the dopants to the atomic layers on the surface of the parent crystal. Then heat governs the diffusion of the dopant from the surface through the parent crystal. Although these well-established methods are suitable for bulk semiconductors, the application of these methods to semiconductor nanostructures, especially colloidal nanostructures, is limited.

Although doping is a necessary step to promote semiconductor nanowires for practical use, it is yet a great challenge in the field. There are some efforts to dope semiconductor nanowires with impurity atoms. Doping during growth has been demonstrated in colloidal and free-standing nanowires.[3–7] In this technique, a dopant precursor is added into a nanowire growth medium during the growth process. More details on nanowire growth will be discussed in the next chapter. The challenge of this approach is that the doping process is governed by solubility of dopants in nanowire growth catalyst, which are metal nanoparticle. This limits type and quantity of dopants that can be

introduced into semiconductor crystal. Alternative doping approaches will certainly be useful to engineer properties of semiconductor nanowire to suit its potential applications

This dissertation will demonstrate a potential of doping approaches via unconventional mechanisms, which have been demonstrated to successfully introduce charge carriers and magnetic dopants into a structure with high surface-to-volume ratio e.g. colloidal quantum dots. Semiconductor nanowires also possess large surface-to-volume ratio, and thus they are suitable candidates for these approaches.

1.4 OVERVIEW OF THE THESIS

This dissertation will demonstrate three approaches to manipulate magnetic and electronic properties of semiconductor nanowires via doping. Chapter 2 will provide some background on nanowire growth techniques and focus on colloidal cadmium selenide (CdSe) nanowire growth via solution-liquid-solid growth mechanism of semiconductor nanowire Moreover, detailed experimental method used to synthesize bismuth nanoparticles used for colloidal CdSe nanowire growth and colloidal CdSe nanowires will be discussed in this chapter. These CdSe nanowires were used as starting materials to demonstrate doping approaches in this dissertation.

The next three chapters will present three semiconductor nanowire doping mechanisms, including nanocrystal diffusion doping, sequential nanocrystal diffusion doping and cation exchange, and photochemical doping, by discussing methods used to prepared doped semiconductor nanowires via those mechanisms as well as the effect of the doping on magnetic and electronic properties of the doped nanowires. The doping mechanisms demonstrated in this thesis is illustrated in Figure 1.4. Chapter 3 will discuss about preparation of Mn(II) doped CdSe nanowire via diffusion doping as an example to

demonstrate the advantage of doping in controlling magnetic property of semiconductor nanowires. Chapter 4 will discuss about using sequential diffusion doping and cation exchange to prepare In(III) doped CdSe nanowires from CdSe nanowire to demonstrate the benefit of doping on controlling electronic property of semiconductor nanowires. The final chapter will discuss a potential of photochemical doping mechanism on semiconductor nanowire doping.

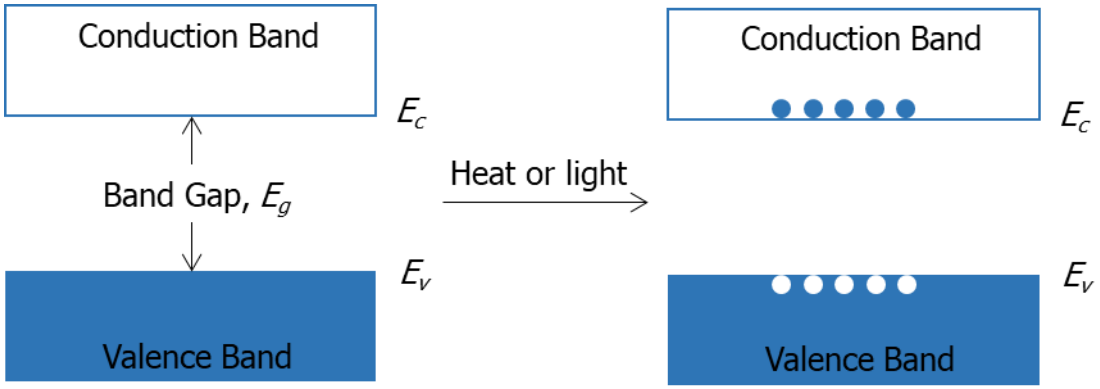

Figure 1.1 Energy band diagrams of a semiconductor at absolute zero (left) and at elevated temperature or under illumination (right). Blue circles represent electrons and white circles represent holes. At absolute zero (left), the valence band is filled with localized electrons and the conduction band is empty. Excited by heat or light (right), electrons from the valence band move to conduction band and leave free holes in the valence band. The conduction band and the valence band is separated by a band gap where there is no allowed electronic states. The band gap energy, E_g, is specified by the highest energy level in the valence band (E_v) and the lowest energy level in the conduction band (E_c), $E_g = E_c - E_v$.

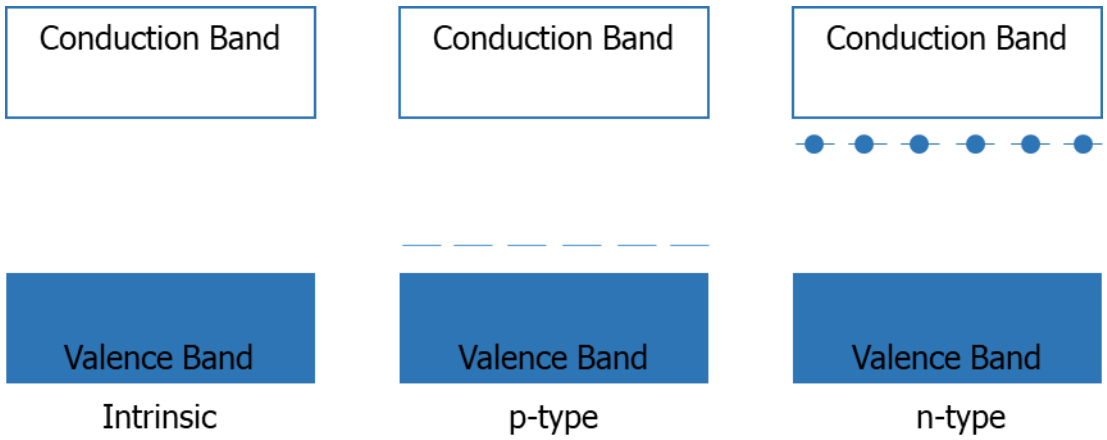

Figure 1.2 Energy diagrams of (A) an intrinsic semiconductor, (B) an n-type semiconductor, and (C) a p-type semiconductor.

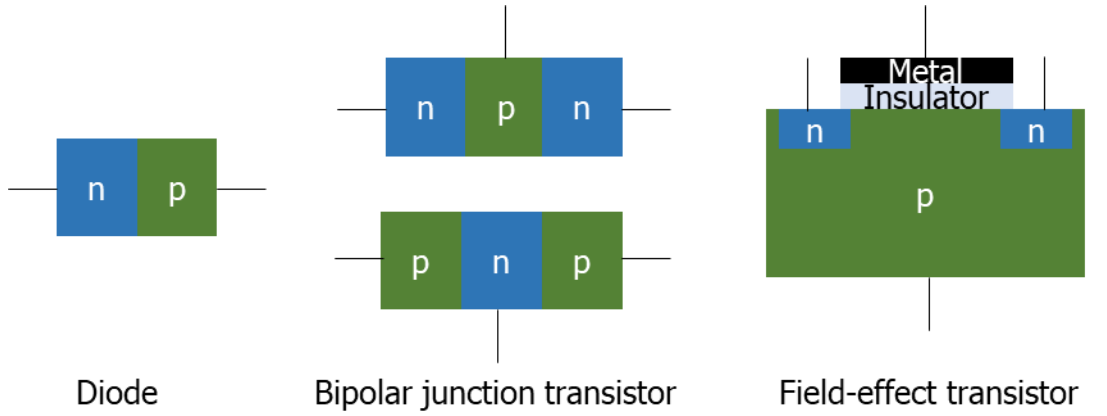

Figure 1.3 Configurations of a diode, a bipolar junction transistor, and a field-effect transistor. Blue blocks represent n-type semiconductor, green blocks represent p-type semiconductor, and black lines represent connections to electronic circuits.

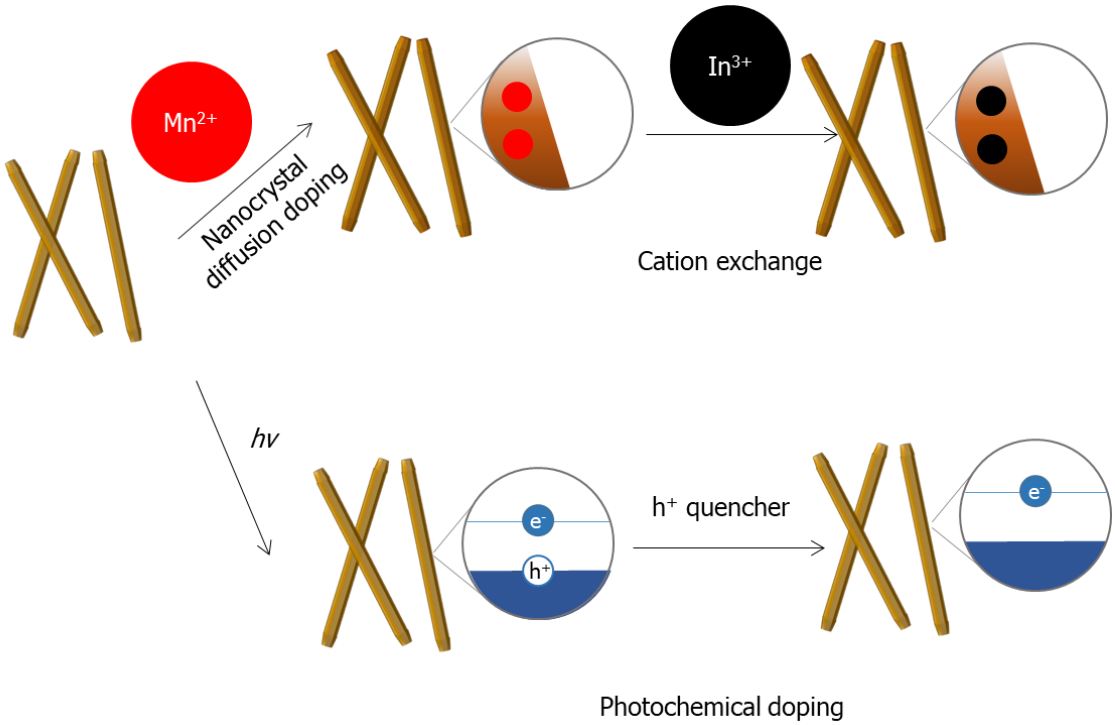

Figure 1.4 Schematic of semiconductor nanowire doping approaches presented in this thesis.

CHAPTER 2

SYNTHESIS AND CHARACTERIZATION OF COLLOIDAL CDSE NANOWIRES VIA SOLUTION-LIQUID-SOLID MECHANISM

The advance in nanotechnology improves the quality of the electronic devices. In the past decades, thin film semiconductor was invented and has been employed as a main component in modern electronic devices. By confining one dimension of bulk structure to micro- or nanoscale, thin film structure is achieved. As compared to their bulk counterparts, thin film semiconductors are more compact and more efficient. The quest to look for more compact and more efficient semiconducting materials is still progressing to improve the quality of existing technology and invent new technology. By confining two dimensions of bulk semiconductor to nanometer scale, semiconductor nanowire can be realized. Not only more compact size as compare to bulk semiconductor, semiconductor nanowire also has unique electronic, optical, mechanic, thermal, chemical, and magnetic properties leading it to be a promising candidate for many applications, such as such as micro-/nanoscale electronic devices, nanosensors, nanophotonics, themoelectrics, photovoltaics, catalysis, and battery. Due to its great potential for many applications, synthesis and properties of semiconductor nanowire has been extensively in the past decades.

2.1 SEMICONDUCTOR NANOWIRE GROWTH

Semiconductor nanowire is a cylindrical shape semiconductor with radial dimension in nanometer scale and length in the range of microns to millimeters. This quasi-one-dimensional structure can be achieved by etching bulk semiconductor, so called top-

down method, or by assembling its subcomponents, so called bottom-up method.[8] Top-down approach requires high-precision etching process, usually assisted by lithography techniques. Therefore, morphology of semiconductor nanowires produced from this approach is determined by lithography pattern, and thus possibility of the morphology is limited by resolution of the lithography technique used. This approach allows semiconductor nanowires for being integrated into electronic device with high precision. However, the yield of semiconductor nanowires produced from this approach limited as compared to that from the other approach. Bottom-up approach be achieved via several methods. These methods usually require either a template or a metal nanoparticle catalyst. In terms of yield, metal nanoparticle assisted semiconductor nanowire growth method is superior. This method can be done in vapor phase or in solution phase.[2,8,9] The method carried out in vapor phase yields free standing semiconductor nanowire while that carried out in solution phase yields colloidal semiconductor nanowires. Among those semiconductor nanowire synthetic methods, solution based method via solution-liquid-solid (SLS) mechanism is most suitable to synthesize semiconductor as a starting material for doping reactions demonstrated in this dissertation because this method yields colloidal semiconductor nanowires with sufficient amount suitable for the doping reactions presented in this dissertation.

2.2 CDSE SYNTHESIS VIA SOLUTION-LIQUID-SOLID (SLS) MECHANISM

There are numerous types of semiconductor based on elemental compositions which serve different purposes in semiconductor applications. Colloidal CdSe nanowire is selected as a starting material in doping reactions demonstrated in this thesis for several reasons. First, CdSe is a direct bandgap semiconductor emitting fluorescence in visible

range. This II-VI semiconductor also has excellent optical properties. Additionally, colloidal chemistry of CdSe nanocrystals is well-established. Finally, doping methods presented in this dissertation are adapted from doping methods successfully used to prepare doped CdSe colloidal quantum dots.[10–12] This chapter will primarily focus on synthesis and characterization of colloidal CdSe nanowire which was used as a starting material for doping reactions that will be discussed in the next chapters.

Solution phase semiconductor nanowire synthesis via SLS mechanism is a bottom-up approach, through which a semiconductor nanowire is assembled from its subcomponents. This mechanism contains many steps. First, the subcomponents dissolve in nanoscale metal droplet forming a nanoscale alloy droplet. The continuous supply of the subcomponents to the alloy droplet supersaturates the alloy inducing the crystallization of the subcomponents. The crystal growth continue in one direction yielding a semiconductor nanowire. Because the nanowire crystal is crystalized from the nanoscale alloy droplet, the size of the metal nanoparticle that forms the droplet determines the radial dimension of a nanowire. The fact that the subcomponents from a solution becomes liquid, and then solid is the origin of the name of this mechanism, SLS.

Many research studies successfully synthesized CdSe nanowires via this mechanism. This mechanism allows CdSe nanowires to be synthesized as colloidal CdSe nanowires as well as CdSe nanowires attached to a substrate or electrodes.[9,13–18] The Colloidal CdSe nanowires are capped by organic ligands, which provide stability in solution and prevent aggregation of the nanowires. In general, CdSe nanowire synthesis reaction media consist of a cadmium precursor, a selenium precursor, bismuth nanoparticles, surfactants, and a high boiling point solvent. The cadmium and selenium

precursors are cadmium and selenium bonded to long-chain organic moieties. The ratio of the cadmium to the selenium precursors,[13,19] the surfactants,[20,21] and the solvent as well as the size of the bismuth nanoparticles determine morphology of CdSe nanowires.[9,13,19] In a CdSe nanowire growth reaction, the precursors decompose and then supply cadmium and selenium to bismuth nanoparticles at elevated temperature. Bismuth nanoparticles are usually used as catalysts in semiconductor nanowire synthesis via SLS mechanism due to its relatively low melting point as compared to other types of metal nanoparticles, such as gold nanoparticles. The low melting point property is suitable for solution phase synthesis because the synthetic temperature cannot go beyond boiling point of the solvent used in a nanowire growth reaction. Bismuth nanoparticles can be synthesized by various methods. Annealing of bismuth thin film[16,18,20] and electrodeposition[22] reported to yield bismuth nanoparticle attached on substrates. There were many research studies reported on synthesis of polymeric ligand capped bismuth nanoparticles, and used them for semiconductor nanowire synthesis.[13,14,20,23,24] However, the production of the polymer used for the polymeric ligand capped bismuth nanoparticle synthesis was discontinued. Yarema and coworkers reported on controlled synthesis of oleate capped bismuth nanoparticle.[25] This method does not require polymeric ligand and yields highly monodisperse colloidal bismuth nanoparticles and thus was modified and employed to synthesize colloidal bismuth nanoparticles used for CdSe synthesis illustrated in this dissertation.

This chapter will illustrate solution phase bismuth nanoparticles synthesis and colloidal CdSe nanowire synthesis via SLS mechanism.

2.3 EXPERIMENTAL SECTION

Chemicals. Lithium bis(trimethylsilyl)amide ($Li[N(SiMe_3)_2]$, 99.0 %) and selenium shot (Se, 99.999%) were obtained from Alfa Aesar. 1-Hexadecylamine (HDA, 90%) and tri-n-octylphosphine oxide (TOPO, 99%) were obtained from ACROS ORGANICS. Cadmium oxide (CdO, 99.999%) and tri-n-octylphosphine (TOP, 97%) were obtained from STREM CHEMICALS. Oleic acid (OA, 99%) was obtained from BEANTOWN CHEMICAL. Bismuth(III) chloride ($BiCl_3$, 99.99%), and tetrachloroethylene (TCE, 99%) were obtained from Aldrich. Acetonitrile (≥99.5%) and hexane (95%) were obtained from Sigma-Aldrich. Toluene (99.9%) was obtained from Fisher Scientific. Ethyl alcohol was (200 proof ethanol) was obtained from Decon Laboratories. Diethyl ether and Tetrahydrofuran (THF) were dried over activated alumina.

Synthesis of $Bi[N(SiMe_3)_2]_3$ as a Bismuth Precursor. The $Bi[N(SiMe_3)_2]_3$ was prepared using a modified literature method.[25,26] All steps of synthesis and purification were carried under an air-free condition with anhydrous solvent. 1.000 g (5.976 mmol) of $Li[N(SiMe_3)_2]$ and 12 mL of diethyl ether were mixed in a septum-capped 50 mL round bottom flask in a nitrogen atmosphere glovebox. Separately, in a nitrogen atmosphere glovebox, 0.6282g (1.992 mmol) of $BiCl_3$, 12 mL of diethyl ether, and 2.4 mL of THF were mixed before adding to a septum-capped addition funnel. The funnel and the round bottom flask were assembled in a nitrogen atmosphere glovebox. The solution of $Li[N(SiMe_3)_2]$ was stirred and cooled in an ice bath. The solution of $BiCl_3$ was added dropwise to the solution of $Li[N(SiMe_3)_2]$ for 2 hours. The reaction mixture, which became light yellow turbid, was centrifuged. The supernatant was then filtered using PTFE syringe filter with 0.45 μm pore size. The filtered solution was dried under vacuum to give a light

yellow solid. To dissolve the solid, 10 mL of hexane was added to give a yellow solution. The solution was filtered using PTFE syringe filter with 0.45 μm pore size and dried under vacuum to yield 165 mg of a yellow solid. $Bi[N(SiMe_3)_2]_3$ is a light sensitive compound, so the product was stored in a freezer inside the glovebox. This product was used as a bismuth precursor without characterizations.

Bi NP growth. Bismuth nanoparticles were prepared using a modified literature method.[25] Briefly, 25 g of HDA was added into a septum-capped 100 mL round bottom flask and heated at 100ºC under vacuum for 30 min in order to dry the HDA. The HDA was then kept at 100 ºC under nitrogen atmosphere. Separately, in a nitrogen atmosphere glovebox, 1.2 mL of toluene was added into 171 mg (0.248 mmol) of $Bi[N(SiMe_3)_2]_3$ to give a yellow solution, and 1.2 mL of toluene was added into 207 mg (1.24 mmol) of $Li[N(SiMe_3)_2]$ to give a brown solution. These solutions were then mixed, and injected into the flask containing the HDA at 100 ºC. The reaction mixture turned to brown solution instantly after the injection. The reaction mixture was kept at 100 ºC for 15 sec before cooling down to room temperature. At 80 ºC, 20 mL of toluene was injected into the reaction mixture. At room temperature, ethanol was added to the reaction mixture (1:1 (v/v)). The reaction mixture was mixed well before being centrifuged at 6000 g to separate Bi nanoparticles. The precipitate was redispersed in TCE; sonication was used to assist the dissolution of the solid. 200 μL of OA was added to the solution to replace HDA ligand with OA. Ethanol was added to the solution (1:1 (v/v)). The mixture was centrifuged to precipitate Bi nanoparticles. The Bi nanoparticles was redispersed in anhydrous toluene, and then stored in a nitrogen atmosphere glovebox for further use. The Bi nanoparticles were characterized by TEM.

CdSe nanowire growth. CdSe nanowires were prepared using a modified literature method.[19] Briefly, in a nitrogen atmosphere glovebox, 1.92 M TOPSe was prepared by adding 11.4 mL of TOP to 1.727g of selenium pellets. The mixture was then stirred at room temperature until the selenium pellets are completely dissolved. Separately, 60 mg (0.47 mmol) of CdO, 530 μL of OA, and 15 g of TOPO were loaded in a septum-capped 100 mL round bottom flask, and then heated at 110ºC under vacuum for 50 min to dry the mixture. The reaction mixture was then kept under nitrogen atmosphere before increasing the reaction temperature to 340 ºC, at which the reaction mixture became clear. The reaction temperature was then reduced to 250 ºC, at which the mixture of 2.935 mL of TOPSe (1.92 M) and 0.180 mL of Bi NP solution in anhydrous toluene (4 mg/mL) was injected into the reaction mixture. The reaction mixture turned to dark brown immediately after the injection. The reaction temperature was kept at 250 ºC for 10 min before cooling the reaction mixture down. At 80ºC, 15 mL of toluene was injected into the reaction mixture to prevent solidification of TOPO. The reaction mixture was then precipitate by mixing with acetonitrile before centrifuge. The precipitate was purified by precipitation/redissolution technique with (1:1 (v/v)) toluene/acetonitrile three times. The nanowires were suspended in toluene for further use.

Physical Characterization. Transmission electron microscope (TEM) samples were prepared by dropping a dilute solution of colloidal suspension of bismuth nanoparticles in toluene on a 400 mesh copper grid (Ted Pella, Inc.) or that of CdSe nanowires in toluene on 200 mesh copper grid with a lacey carbon film (Ted Pella, Inc.) and allowing this substrate to dry under vacuum. TEM images were obtained on a Hitachi HT7800 TEM, 100 kV microscope. Bismuth nanoparticles and CdSe nanowires sizes and

size distributions reported were determined by analysis of the images of 207 and 104 individual nanocrystals, respectively. Energy-dispersive X-ray spectroscopy (EDS) spectra were obtained using a Hitachi HT7800 TEM equipped silicon drift detector (Oxford Instruments X-Max^N-80T). Relative atomic contents were extracted from the EDS spectra using Aztec software package version 3.3. A PXRD pattern were collected from dried CdSe nanowire powder on a Zero Background holder using a Bruker D2 Phaser with LYNXEYE silicon strip detector. Lithium fluoride (LiF) was mixed into a nanowire powder sample by grinding in a mortar for < 30 s to provide reference peaks. Thermogravimetric Analysis (TGA) data were collected using a TA Instruments Q5000 with a nitrogen flow rate of 25 mL min^{-1} and heating rate of 10 °C min^{-1}.

2.4 RESULTS AND DISCUSSION

Bismuth precursor and bismuth nanoparticle synthesis. $Bi[N(SiMe_3)_2]_3$ was synthesized from $BiCl_3$ and $Li[N(SiMe_3)_2]$ to be used as bismuth precursor for bismuth nanoparticle synthesis. The yellow solid product from the synthesis was assumed to be $Bi[N(SiMe_3)_2]_3$ without characterizations and used for bismuth nanoparticle synthesis. From $Bi[N(SiMe_3)_2]_3$, bismuth nanoparticles were synthesized to be used as metal nanocatalysts in colloidal CdSe nanowire synthesis. The mechanism of the bismuth nanoparticle synthesis is assumed to be a homolytic cleavage of Bi-N bonds in the precursor molecule at temperature above 100 °C generating elemental bismuth. $Li[N(SiMe_3)_2]$ was added to control the shape of the bismuth nanoparticles; $N(SiMe_3)_2$ is believed to coordinate to bismuth atoms on the surface of the nanoparticle during the growth allowing the spherical shape of bismuth nanoparticle to form. HDA was used as a solvent as well as a weakly coordinated ligand to bismuth nanoparticle; strongly

coordinated ligand, such as oleate induces the formation of bismuth $(oleate)_3$ and thus hamper the formation of bismuth nanoparticles. HDA ligand was replaced by oleate ligand in a post-synthetic modification step to stabilize the bismuth nanoparticles. Size of the bismuth nanoparticles is primarily controlled by the synthetic temperature. A representative micrograph of the bismuth nanoparticles taken by Transmission electron microscope (TEM) shown in Figure 2.1 indicates that the Bi nanoparticles are spherical. The size distribution of the bismuth nanoparticles collected from several TEM images is represented by a histogram shown in Figure 2.2. The diameter of Bi nanoparticles ranges from 5.8 to 18.1 nm with the average diameter of 10.7 ± 2.2 nm where the uncertainty represents sample standard deviation among the nanoparticles measured.

Colloidal CdSe nanowire synthesis. Colloidal CdSe nanowires were synthesized from $Cd(oleate)_2$ and TOPSe catalyzed by bismuth nanoparticles. $Cd(oleate)_2$ was generated from CdO and OA around 340°C while TOPSe was synthesized from elemental selenium and TOP at room temperature. The impurities in TOPO were reported to have an effect on the morphology of CdSe nanowires, so high purity TOPO (99%) was used as a solvent for the nanowire synthesis. CdSe nanowires were synthesized at 250°C at which the bismuth nanoparticle melts in the presence of cadmium and selenium.[4,27] A representative TEM image of the nanowires shown in Figure 2.3 indicates that the nanowires have high aspect ratio. The lengths of the nanowires are in micron scale while the diameters of the nanowires are in nanometer scale. There is a nanocrystal attached to a tip of a nanowire shown in Figure 2.3. This is typical for a nanowire synthesized via SLS mechanism because the nanowire is crystalized from the alloy droplet of precursors of the nanowire and a metal nanoparticle used as a catalyst in the synthesis. The distribution of

the nanowire diameters is represented by a histogram shown in Figure 2.4, which indicates the diameters of the nanowires ranging from 7.0 to 82 nm. The average diameter of the nanowires is 43 ± 16 nm, where the uncertainty represents sample standard deviation among the nanowires measured. which is larger than the average dimeter of the Bi nanoparticles. A semiconductor nanowire synthesized via SLS mechanism normally has larger radial dimension than that of the metal nanoparticles used as a catalyst for the nanowire synthesis because the nanowires are crystalized from alloy droplets of the metal nanoparticles and semiconductor precursors, which is larger than the size of the metal nanoparticles. EDS spectra collected using TEM equipped with Energy Dispersive X-ray spectroscopy (TEM-EDS) detector suggests that the nanowires are selenium-rich; the atomic ratio of cadmium to selenium is 47.4 ± 0.5 to 52.6 ± 0.5, where the uncertainties represent sample standard deviation among the spots measured. The atomic ratio was calculated from Kα peaks of cadmium and selenium at 23.17 and 11.21 eV as shown in Figure 2.5, respectively. The peaks at 0.93 (Lα), 8.04 (Kα), and around 9 (Kβ) eV is attributed to Cu from the TEM grid. The PXRD pattern of the nanowires shown in Figure 2.6 matches that of CdSe in wurtzite phase obtained from Inorganic Crystal Structure Database (ICSD), confirming the chemical compositions of the CdSe nanowires. The PXRD pattern suggests that the crystal structure of CdSe nanowires is primarily wurtzite. Even though the PXRD pattern matches wurtzite CdSe, according to the PXRD data from ICSD, every peak attributed to zincblende CdSe is very close to peaks attributed to wurtzite CdSe in the range of measured 2θ angle. Therefore, we cannot rule zincblende out as a minor crystal structure in the nanowire crystal. CdSe nanowires synthesized via SLS mechanism typically have an admixture of wurtzite and zincblende phases because the

nanowire growth is fast and the energy difference between wurtzite and zincblende structures is small. TGA measurement conducted on a dried sample of the nanowires (Figure 2.7) suggested that there is around 4% of ligands by weight. Excess OA added to generate Cd(II) $(oleate)_2$ as a cadmium precursor and excess TOP added to create TOPSe as a selenium precursor are potential sources of the ligands. The ligands could also come from the oleate and TOP decomposed from the Cd $(oleate)_2$ and the TOPSe during the nanowire synthesis. It was reported that TOPO used as a solvent in the synthesis does not bind to CdSe quantum dot surfaces. All of these measurements confirm that colloidal CdSe nanowires were obtained.

2.5 CONCLUSIONS

Bismuth nanoparticles with the average diameter of 10.7 ± 2.2 nm were obtained and used as a catalyst for colloidal CdSe nanowire synthesis. Selenium-rich colloidal CdSe nanowires with average diameter of 43 ± 16 nm and lengths in microns scale were synthesized. These nanowires were used as starting materials for doping reactions that will be presented in the next chapters.

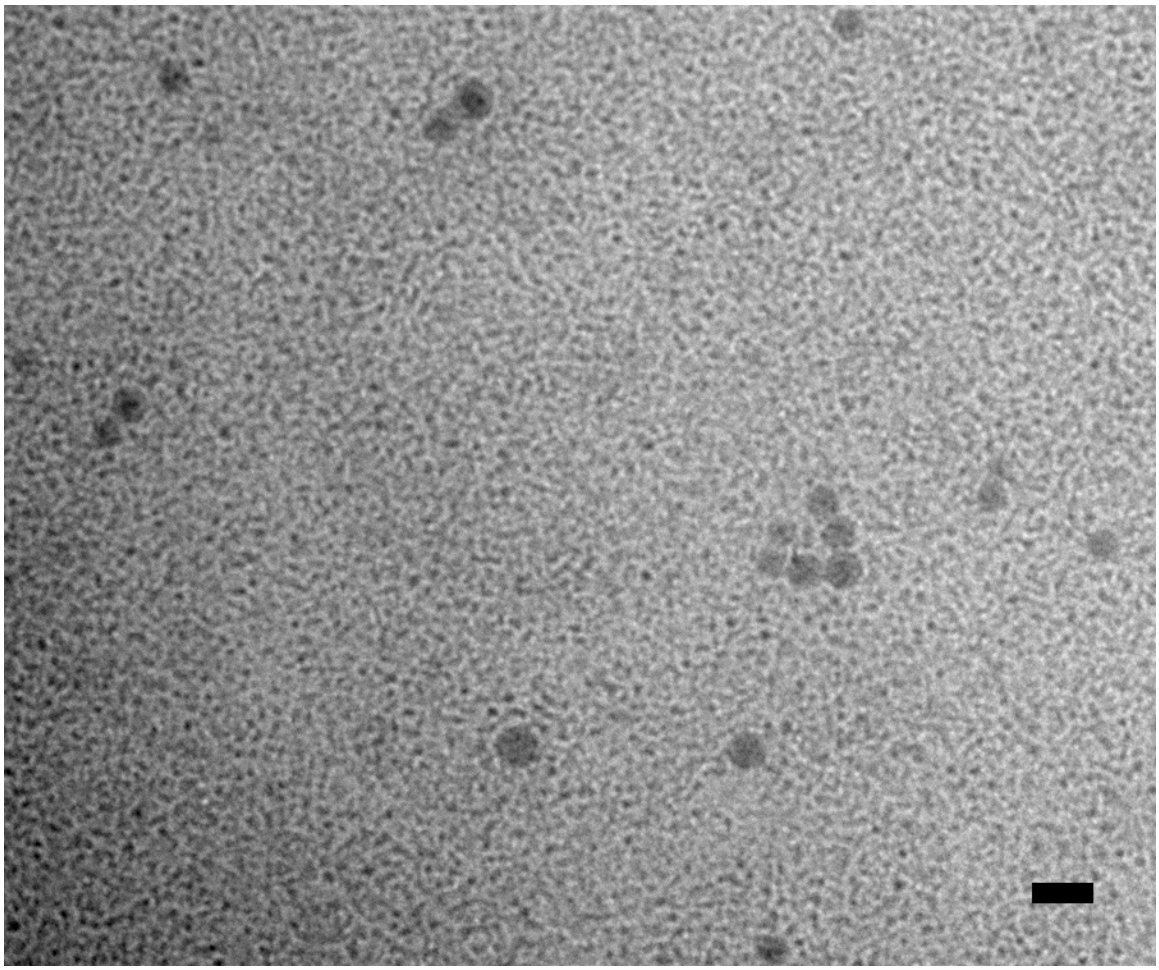

Figure 2.1 A representative TEM image of Bi nanoparticles. Scale bar is 10 nm.

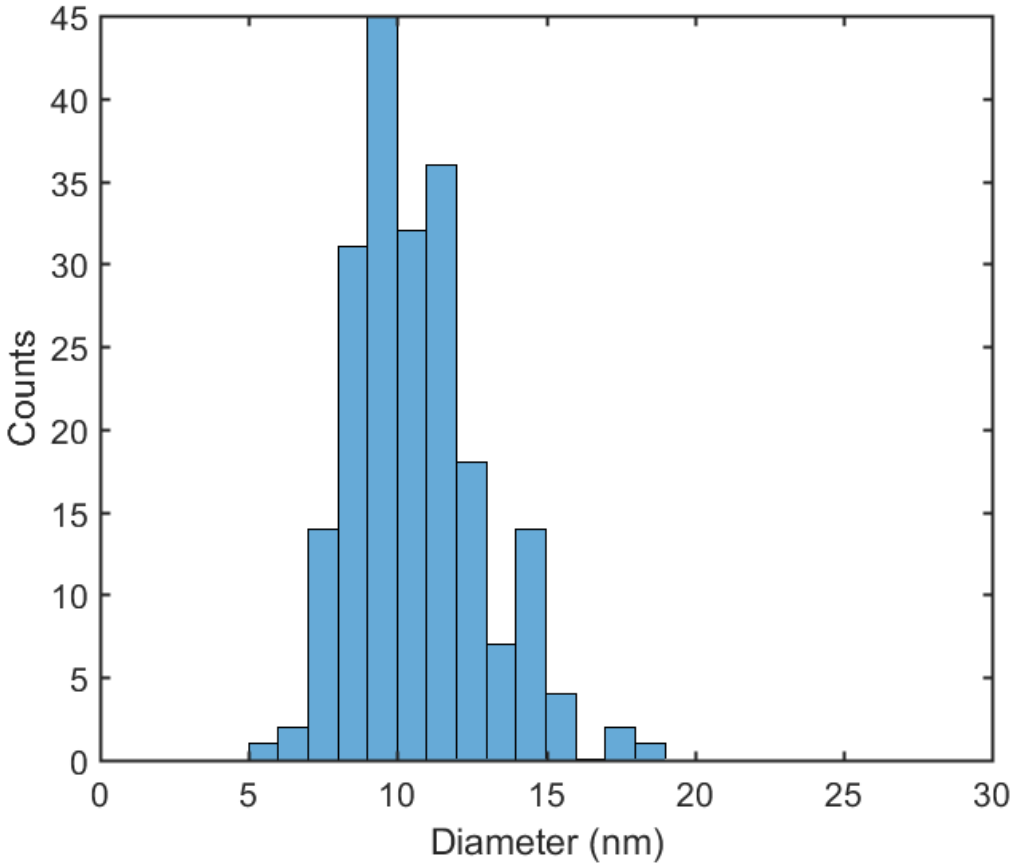

Figure 2.2 Size distribution of the Bi nanoparticles used for colloidal CdSe nanowire synthesis.

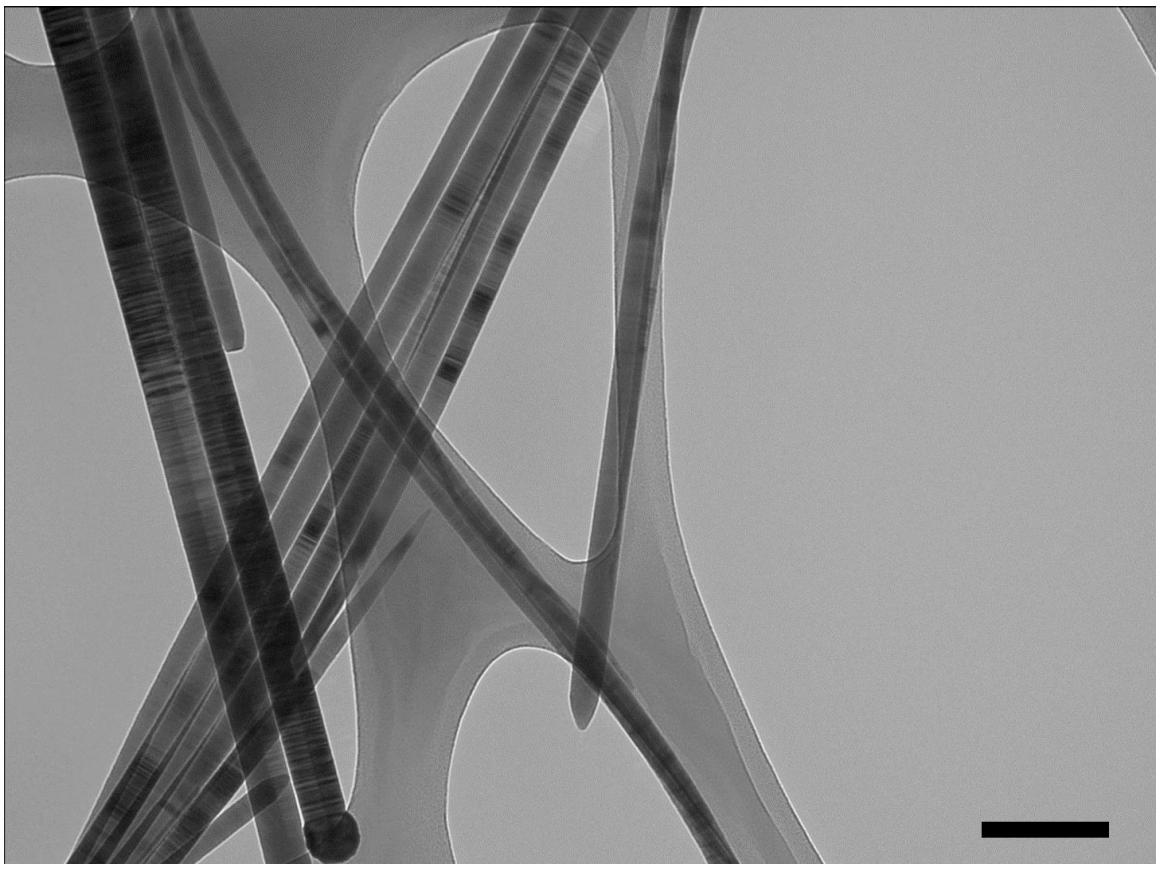

Figure 2.3 A representative TEM image of CdSe nanowires. Scale bar is 200 nm.

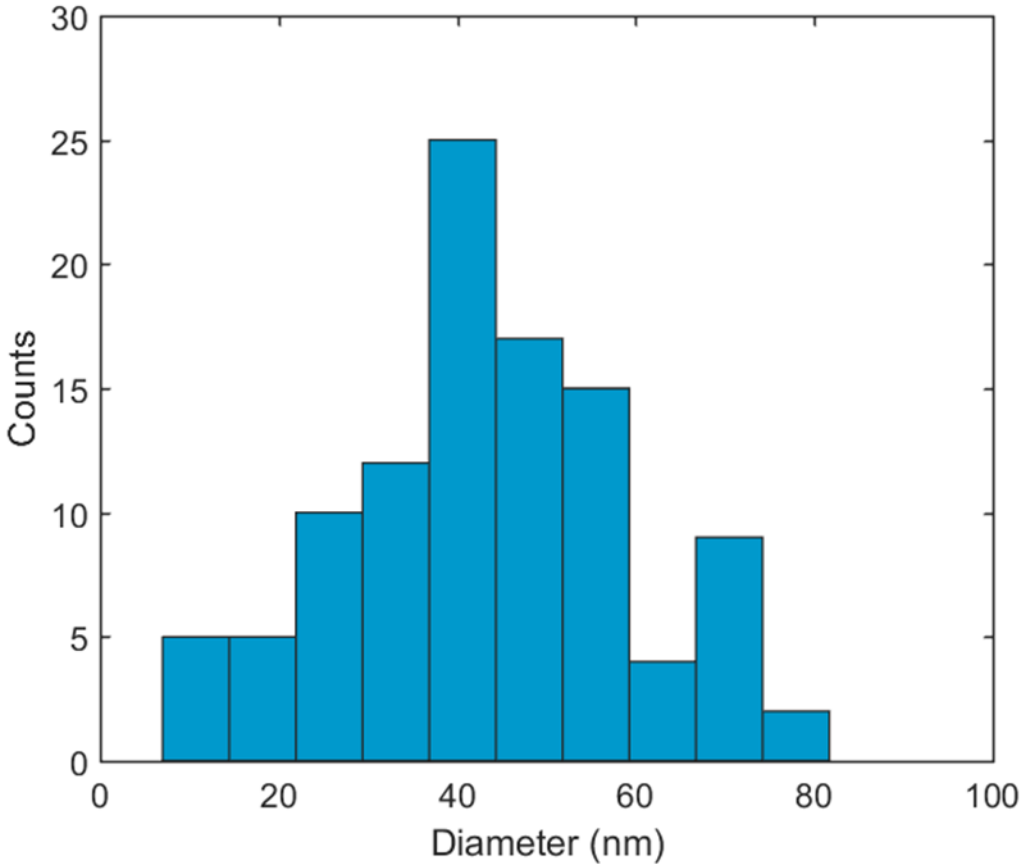

Figure 2.4 Size distribution of the colloidal CdSe nanowires

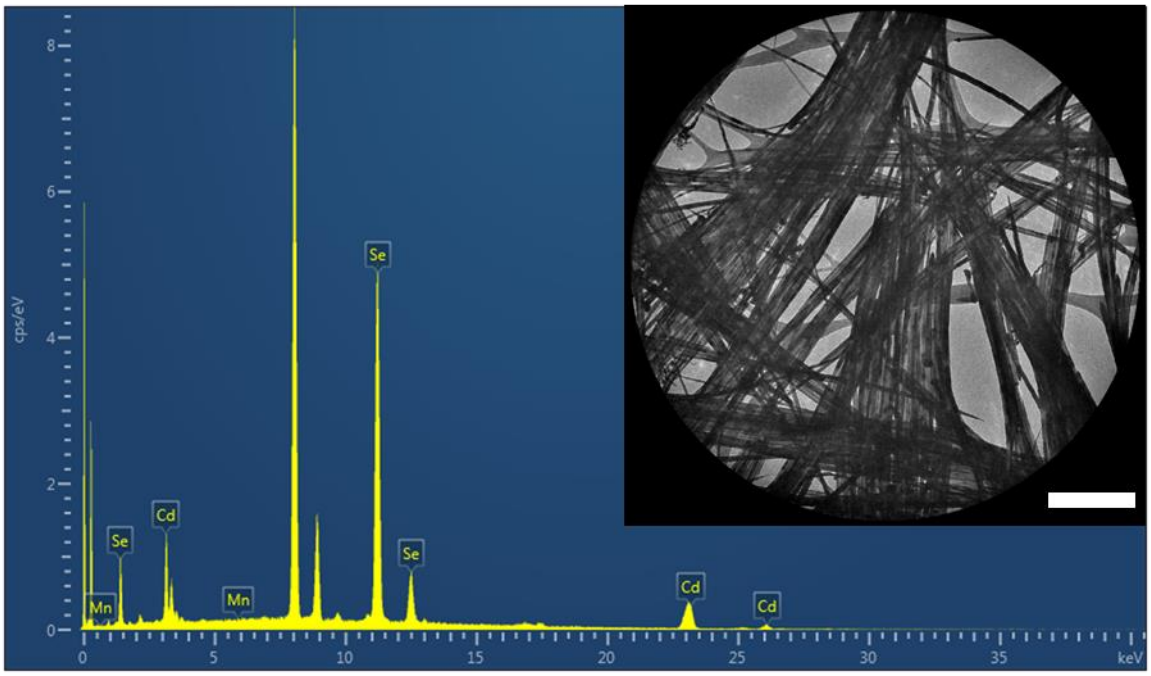

Figure 2.5 A representative EDS spectrum of the CdSe nanowires. Inset: the TEM image of the spot where the EDS spectrum is measured. Scale bar is 1 μm.

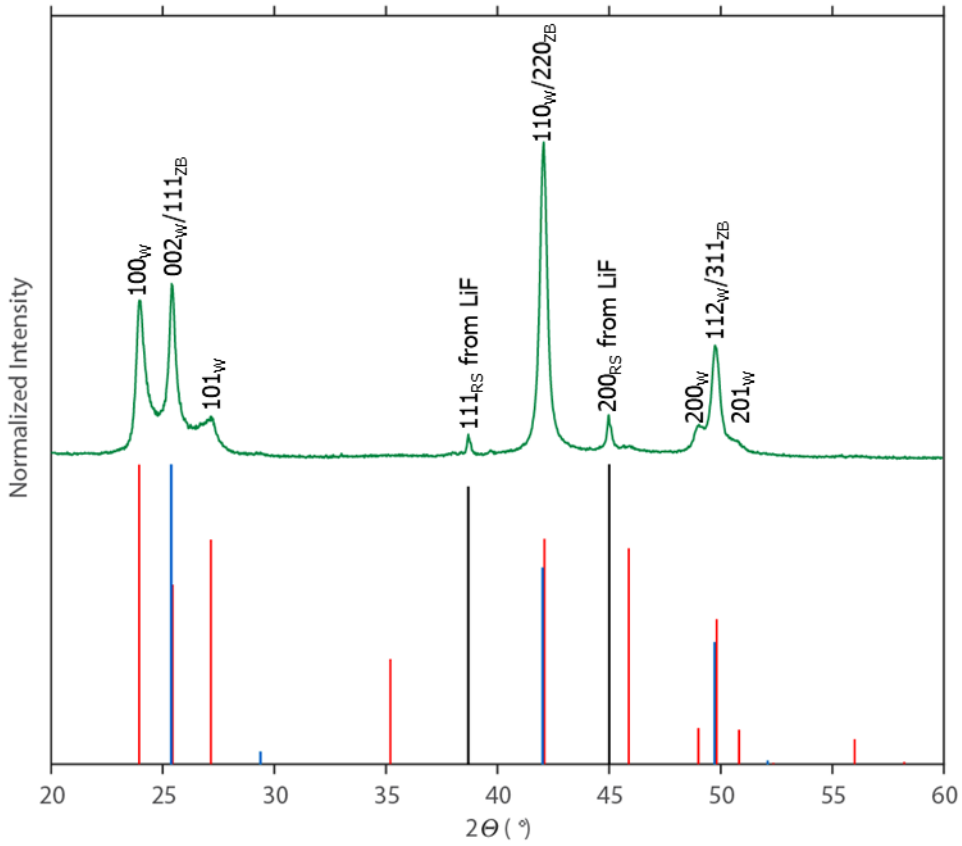

Figure 2.6 A PXRD pattern of colloidal CdSe nanowires. Stick pattern of wurtzite phase of CdSe (red), zincblende phase of CdSe (blue) and LiF are presented for comparison. The measurement was conducted on a zero-background stage leading to a shift of peaks attributed to CdSe nanowires, thus LiF was added to the CdSe nanowire sample to provide reference peaks.

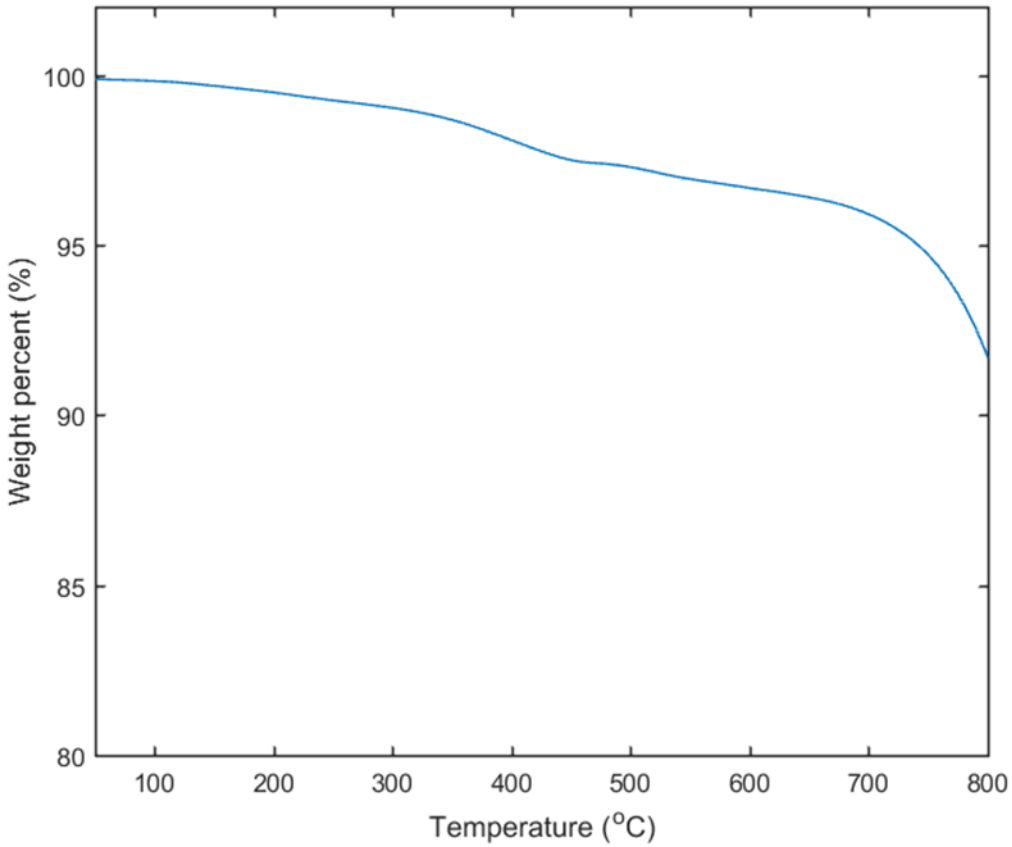

Figure 2.7 TGA measurement on the CdSe nanowires

CHAPTER 3

CONTROLLING MAGNETIC PROPERTY OF CDSE NANOWIRES VIA DIFFUSION DOPING OF MANGANESE AND LIGAND EXCHANGE

3.1 INTRODUCTION

Modern technology utilized fundamental properties of electrons: charge and spin. Electronic devices operate base on controlling electron charge while magnetic devices operate based on controlling electron spin. These two types of devices are foundation of modern technology. One approach to move beyond the efficiency of existing technology is to develop a new technology that can harness both electron spin and electron charge synergistically, which is a primary goal of spintronics. A dilute magnetic semiconductor (DMS) material, prepared by doping a semiconducting material with a proper rare-earth or transition metal, a magnetic dopant, at low atomic percentage. This material is a prime candidate for spintronic application because they provide a medium in which charge carriers from the host semiconductor can interact with spins introduced by the magnetic dopant. DMS is an excellent tool to aid in understating fundamental spintronic properties that have not been revealed. Not only spintronics, DMS is also a promising material for many applications such as, bioimaging and interference information processing.

Many research studies have been conducted in an effort to prepare DMS in various form and compositions. One of most widely used method to prepare DMS is molecular beam epitaxy.[28] This expensive method is suitable to prepare thin-film DMS, which have

a potential to be integrated with well-established thin-film semiconductor technology. DMS has also been prepared in other morphologies such as nanocrystals[29] and nanorods.[30] As compared to those morphologies, nanowire has higher potential for being integrated into electronic devices, which will allow for fabrication of micro-/nanoscale spintronic devices as well as fundamental property study of DMS materials in two-dimensional confinement structure. There were few studies reported on preparation of DMS nanowires, mostly free standing DMS nanowires.[3,31] So far, only one study reported on preparation of colloidal DMS nanowires.[4] The advantageous of colloidal nanowires over free standing nanowires are potential for surface functionalization, processability, and scalability. Moreover, colloidal nanowires with radial dimension in quantization regime can be achieved.[4,32] DMS nanowires at this size regime can provide a platform for studying interactions of electron charge and spin, and thus allow for possibility of novel fundamental physics discovery and novel technology invention. Doping during growth is a primary technique used for DMS nanowires preparation via metal nanoparticle mediated methods, such as vapor-liquid-solid (VLS) and solution-liquid-solid (SLS). In doping during growth technique, a dopant precursor is added into a nanowire growth medium during the growth process. The challenge of this approach is the solubility of dopants in nanowire growth metal nanoparticle catalyst, which limits type and quantity of dopants that can be introduced into semiconductor nanowire crystal. This chapter presents an alternative approach, diffusion doping, to introduce a magnetic dopant into a semiconductor nanowire crystal. Preparation of Mn(II) doped CdSe nanowires and the effect of the doping on magnetic property of the nanowires will be demonstrated. CdSe is a direct bandgap semiconductor emitting fluorescence in visible range and has unique optical properties.

Mn^{2+} ion has the highest effective magnetic moment among the first-row transition-metal ions. Moreover, it has been reported by many studies that Mn(II) doped CdSe is a DMS exhibiting ferromagnetic behavior at low temperature.[3,4] Additionally, Mn-Se bond strength is moderate leading to the versatility to exchange Mn^{2+} in CdSe lattice with another cation. This allows more possibility to control properties of CdSe semiconductor. This strategy is demonstrated in the next chapter.

Introducing Mn(II) ion into CdSe lattices can be challenging due to poor surface absorption of Mn(II) ion on Cd-rich CdSe surface, lower bond strength of Mn-Se as compared to Cd-Se, and intrinsic self-purification.[33] However, it has been reported that diffusion doping has been successfully used to dope Mn^{2+} ion into colloidal CdSe nanocrystals in a controlled fashion.[11,33] In this approach, an anion precursor, a Se precursor, is added to the surface of CdSe nanocrystal to reduce chemical potential of Mn(II) ions on the surfaces and within the crystal of the CdSe nanocrystal as well as chemical potential of Cd(II) ions in the CdSe nanocrystal lattice. Consequently, this attracts Mn(II) ion to the surfaces of the nanocrystal and prevents Cd(II) ions from leaving the nanocrystal lattice. Then heat accelerates the diffusion of Mn(II) ions from the surfaces to the core. Diffusion doping can introduce Mn(II) ion into CdSe nanocrystal up to 20 percent of Mn(II)/cations ratio which can be controlled by equivalent of a selenium precursor to CdSe nanocrystal or reaction time.[11,33] This dissertation demonstrates Mn^{2+} doping in colloidal CdSe nanowires in a controlled manner via diffusion doping as a mean to control magnetic property of colloidal CdSe nanowires. Additionally, ligands on the Mn(II) doped CdSe nanowires was found to have a crucial role in magnetic properties of the nanowires.

3.2 EXPERIMENTAL SECTION

Chemicals. Manganese(II) acetate tetrahydrate ($Mn(II)(OAc)_2 \cdot 4H_2O$, 99.999%), selenium shot (Se, 99.999%), and L-cysteine (≥98%) were obtained from Alfa Aesar. 1-Hexadecylamine (HDA, 90%) and 1-octadecene (ODE, 99%) were obtained from ACROS ORGANICS. Tri-n-butylphosphine (TBP, 99%) was obtained from STREM CHEMICALS. Oleic acid (OA, 99%) was obtained from BEANTOWN CHEMICAL. Stearic acid (SA, ≥98.0%) was obtained from TCI America. Acetonitrile (≥99.5%) and Chloroform (≥99.8%) were obtained from Sigma-Aldrich. Toluene (99.9%) was obtained from Fisher Scientific.

Preparation of Mn(II) doped CdSe nanowires. Mn(II) doped CdSe nanowires were prepared using a modified literature method. Briefly, in a nitrogen atmosphere glovebox, 2.13 M TBPSe was prepared by adding 11.4 mL of TBP to 1.727g of selenium pellets. The mixture was then stirred at room temperature until the selenium pellets are completely dissolved. Separately, 0.8159 g of HDA, 0.4080 g of SA, and 16 mL of ODE were loaded into a septum-capped 100 mL round bottom flask, and then heated at 110 ºC under vacuum for 30 min to dry the mixture. Under nitrogen atmosphere, 26.1 mg of $Mn(OAc)_2 \cdot 4H_2O$ was then added into the reaction mixture against nitrogen overpressure. After that, the reaction mixture was kept under vacuum for 1 h to remove acetic acid and water before heating the mixture to 300 ºC under nitrogen atmosphere. In the glovebox, 21.1 mg of CdSe nanowire (20.3 mg of CdSe according to TGA, 0.106 mmol) in 2 mL of ODE and 50 µL of 2.13 M TBPSe solution were mixed. The mixture was then injected into the reaction mixture. The reaction mixture was kept at 300 ºC under nitrogen atmosphere for 1 h, 2 h, or 4 h before cooling it down to room temperature; toluene was injected into

the reaction mixture at 80 ºC to prevent solidification. The reaction mixture was purified by precipitation/redissolution technique with chloroform/acetonitrile toluene/acetonitrile mixture and pure toluene. The nanowire product was suspended in toluene before further characterizations.

Ligand exchange on Mn(II) doped CdSe nanowires. L-cysteine solution was prepared by dissolving 0.8625 g of L-cysteine in 50 mL of PBS buffer (pH = 7.41). 3:2 (v/v) of a solution of Mn(II) doped CdSe nanowires dispersed in toluene to L-cysteine solution was vortex mixed. The complete of the reaction was monitored by phase exchange of the nanowires from organic phase to aqueous phase. The nanowires were purified by centrifugation and redissolution in DI water for 4 times. The preparation method of Mn(II) doped CdSe nanowires for this ligand exchange experiment were modified from the method described above by using OA instead of SA with the same equivalent to the CdSe nanowires. Additionally, the reaction time for Mn(II) doping reaction was 2 h, 4 h, or 8 h instead of 1-4 h as listed above. Finally, the equivalent of the TBPSe to CdSe was increased from 1 to 3.

Physical Characterization. TEM samples were prepared by dropping a dilute solution of colloidal suspension of nanowires in toluene or DI water on 200 mesh copper grid with a lacey carbon film (Ted Pella, Inc.) and allowing this substrate to dry under vacuum. TEM images of ensemble nanowires were obtained on a Hitachi HT7800 TEM, 100 kV microscope. TEM images of single nanowires were obtained on a JEM-2100 Electron Microscope. EDS spectra of ensemble nanowires were collected using Hitachi HT7800 TEM equipped with a silicon drift detector (Oxford Instruments X-Max^N-80T). EDS spectra of single nanowires were collected using a JEOL JEM-2100 electron

microscope equipped with 30 mm^2 Si(Li) detector (Oxford Instruments). The relative atomic percentages from the EDS spectra are calculated by Inca software package. PXRD data were collected from dried nanowire powders on a Zero Background holder using a Bruker D2 Phaser with LYNXEYE silicon strip detector. Lithium fluoride (LiF) was mixed into some nanowire powder samples by grinding in a mortar for < 30 s to provide reference peaks. X-ray photoelectron spectroscopy measurements were performed using a Kratos AXIS Ultra DLD XPS system, with a monochromatic Al Kα source, operated at 15 keV and 150W and a hemispherical energy analyzer. The X-rays were incident at an angle of 45° with respect to the surface normal and analysis was performed at a pressure below $1x10^{-9}$mbar. High resolution core level spectra were measured with a pass energy of 40 eV, and survey scans were measured with a pass energy of 160 eV. The analysis of the XPS spectra was performed with XPSPEAK 4.1 software. Magnetization data were collected on a Quantum Design MPMS 3 SQUID magnetometer. Temperature-dependent magnetization data were collected under zero-field-cooled (ZFC) and field-cool-worm (fcw) conditions from 2 to 300 K at 100 Oe and M-H loop were collected at 25K.

3.3 RESULTS AND DISCUSSION

Preparation of Mn(II) doped CdSe nanowires via nanocrystal diffusion doping method. Mn(II) doped CdSe nanowires were prepared from colloidal CdSe nanowires via a nanocrystal diffusion doping reaction. In this reaction, TBPSe were added to supply selenium to surfaces of the nanowires to reduce chemical potential of Mn^{2+} on the surface as well as the chemical potential of Cd in the nanowire crystals. This chemical potential reductions attract Mn^{2+} ions to the surface of the nanowire and prevent Cd^{2+} ions from leaving the nanowire crystals. $Mn(SA)_2$ were synthesized from $Mn(OAc)_2 \cdot 4H_2O$ and SA

to be used as a source of Mn^{2+} ions in the doping reaction. HDA and SA were added as ligands coordinated to Mn^{2+} in the reaction mixture. ODE was used as a solvent. The reaction time was used to control the manganese content in the doped nanowires. Aliquots from the reaction mixture were collected at 1 h, 2 h, and 4 h, then purified to remove the excess precursors, the surfactants, and the high-boiling point solvent. Morphology of the doped nanowires was observed via TEM. Figure 3.1 (inset) and 3.2 (inset), are representative TEM images of ensemble and single nanowires from the 4-h aliquot sample, respectively. The TEM images show that the nanowire morphology is preserved after the doping reaction was performed on the CdSe nanowires. This is also true for nanowires from the 1-h and the 2-h aliquots. The EDS spectra of the samples were collected using TEM-EDS to confirm the presence of a manganese species and determine manganese content in the Mn(II) doped CdSe nanowires. Figure 3.1 shows a representative EDS spectrum collected from an ensemble of the doped CdSe nanowires from the 4-h aliquot. The spectrum shows a peak attributed to a manganese species ($K\alpha$) at 5.89 eV that is not present in the EDS spectrum of the CdSe nanowires before doping as shown in Figure 2.5. From EDS spectra of Mn(II) doped CdSe nanowire samples collected from the 1-h, 2-h, and 4-h aliquots, the manganese atomic percentage of each sample was extracted and plotted in Figure 3.3. The manganese atomic percentage in Mn(II) doped CdSe nanowires increases with increasing reaction time. Although the manganese percentages from 1-h (0.18 ± 0.06) and 2-h (0.20 ± 0.17) samples are not significantly different, those values are much smaller than the manganese atomic percentage of the 4-h sample (0.85 ± 0.17). The atomic percentage of manganese in these samples are much smaller than that in Mn(II)CdSe quantum dots prepared by Vlaskin and coworkers using nanocrystal diffusion

doping method.[11] There are two main factors causing the small manganese doping level in the nanowire samples. First, the ratio of selenium precursor to CdSe used for preparing these doped nanowires (1 to 1 ratio) are much smaller than that used by Vlaskin (16 to 1 ratio). This agrees with the results reported by Barrows and coworkers, which explains the effect selenium precursor to CdSe ratio on the doping level.[33] Second, the radial dimension of the nanowires (43 ± 16 nm) is much larger than that of the quantum dots (4.37 ± 0.18 nm). The effect of nanocrystal radial dimension on manganese doping level is demonstrated here. EDS spectra of a single nanowires allows for investigating a relationship between manganese content and radial dimension of the doped nanowires collected at different reaction times. Figure 3.4 shows a plot of manganese atomic percentage in the doped nanowire as a function of its radial dimension. Assuming that the doped nanowires contain manganese, cadmium, and selenium, the manganese atomic percentage is calculated from the manganese Kα peak at 5.89 eV, cadmium Kα peak at 23.17 eV, and selenium Kα peak at 11.21 eV. The radius of the nanowire is determined from corresponding TEM images. The plot indicates that nanowires with smaller diameters have higher manganese content at every demonstrated doping time. Moreover, from the effect of doping time on manganese atomic percentage of the single nanowires, it is clear that the nanowires with similar radial dimension have higher manganese atomic percentage at longer doping reaction time indicating that the longer doping reaction time led a larger manganese content doped into the nanowires. This result corresponds to the result obtained from the ensemble TEM-EDS measurement. The manganese percentage data from the single nanowires were compared with diffusion in cylindrical model[34] which is explained by equation 3.1-3.3.

$$x = \int \frac{2\pi\, c(r,t)dr}{\pi R^2} \tag{3.1}$$

$$c(r,t) = u(r,t)(c_0 - c_R) + c_R \tag{3.2}$$

$$u(r,t) = \sum_{n=1}^{\infty} e^{-D\left(\frac{\alpha_{n0}}{R}\right)^2 t} J_0\left(r\left(\frac{\alpha_{n0}}{R}\right)\right) \frac{2}{\alpha_{n0} J_1(\alpha_{n0})} \tag{3.3}$$

Here, R is the radius of the nanowire, $c(r,t)$ is the manganese concentration within the wire at a distance r from the nanowire core (axis) at a time t, and x is the average manganese atomic percentage. The initial concentration of manganese in the nanowire, c_0, is assumed to be 0, c_R is the saturated concentration of the manganese in the crystal, and D is the diffusion constant. A rough estimate of manganese diffusion constant during the doping process is 2×10^{-4} nm^2/s when c_R is assumed to be 6% as demonstrated as the manganese concentration in Mn(II) doped CdSe quantum dots at equilibrium at corresponding equivalent ratio of selenium precursor to CdSe (1:1) at 24 h reaction time reported by Barrows and coworkers.[33] Particles with high manganese content was also found in the doped nanowire samples from all aliquots. Their representative TEM image is shown in Figure 3.5. The particles were later confirmed as MnO particles by TEM-EDS and PXRD measurements. Figure 3.6 shows PXRD patterns of the 1-h, 2-h, and 4-h Mn(II)CdSe nanowire samples as well as a CdSe nanowire sample. The PXRD patterns indicates that crystal structure of the doped samples remains the same as that of the CdSe nanowire sample. The PXRD patterns suggest that the crystal structure of the doped and intrinsic

nanowires is primarily wurtzite; stacking faults and zincblende phases can potentially be present in the samples. The enhancement of $(002)_w$, $(111)_z$, $(101)_w$, $(103)_w$, $(112)_w$, and $(311)_z$ peaks from the doped sample as compared to the CdSe nanowire sample suggest that the doping reaction may be accompanied by a reduction in defects in nanowire crystal, which is possibly caused by annealing under the doping temperature (300 °C). Furthermore, peaks attributed to cubic MnO appear in the PXRD patterns of the doped nanowires samples, confirming the present of MnO particle as a contaminant in the doped samples. XPS was used to investigate the manganese content on the surficial layer of the doped nanowires and the oxidation state of the manganese species in the doped sample. An XPS survey scan and high-resolution core level XPS spectra of the doped nanowires from the 4-h aliquot shown in Figure 3.7 confirms the present of manganese species in the doped nanowire sample. A XPS data of the sample is summarized in Table 3.1. The high-resolution spectra show peaks attributed by Mn^{2+} (doublet Mn 2p) at 641.1eV and 652.0 eV, cadmium species (doublet Cd 3d) at 404.8 and 411.5 eV, and selenium species (doublet Se 3d) at 53.5 and 54.2 eV. Assuming that the doped nanowires contain manganese, cadmium, and selenium, the manganese atomic percentage is calculated from the deconvoluted peaks to be 6.3%, which is higher than the manganese atomic percentage obtained from TEM-EDS measurements. There are two possible reasons supporting this result. First, XPS measurement probes relative atomic contents on the surface of the samples (from the surface to approximately 10 nm beneath the surface). In nanocrystal diffusion doping mechanism, a dopant diffuses from surfaces of a nanocrystal creating a concentration gradient of the dopants. This results in a higher dopant concentration at the surface layers as compared to the core layers in the nanocrystal before the doping process

reaches its equilibrium. Mn(II) doped CdSe nanocrystals with 6% of manganese atomic percentage can be achieved at equilibrium via nanocrystal diffusion mechanism as mention above. The highest concentration of manganese in Mn(II) doped CdSe nanowires reported here (2.3% as shown in Figure 3.4) suggests that the doping process does not reach the equilibrium point, and thus the dopant concentration gradient is observed via the XPS measurements. Another reason causing manganese atomic percentage obtained from the XPS measurements to be higher than that from the TEM-EDS measurements is the MnO particles contaminated in the doped nanowire samples. The MnO particles were in the TEM and PXRD measurements; the signals from the MnO particles were excluded from the data obtained from TEM-EDS measurement by selectively detecting an area that does not contain MnO particles. A high-resolution XPS spectrum scanning from 631 to 668 eV (Figure 3.7 B) shows a deconvoluted peaks attributed by Mn $2p_{3/2}$ and $2p_{1/2}$ at 641.1 and 652.0 eV. Mn doped CdSe nanowire prepared by doping during growth method through gas phase reported by Chen and coworkers also show the Mn $2p_{3/2}$ and Mn $2p_{1/2}$ peaks at 641.5 and 653.8 eV, respectively.[3] The difference of the Mn $2p_{1/2}$ peak positions is caused by the overlapping of Mn $2p_{1/2}$ and Cd $p_{1/2}$ peaks leading to the difficulty in resolving the Mn $2p_{1/2}$ peak. Nevertheless, the peak positions of Mn $2p_{3/2}$ suggests the success of the manganese doping reaction by revealing the presence of Mn-Se bond as well as the absent of elemental manganese Mn-Mn, which shows Mn 2p at 638.7 eV.[35] The results from TEM, TEM-EDS, PXRD, and XPS measurements discussed above indicate that Mn(II)CdSe nanowires with different manganese contents were successfully prepared from colloidal CdSe nanowires via diffusion doping mechanism.

The effect of manganese doping on magnetic property of Mn(II) doped CdSe nanowires. The doped samples from 2-h and 4-h aliquots show ferromagnetism at low temperature (25K) as shown in Figure 3.8. The saturated magnetization per sample mass of the doped nanowires increases with increasing doping reaction time, which is proportional to the Mn^{2+} content in the Mn(II) doped CdSe nanowires, suggesting that the magnetization per sample mass increases with increasing Mn^{2+} content in the doped nanowires at this low manganese content range. Mn^{2+}, which has 5 unpaired electrons, is a source of magnetic moment in the Mn(II)CdSe nanowires. Therefore, increasing Mn^{2+} concentration in the Mn(II)CdSe nanowires would increase number of component with magnetic moment in the material, and thus magnetization. Furthermore, temperature-dependent magnetizations of the doped nanowires from 1-h, 2-h, and 4-h aliquots and CdSe nanowire are shown in Figure 3.9. Above a critical temperature called Curie temperature, T_C, intrinsic magnetic moments arising from magnetic components in a material are randomly oriented causing zero net magnetic moment in the material. These distributions of intrinsic magnetic moment orientations can be aligned with the direction of external magnetic field. Under T_C, majority of the intrinsic magnetic moment spontaneously aligned in one direction (a major magnetic domain) increasing the net magnetic moment of the material. The present of an external magnetic field can increase the size of the magnetic domain, and the thus net magnetic moment of the material. The temperature-dependent magnetization measurements were conducted in two modes: field cool warm (fcw) and zero field cool (zfc). The measurements were started by cooling down the samples with (fcw) and without (zfc) applying external magnetic field from room temperature to 2K. Then the magnetizations of the samples were collected while the temperature of the sample

were increased with applied magnetic field of 100 Oe. In an fcw mode measurement, the size of the major magnetic domain of a sample is larger as compared to that from a corresponding zfc mode measurement due to the applied external magnetic field during the cooling process in fcw mode. Therefore, the fcw mode measurement on each of the doped nanowire samples shows higher magnetization as compared to that from zfc mode. The samples from 2-h and 4-h aliquots show the same T_C of 40K. While the magnetization per sample mass of the sample form 4-h aliquot is higher than that from 2-h aliquots. From the zfc mode measurements, the samples from 2-h and 4-h aliquots exhibit superparamagnetic behavior at low temperature, which is found in nanometer scale ferromagnetic materials;[3,36–39] below the T_C, the values of magnetization per sample mass of those samples increase with decreasing temperature to a maximum point at a critical temperature called blocking temperature, T_B, at 36K, then decrease with decreasing temperature. Below T_B, the divergence of zfc and fcw curves indicates ferromagnetic behavior of the samples. Between T_C and T_B, the complete overlapping of two curves implies the paramagnetic – like behavior. These features indicates superparamagnetic behavior of the materials. Superparamagnetic behavior was also observed in Mn(II) doped CdSe nanowires prepared by doping during growth method.[3] The agreement of temperature-dependent magnetization features of those nanowires confirms the success of manganese doping via nanocrystal diffusion doping presented in this chapter. The values of magnetization per sample mass start to rise again at lower temperature (at 26 K for 2-h sample and at 25 K for 4-h sample). The increase in the magnetization is possibly caused by paramagnetic contribution from a residue of isolated Mn^{2+} ions present in the samples. Although MnO particle in hexagonal phase exhibits paramagnetic behavior at low temperature,[40] the MnO particle contaminated

in the samples is in cubic phase, which was reported as an antiferromagnetic material,[41] and thus not a source of the increase in magnetization at the low temperature region in the zfc mode measurement. It is worth mentioning that Mn^{2+} at high-spin state has a theoretical mass magnetization of 601 emu/g since high-spin Mn^{2+} has spin-only magnetic moment of 5.92 B.M/ion (5.49×10^{-20} emu/ion).

The effect of ligand exchange on magnetic property of Mn(II) doped CdSe nanowires. In an attempt to obtain Mn(II) doped CdSe nanowires without contaminated MnO particles, SA was replaced by OA in order to increase the solubility of the nanowires in organic solvents. The higher solubility was expected to assist separation between the doped nanowires and MnO particles through precipitation/redissolution methods. The surfactant replacement did not help to achieve the separation. Additionally, the manganese content in these doped nanowires is less as compared to the doped nanowires prepared by the reaction using SA as a surfactant even though higher equivalent of TBPSe to CdSe ratio was used in the reaction using OA as a surfactant; the higher equivalent of TBPSe to CdSe ratio is supposed to increase the manganese content in the nanowires.[33] Figure 3.10 shows a plot of manganese atomic percentage in the doped nanowires as a function of nanowire radius at three doping reaction times. The plot indicates that the manganese content in the doped nanowires was saturated since 2 h of doping reaction time. The highest manganese content is around 1.6%. Another attempt to remove MnO from the dope nanowires is to use a ligand exchange reaction. L-cysteine was used to exchange with the long-chain ligands on the doped nanowires because it was reported as a strong ligand to CdSe nanocrystal surfaces.[42] The L-cysteine-capped doped nanowires was transferred from an organic solution to an aqueous solution after the ligand exchange reaction was completed.

This ligand exchange reaction was expected to separate the doped nanowires from the MnO particles. The ligand exchange reaction was found to have an effect on magnetic properties of the doped nanowires as shown in Figure 3.11. T_C and T_B of the L-cysteine-capped doped nanowires obtained from temperature dependent magnetization measurements in fcw and zfc modes at 100 Oe (15 K and 13 K, respectively) are smaller than the T_C and T_B of the doped nanowires at 100 Oe that were not gone through the ligand exchange reaction (40 K and 36 K, respectively). It is worth noting that the irreversible temperature, at which the magnetizations measured in fcw and zfc start to diverge, of the L-cysteine-capped doped nanowires from 2-h, 4-h, and 8-h aliquots are 28, 42, and 44 K, respectively, while the irreversible temperature of the nanowire samples without ligand exchange from 1-h, 2-h, and 4-h aliquots are 5, 43, and 43 K, respectively. The effect of ligand identity on magnetic property was also reported in Mn doped nanocrystal.[43] Though the manganese concentrations in the doped nanowire samples collected at different doping reaction time are not significantly different as shown in Figure 3.10, the magnitude of magnetization per sample mass of each samples through entire temperature range measured in both fcw and zfc modes in this are different (4h>8h>2h). This might be caused by the annealing effect during the doping reaction. Annealing was reported to change magnetic property of Mn(II) doped CdSe quantum dots by arranging the position of the Mn^{2+} in the doped CdSe crystals.[37] The PXRD patterns of the doped nanowire samples at various doping duration, shown in Figure 3.12, indicate that MnO particles were removed from the Mn(II) CdSe nanowires via the ligand exchange reaction. Without MnO particles, the doped nanowire samples from 2-h, 4-h, and 8-h aliquots still show the increase in magnetization at low temperature starting at 13, 11, and 12 K toward the lower temperatures. This remaining of

this features after MnO particles are removed from the samples suggests that this feature is caused at least in part by other components that are distinct from the MnO particles.

3.4 CONCLUSIONS

The novel method for preparing dilute magnetic semiconductor nanowires was demonstrated in this chapter. Mn^{2+} can be introduced into colloidal CdSe nanowire crystal via nanocrystal diffusion doping mechanism in a controlled fashion yielding colloidal Mn(II) doped CdSe nanowires exhibiting superparamagnetic behavior at low temperature. Moreover, it was demonstrated that the doping content can be controlled by the nanowire radial dimension and doping reaction time and a surfactant used in the doping reaction. Moreover, the effect of ligand identity on magnetic behavior of Mn(II) doped CdSe nanowires was demonstrated. These discoveries provide knowledge that will aid in improving doping technology in semiconductor nanowires.

Table 3.1 Summary of XPS data of the Mn(II) doped CdSe nanowires from 4h aliquot.

Element	Peak	Binding Energy (eV)[a]	Raw Area (CPS)[b]	Relative Atomic Sensitivity[c]	Atomic Percentage[d]
Mn	Mn $2p_{3/2}$	641.1	1100.6	2.659	0.88
	Mn $2p_{1/2}$	652.0			
Cd	Cd $3d_{5/2}$	404.8	22247.2	6.623	7.24
	Cd $3d_{3/2}$	411.5			
Se	Se $3d_{5/2}$	53.5	2286.6	0.853	5.77
	Se $3d_{3/2}$	54.2			

[a]Binding energy is extracted from Gaussian-Lorentzian fit of the data using XPSPEAK 4.1 software.
[b]Raw peak area is obtained from signal above background using XPSPEAK 4.1 software.
[c]Relative atomic sensitivity is provided by XPSPEAK 4.1 software.
[d]Atomic percentage is calculated using XPSPEAK 4.1 software. Numbers do not add to 100% because of contributions from carbon and oxygen signals (not shown).

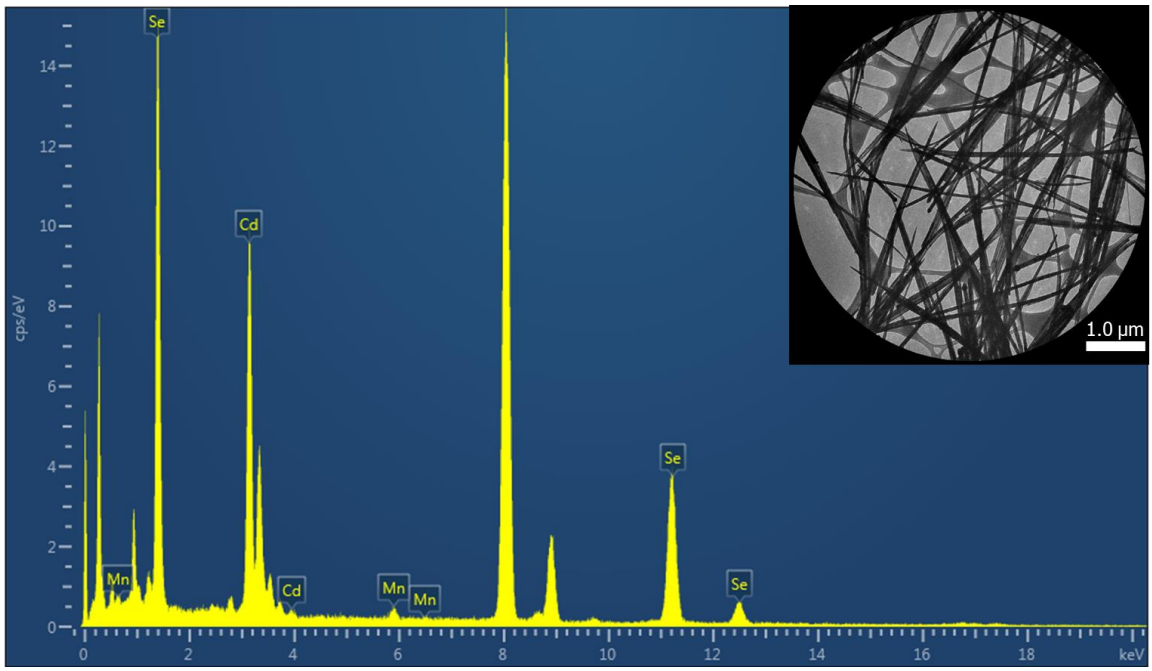

Figure 3.1 A representative EDS spectrum of the Mn(II) doped CdSe nanowires from 4h aliquot. Inset: the TEM image of the spot where the EDS spectrum is measured.

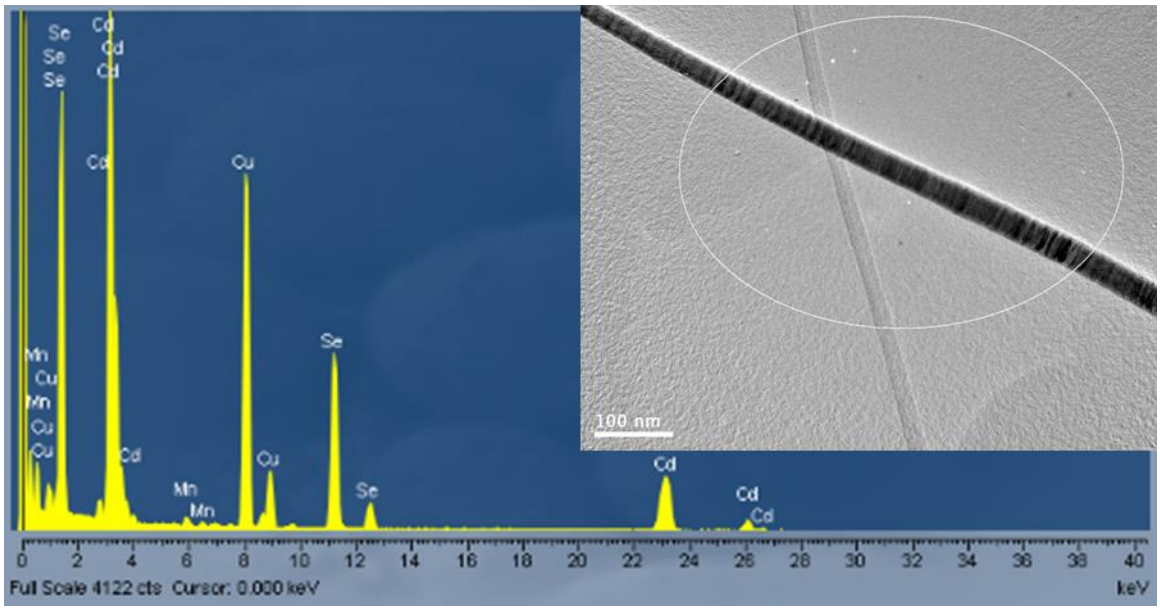

Figure 3.2 A representative EDS spectrum of a single Mn(II) doped CdSe nanowires collected from 4h aliquot. Inset: the TEM image of the corresponding doped nanowires; the circle specifies the spot where the EDS spectrum is measured.

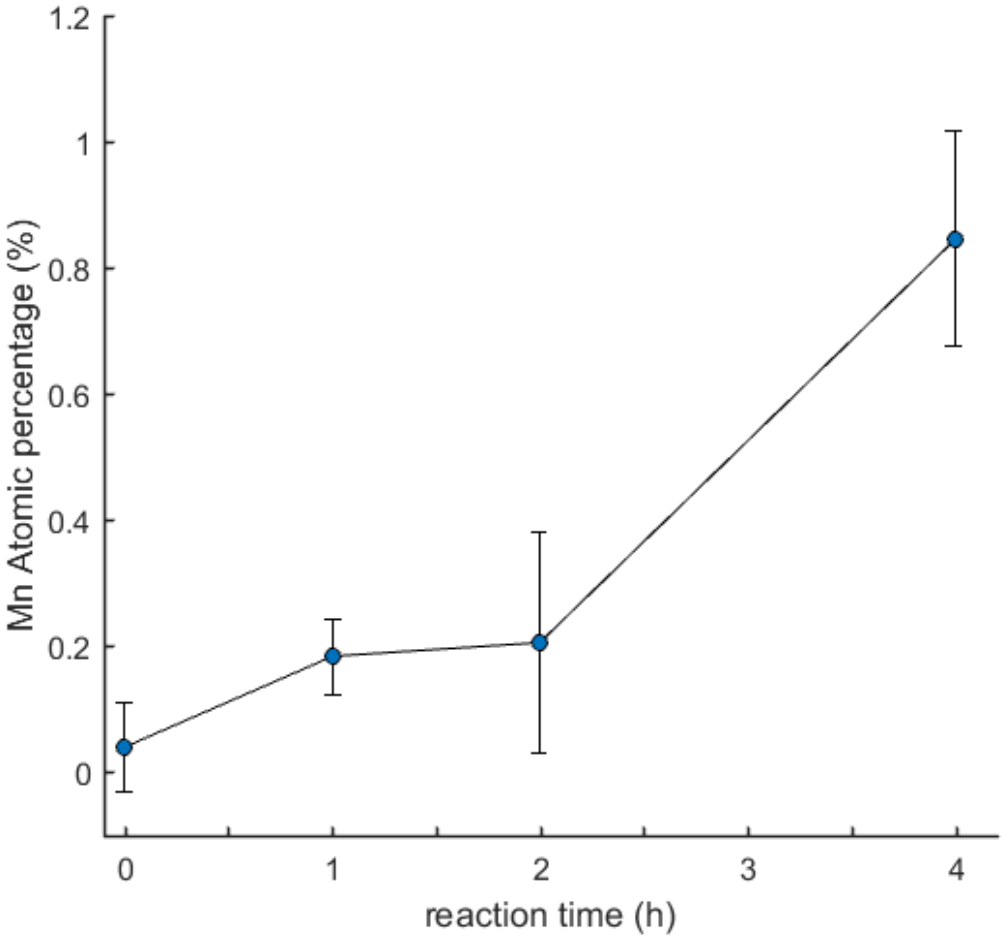

Figure 3.3 Manganese atomic percentage of Mn(II) doped CdSe nanowire samples collected from the diffusion doping reaction at 1, 2, and 4 hours compared to CdSe nanowire sample (0 h). The ammonic percentage data were obtained from TEM-EDS measurements of ensemble nanowire samples. The solid lines are guides to the eyes. The error bars represent sample standard deviations of the data.

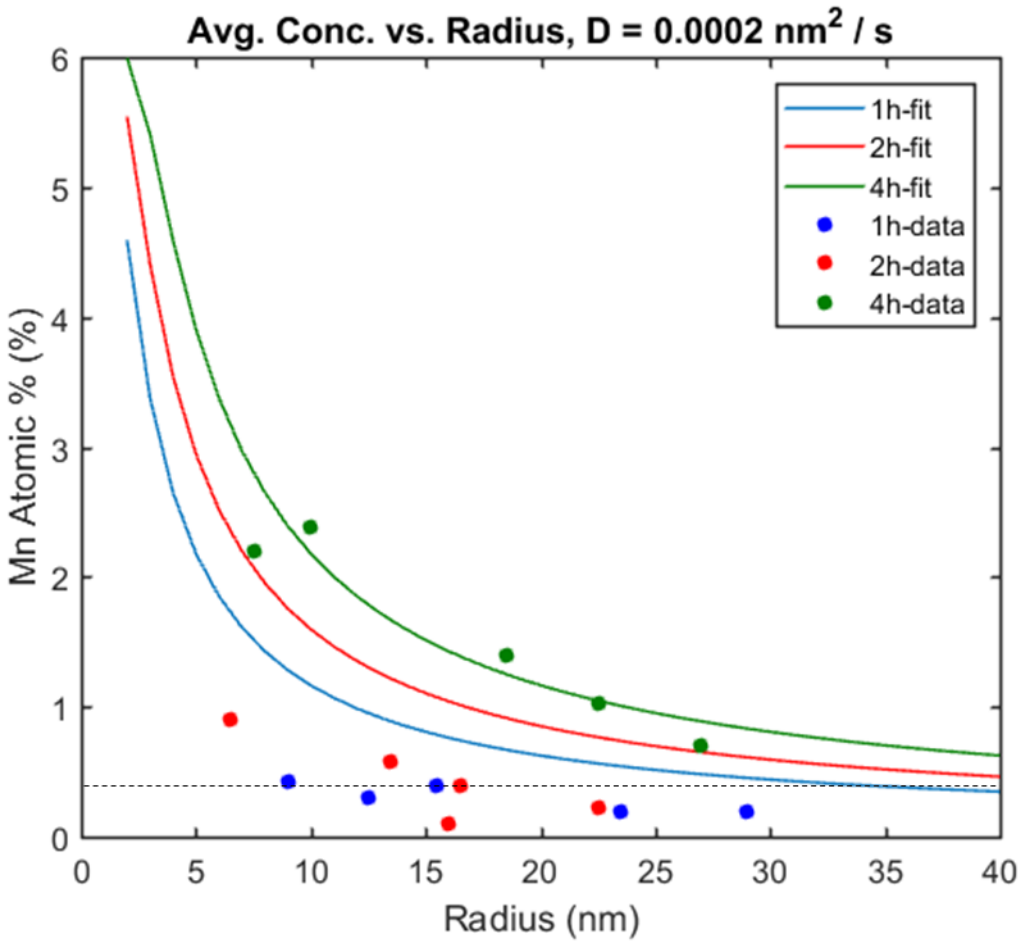

Figure 3.4 Mn atomic percentage vs radius of the doped nanowires from 1h (blue circle), 2h (red circle), and 4h (green circle) aliquots. Solid lines are generated by the diffusion in cylindrical model explained in the text to compare the data from 1h (blue), 2h (red), and 4h (green) aliquot. The black dash line indicates detection limit of the EDS measurement. The detection limit was indicated by the detectability of signals to the baseline in the corresponding EDS spectra. At atomic percentage below 0.40%, Mn peak in EDS spectrum is indistinguishable from background.

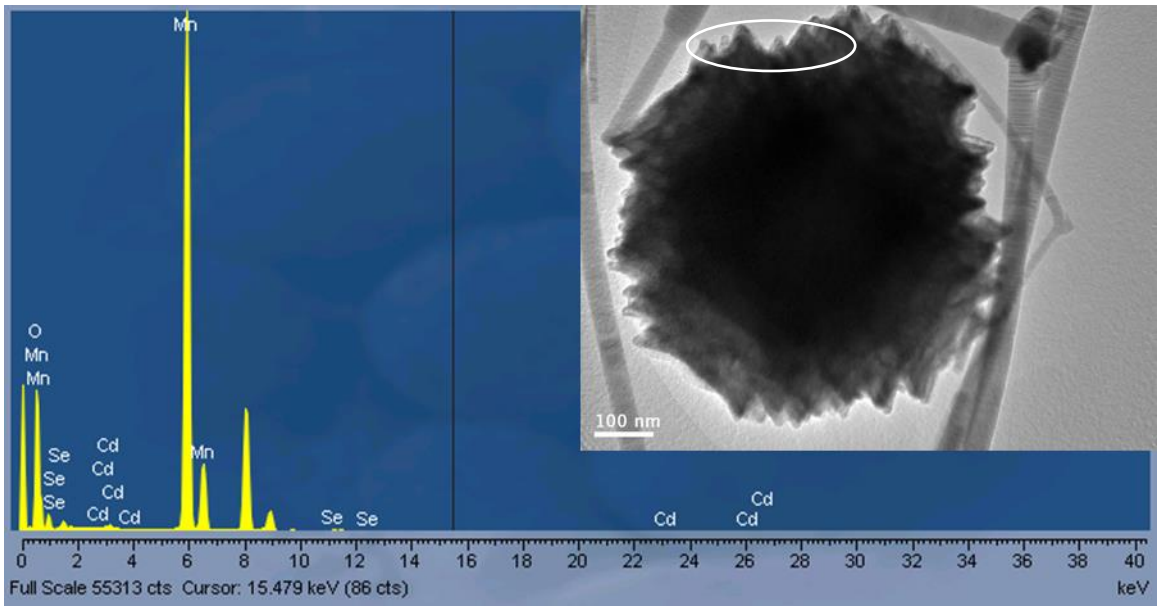

Figure 3.5 A representative EDS spectrum of a MnO particle contaminated in a doped nanowire sample. Inset: the TEM image of the corresponding MnO particle; the circle specifies the spot where the EDS spectrum is measured.

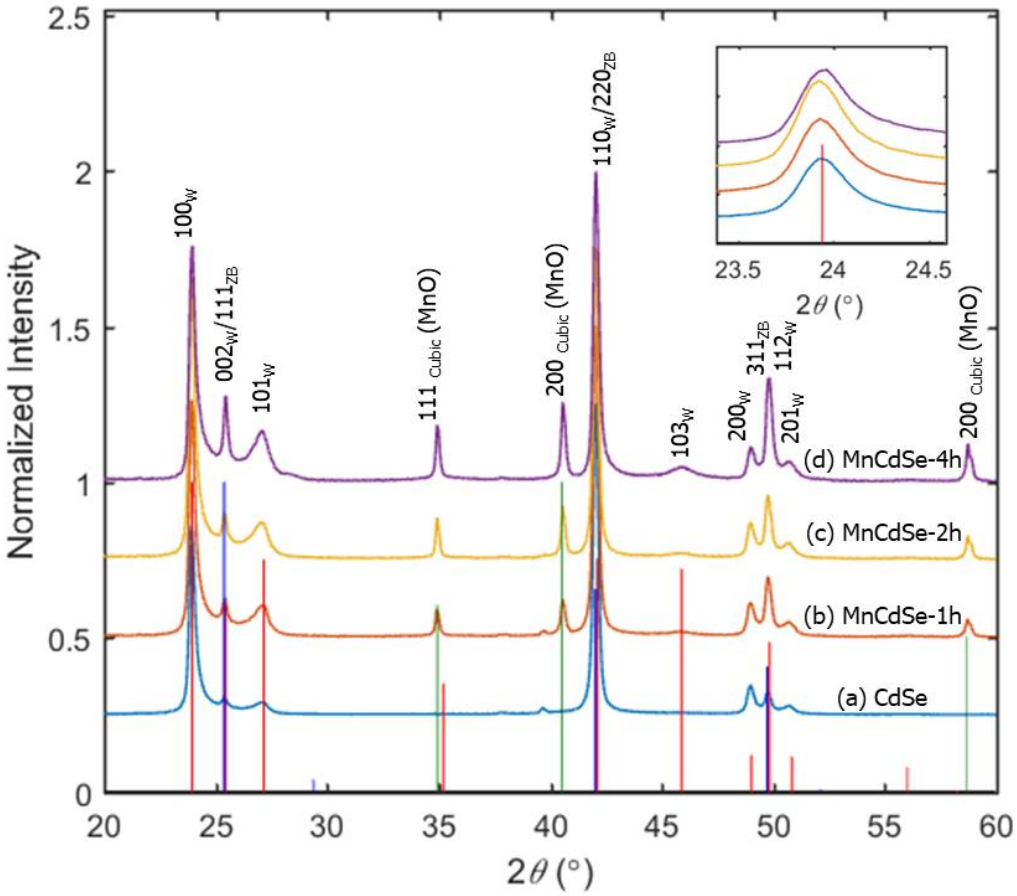

Figure 3.6 PXRD patterns of (a) colloidal CdSe nanowires, (b) Mn(II)CdSe nanowires collected from 1h aliquot, (c) Mn(II)CdSe nanowires collected from 2h aliquot, and (d) Mn(II)CdSe nanowires collected from 4h aliquot. Stick patterns of wurtzite phase of CdSe (red), zincblende phase of CdSe (blue) and cubic MnO (green) are presented for comparison. The measurement was conducted on a zero-background stage leading to a small shift of the PXRD patterns between samples. To compensate the shift, the PXRD pattern of CdSe nanowire sample is adjusted to align to the ICSD 100_W peak position, while those of Mn(II) doped nanowire samples are shifted to align to ICSD 200_{cubic} (MnO), assuming that MnO diffraction angles are the same in all samples.

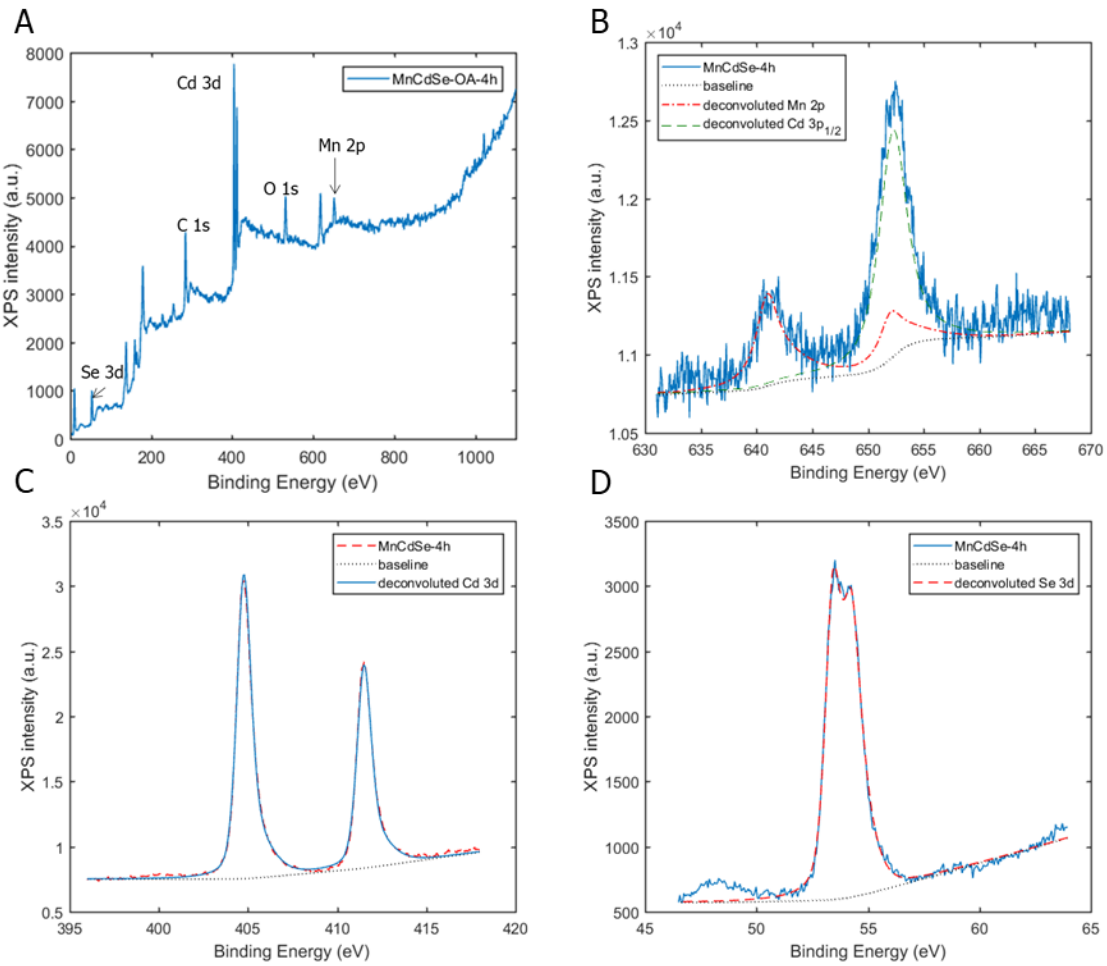

Figure 3.7 XPS spectra of Mn(II) doped CdSe nanowires from the 4-h aliquot: (A) survey scan and (B-D) high resolution core level spectra. Peak deconvolutions in panel B, C, and, D show the presence of Mn 2p, Cd 3D, and Se 3D peaks, respectively.

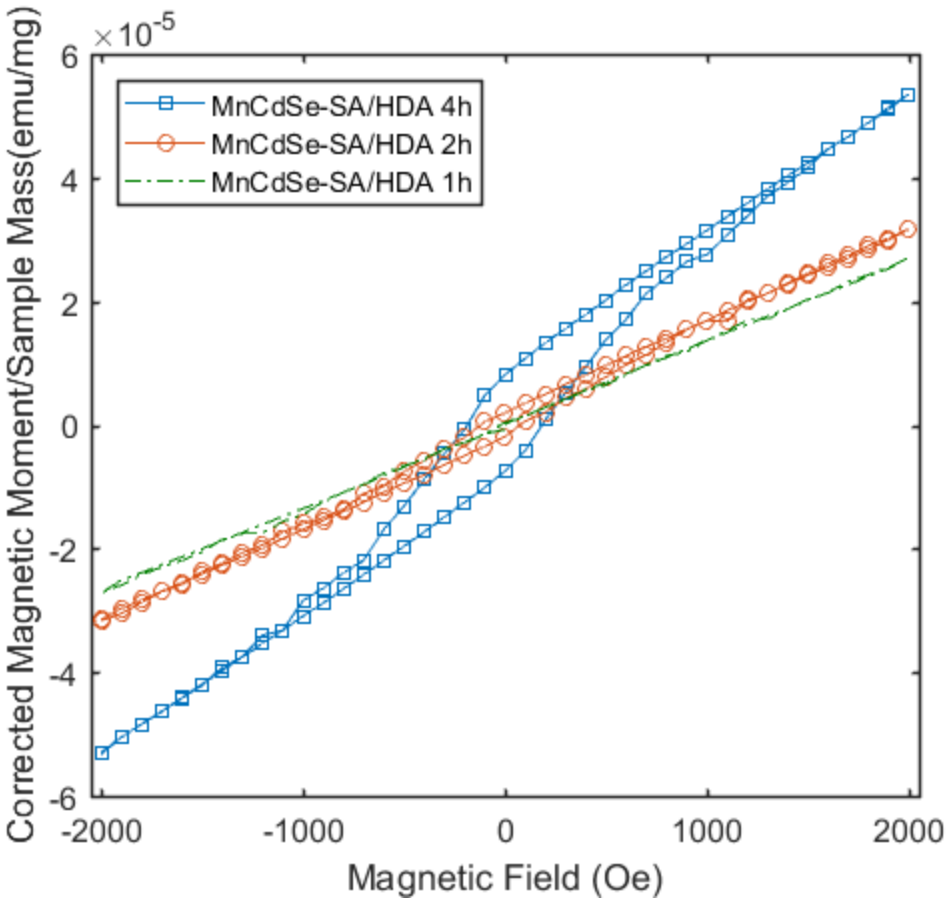

Figure 3.8 M-H loops of manganese doped CdSe nanowires from 1h (green dot), 2h (orange circle), and 4h (blue square) aliquots measured at 25K.

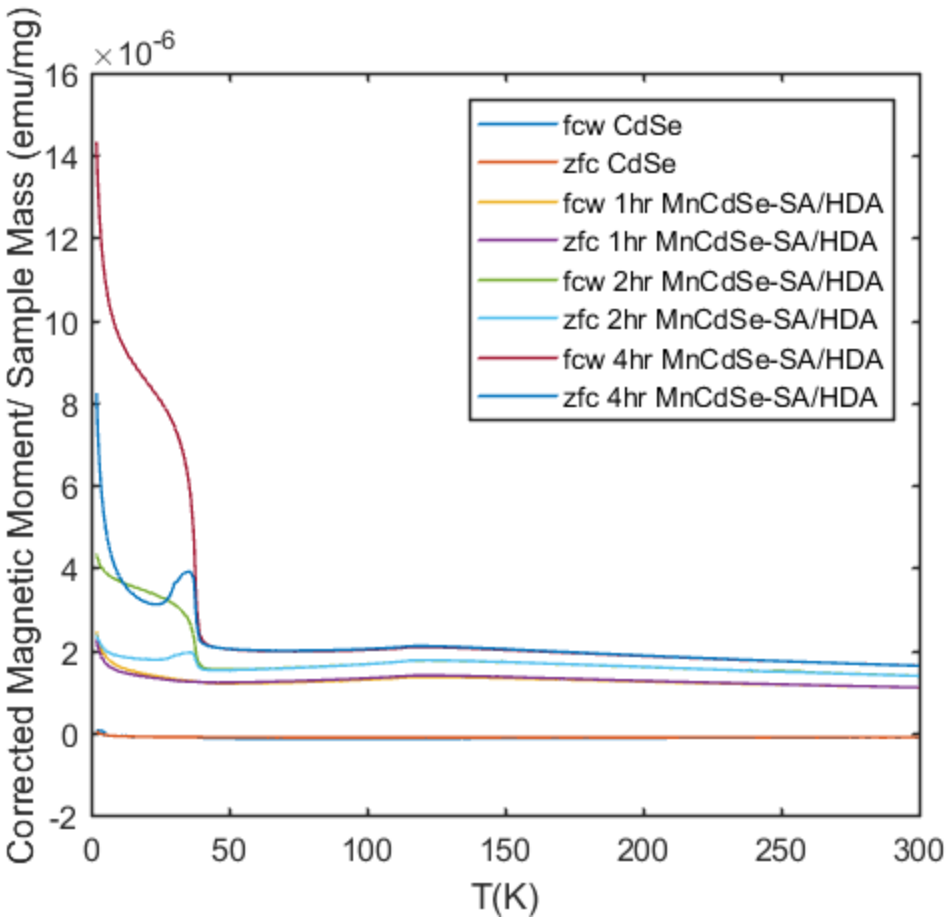

Figure 3.9 Temperature-dependent magnetization in fcw and zfc modes conducted at 100 Oe of Mn-doped CdSe nanowires from 1h, 2h, and 4h aliquots.

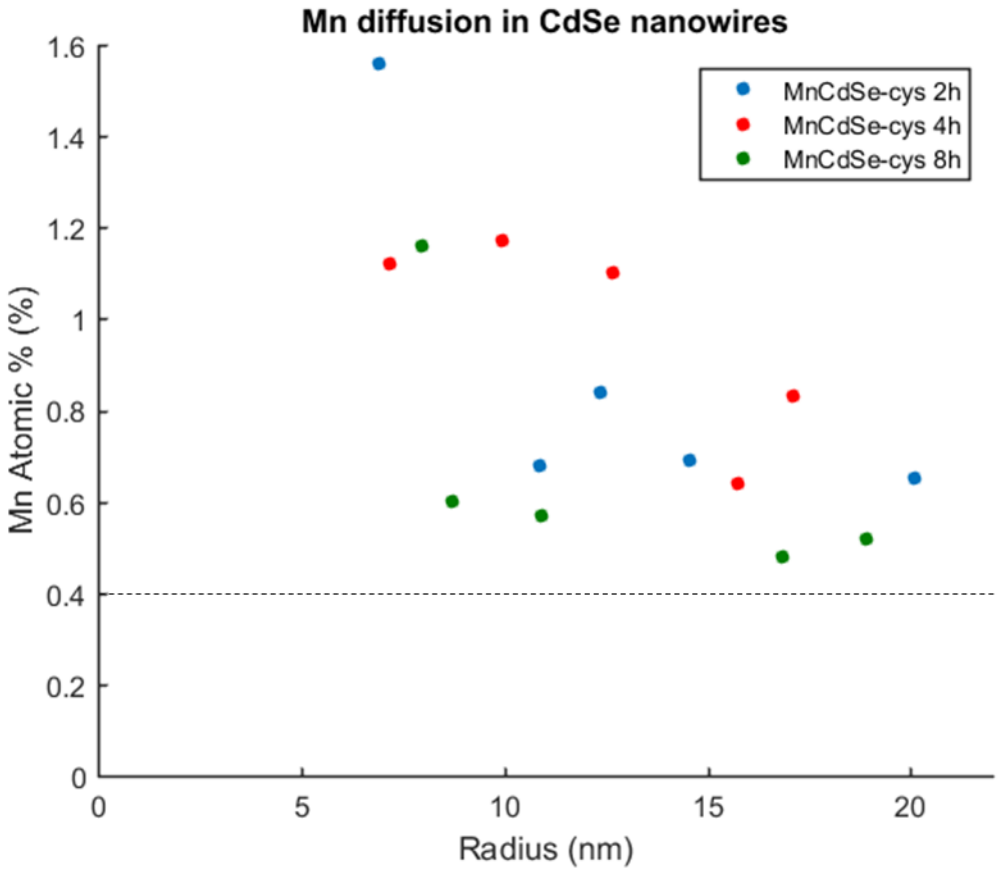

Figure 3.10 Mn atomic percentage vs radius of the Mn(II) doped CdSe nanowires prepared by replacing SA with OA from 2h (blue circle), 4h (red circle), and 8h (green circle) aliquots. The black dash line indicates detection limit of the EDS measurement. The detection limit was indicated by the detectability of signals to the baseline in the corresponding EDS spectra. At atomic percentage below 0.40%, Mn peak in EDS spectrum is indistinguishable from background.

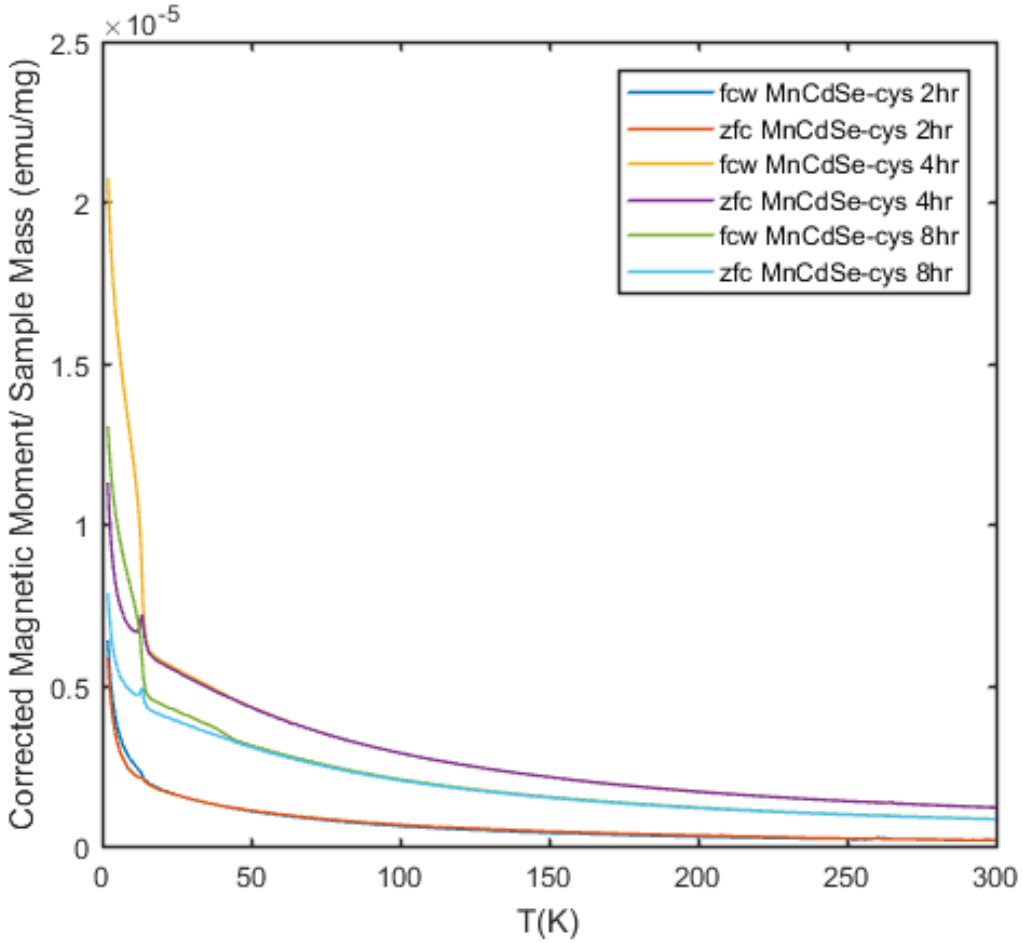

Figure 3.11 Temperature-dependent magnetization in fcw and zfc modes conducted at 100 Oe of L-cysteine-capped Mn(II) doped CdSe nanowires from 2h, 4h, and 8h aliquots.

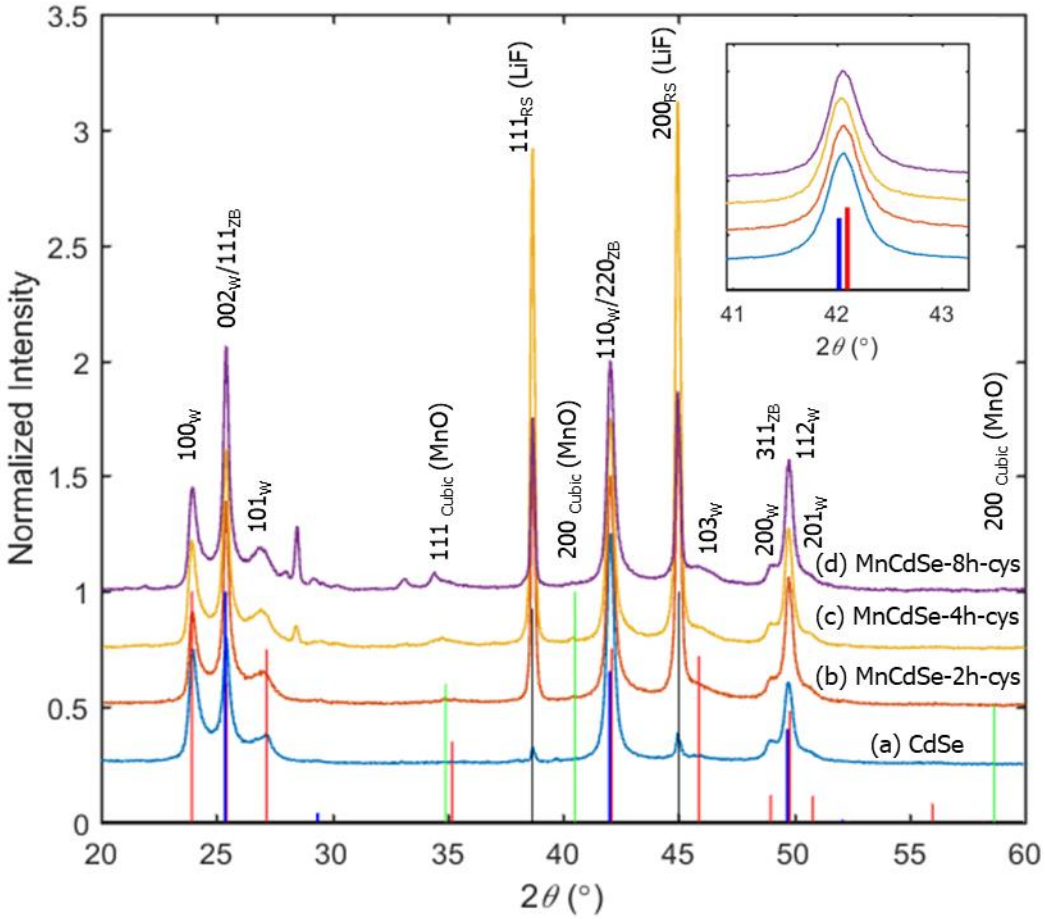

Figure 3.12 PXRD patterns of (a) colloidal CdSe nanowires, (b-d) Mn(II)CdSe nanowires after cysteine ligand exchange collected from (b) 2h aliquot, (c) 4h aliquot, and (d) 8h aliquot. Stick patterns of wurtzite phase of CdSe (red), zincblende phase of CdSe (blue), cubic phase of MnO (green), and rock salt phase of LiF (black) are presented for comparison. The measurement was conducted on a zero-background stage leading to a shift of a PXRD pattern, thus LiF was added to the samples to provide reference peaks.

CHAPTER 4

CONTROLLING ELECTRONIC PROPERTIES OF CDSE NANOWIRES VIA SEQUENTIAL DIFFUSION DOPING OF MANGANESE AND CATION EXCHANGE WITH INDIUM

4.1 INTRODUCTION

Tuning electronic property allows semiconductors to be fundamental materials for many applications, such as electronics, photovoltaics, and optoelectronics. For example, to be used as a component in electronic device fabrications, charge carriers are introduced into intrinsic semiconductors generating p-type or n-type semiconductors. Doping has been used as a primary method to control electronic properties of semiconductors by introducing charge carriers to the semiconductors. In semiconductor industry, doping is accomplished by introducing proper impurity atoms, so called dopants, into a semiconductor crystal. Doping technology for bulk semiconductors is mature; diffusion and ion implantation are primarily techniques employed for doping in bulk materials.

In the past two decades, semiconductor nanostructures, e.g. semiconductor nanocrystals, have been extensively studied to be employed as components in electronic devices due to their potential to provide more compact, more efficient, and more cost-effective electronic devices. Similar to bulk semiconductors, doping is necessary to enable semiconductor nanostructures as electronic device components. However, doping techniques used for bulk semiconductor are not suitable for nanoscale semiconductor, such

as semiconductor nanocrystals. Several electronic doping techniques has been invented to dope semiconductor nanocrystal.[44,45] Semiconductor nanowires are one of the most extensively studied semiconductor nanocrystals due to their potential for many applications.[1,2] Several prototype devices for those applications have been achieved.[46–48] Their unique morphology allows for superior advantages in electronic device application as compared to other nanostructures such as quantum dots and nanorods as well as conventional planar semiconductor electronics. Highly efficient methods to integrate nanowire into electronic devices has been demonstrated. Additionally, the nanowire structure allows for gate-all-around architectures leading to highly efficient control of charge carriers in channels of nanowire field-effect transistors.[49] Despite its great potential for practical use, the knowledge on semiconductor nanowire doping is limited. CdSe nanowire, a direct band gap semiconductor nanowire with fluorescence emission in visible range, is a promising candidate for many applications due to its unique characteristics. In bulk CdSe, CdSe film, and CdSe quantum dot film, indium have been used to tune their properties as an n-type dopant.[50–55] In free standing CdSe nanowires, doping during growth has been demonstrated to introduce indium to a CdSe crystal creating n-type semiconductor nanowire.[5] This process was done by introducing an indium precursor to VLS growth system of CdSe nanowires. Despite their great potential in being integrated into electronic devices, indium doping of colloidal CdSe nanowires has not been achieved. This chapter presents a novel approach to doped indium to colloidal CdSe nanowires in a controlled fashion and the effect of the doping on electronic property of the nanowires. This approach, which is modified from an approach used to introduce indium into CdSe colloidal quantum dots, contains two steps.[56] First, Mn^{2+} is doped into CdSe nanowires via nanocrystal

diffusion doping method, which is explained in the previous chapter. Then the Mn^{2+} in the doped CdSe nanowires, is replaced with In^{3+} via cation exchange. By controlling the concentration of indium in the In(III) doped CdSe nanowires, the electronic properties of the doped nanowires can be tuned.

4.2 EXPERIMENTAL SECTION

Chemicals. Manganese(II) acetate tetrahydrate ($Mn(II)(OAc)_2 \cdot 4H_2O$, 99.999%) and selenium shot (Se, 99.999%) were obtained from Alfa Aesar. 1-Hexadecylamine (HDA, 90%) and 1-octadecene (ODE, 99%) were obtained from ACROS ORGANICS. Tri-n-butylphosphine (TBP, 99%) and indium(III) acetate ($In(III)(OAc)_3$. 99.99%) were obtained from STREM CHEMICALS. Oleic acid (OA, 99%) was obtained from BEANTOWN CHEMICAL. Stearic acid (SA, ≥98.0%) was obtained from TCI America. Acetonitrile (≥99.5%) was obtained from Sigma-Aldrich. Toluene (99.9%) was obtained from Fisher Scientific.

Preparation of In doped CdSe nanowires. InCdSe nanowires were prepared using a modified literature method.[56] Briefly, in a nitrogen atmosphere glovebox, 2.13 M TBPSe was prepared by adding 11.4 mL of TBP to 1.727g of selenium pellets. The mixture was then stirred at room temperature until the selenium pellets are completely dissolved. $In(III)(OA)_3$ was prepared separately by loading 63 mg $In(III)(OAc)_3$, 0.8808 g of OA and 6.5 g of ODE into a septum-capped 50 mL round bottom flask. The mixture was then dried by heating at 115 ºC under vacuum for 1 h. After that, it was heated to 280 ºC under nitrogen atmosphere until the mixture is clear before cooling the mixture to room. In a nitrogen atmosphere glovebox, anhydrous ODE was added into the mixture to the total volume of 10.0 mL to obtain 21.7 mM $In(III)(OA)_3$. Separately, 0.4672 g of HDA, 0.2348 g of SA,

and 6 mL of ODE were loaded into a septum-capped 50 mL round bottom flask, and then heated at 110 ºC under vacuum for 30 min to dry the mixture. Under nitrogen atmosphere, 14.9 mg of $Mn(OAc_2)\cdot 4H_2O$ was then added into the reaction mixture against nitrogen overpressure. After that, the reaction mixture was kept under vacuum for 1 h to remove acetic acid and water before heating the mixture to 300 ºC under nitrogen atmosphere. In the glovebox, 11.6 mg of CdSe nanowire (12.1 mg of CdSe according to TGA, 0.0606 mmol) in 2 mL of ODE and 28 (14, or 55) μL (0.0596 (0.0298, or 1.17) mmol) of 2.13 M TBPSe solution were mixed. The mixture was then injected into the reaction mixture. The reaction mixture was kept at 300 ºC under nitrogen atmosphere for 4 h before injecting 1.4 mL of 21.7 mM $In(III)(OA)_3$ reducing the reaction temperature to 280 ºC. The reaction mixture was kept at 280 ºC under nitrogen atmosphere for 10 min before cooling it down to room temperature; toluene was injected into the reaction mixture at 80 ºC to prevent solidification. The reaction mixture was purified by precipitation/redissolution technique with toluene/acetonitrile mixture and pure toluene. The nanowires product was suspended in toluene before further characterizations.

Electrode fabrication. Devices were fabricated on a heavily p-doped Si wafer with 285 nm dry thermal oxide obtained from Addison Engineering, Inc. First, the Si wafer was rinsed thoroughly with acetone, isopropyl alcohol, and DI water, and then immediately dried with a nitrogen stream. The wafer was then heated at 180 ºC for 5 min to remove water on the SiO_2 surface. Metal contacts on the SiO_2 surface were defined by photolithography and electron-beam evaporation of titanium/gold (30 nm/70 nm) at 3×10^6 torr.

Nanowire FET device fabrication. First, a nanowire solution was prepared by mixing a stock solution of nanowires suspended in toluene (1-5 mg/mL) and ODE at a 2:1 (v/v) ratio. Then the nanowires were deposited to bridge between two metal electrodes via dielectrophoretic alignment in a nitrogen atmosphere glovebox; the nanowire solution was dropped between the electrodes on the device fabricated by the method explained above under a DC electric field (2.5×10^6 V/m) between the electrodes, and then the electric field was kept constant for 5 min. After that, the device was rinsed with toluene, and dried by wicking the remaining toluene. The device was left in the glovebox at least 10 min before electronic measurements.

Physical Characterization. TEM samples were prepared by dropping a dilute solution of colloidal suspension of nanowires in toluene or DI water on 200 mesh copper grid with a lacey carbon film (Ted Pella, Inc.) and allowing this substrate to dry under vacuum. TEM images of nanowires were obtained on a Hitachi HT7800 TEM, 100 kV microscope. EDS spectra of ensemble nanowires were collected using Hitachi HT7800 TEM equipped with a silicon drift detector (Oxford Instruments X-Max^N-80T). Relative atomic concentrations were extracted from the EDS spectra using Aztec software package version 3.3 and from an ensemble elemental analysis using Finnigan ELEMENT XR double focusing magnetic sector field inductively coupled plasma-mass spectrometer (SF-ICP-MS) with Rh as internal standards. 0.2 ml/min Micromist U-series nebulizer (GE, Australia), quartz torch and injector (Thermo Fisher Scientific, USA) were used for sample introduction. The samples analyzed by ICP-MS were prepared by dissolving dried nanowire samples in aqua regia at 70ºC overnight. PXRD data were collected from dried nanowire powders on a Zero Background holder using a Bruker D2 Phaser with

LYNXEYE silicon strip detector. Lithium fluoride (LiF) was mixed into some nanowire powder samples by grinding in a mortar for < 30 s to provide reference peaks X-ray photoelectron spectroscopy measurements were performed using a Kratos AXIS Ultra DLD XPS system, with a monochromatic Al Kα source, operated at 15 keV and 150W and a hemispherical energy analyzer. The X-rays were incident at an angle of 45° with respect to the surface normal and analysis was performed at a pressure below 1x10-9mbar. High resolution core level spectra were measured with a pass energy of 40 eV, and survey scans were measured with a pass energy of 160 eV. The analysis of the XPS spectra was performed with XPSPEAK 4.1 software. Scanning electron microscopy (SEM) images were collected directly from nanowire FET devices using Zeiss Ultra plus FESEM.

Electronic characterization. All measurements were performed in a nitrogen glovebox under dark. Transfer characteristics were collected using the following instruments. Gate biases were swept linearly at 14.6 V/s using a 2 MHz function generator (BK Precision 4010A) while a constant drain voltage was supplied by a DC power supply (Keithley 2636A SourceMeter). Drain current was amplified by a current amplifier (1211 DL-Instruments) and collected by analog discovery. Gate dependent-*IV* curves were collected by the Keithley 2636A SourceMeter at constant sweeping rate of 2 V/s.

4.3 RESULTS AND DISCUSSION

Preparation of In(III) doped CdSe nanowires via sequential nanocrystal diffusion doping and cation exchange method. In(III) doped CdSe nanowires were prepared using a two-step process. First, Mn(II) doped CdSe nanowires were prepared from colloidal CdSe nanowires via the nanocrystal diffusion doping mechanism described in chapter 3. Then without purification, the Mn^{2+} in the Mn(II) doped CdSe nanowires were

replaced by In^{3+} supplied from $In(III)(OA)_3$ to yield In(III) doped CdSe nanowires CdSe nanowires via a cation exchange mechanism. Three In(III) doped CdSe nanowire samples were prepared by varying the equivalents ratio of TBPSe, a selenium precursor, to CdSe nanowires (0.5, 1, and 2) during the first step ,which Mn(II) doped CdSe nanowires were generated. An equivalent ratio of a selenium precursor to CdSe quantum dots was reported to influence the manganese content in Mn(II) doped CdSe nanowires synthesized via nanocrystal diffusion doping mechanism.[33] Therefore, it was expected to influence the indium content in In(III) doped CdSe nanowires generated from Mn(II) doped CdSe nanowires via a cation exchange mechanism. Although the reaction condition in the second step can possibly allow for doping indium into the CdSe nanowire crystal via nanocrystal diffusion doping mechanism, the reaction time (10 mins) is not sufficient to achieve diffusion doping; kinetics of nanocrystal diffusion doping mechanism is very small as compared to that of cation exchange mechanism, and thus the introduction of indium to the CdSe nanowire crystals was achieved via sequential nanocrystal diffusion doping and cation exchange mechanism instead of nanocrystal diffusion doping mechanism. The indium doping reaction preserves nanowire morphology; the products from the indium doping reactions, regardless of the selenium precursor to CdSe nanowire ratio, retain the nanowire morphology of the CdSe nanowires used as starting materials as demonstrated by a representative TEM image of indium doped CdSe nanowires in Figure 4.1 (inset). EDS spectra of the indium doped CdSe nanowires were collected at several random spots on TEM grids containing indium doped CdSe nanowires in order to confirm the presence of indium and quantify the indium contents in the indium doped CdSe nanowires. Indium ($K\alpha$) peak at 24.21 eV appears in all EDS spectra, as demonstrated in Figure 4.1, indicating

the presence of indium species in the indium doped CdSe nanowires. Additionally, manganese (Kα) peak at 5.90 eV is not observed in any EDS spectrum collected from the indium doped CdSe nanowire samples indicating the completion of manganese species replacement by indium species. An indium atomic percentage in indium doped CdSe nanowires was calculated from indium (Kα) peak at 24.21 eV, cadmium (Kα) peak at 23.17 eV, and selenium (Kα) peak at 11.21 eV. A plot of the indium atomic percentage in indium doped CdSe nanowires measured by TEM-EDS and ICP-MS *vs.* the equivalent ratio of a selenium precursor to CdSe is shown in Figure 4.2. The results from both measurements indicates that the indium atomic percentage increases with more selenium precursor added to the doping reaction. From the TEM-EDS measurements, the atomic percentage of indium in the indium doped CdSe nanowire samples prepared with 0.5, 1, and 2 equivalent ratios of TBPSe to CdSe are 1.3 ± 0.4, 1.9 ± 0.7, and 3.8 ± 0.8 %, respectively, where the uncertainties represent sample standard deviation among the random spots measured. The indium atomic percentages are used as labels to the corresponding indium doped nanowire samples. PXRD patterns of the CdSe nanowires and indium doped CdSe nanowires shown in Figure 3.3 indicates that hexagonal wurtzite is a primary crystal structure of both intrinsic and doped nanowires without formation of other impurity phases such as those from CdO or MnO. Peak shift to the higher 2θ region with higher indium concentration is observed (Figure 3.3 inset). The substitution of Cd^{2+} with smaller In^{3+} ion causes the reduction of lattice constants resulting in the peak shift which was also observed in Mn doped CdSe nanowires.[4] This also confirms success of the indium doping reaction. Additionally, XPS measurements on 3.8 atomic % indium sample were conducted in order to determine oxidation state and concentration of In species at surface

layers of In(III) doped CdSe nanowires. The data from the measurements is summarized in Table 4.1. XPS high-resolution scans of the 3.8 atomic % indium sample shows In 3d peaks at 444.8 and 452.3 eV; Cd 3d peaks at 405.0 and 411.8 eV; and Se 3d peaks at 53.9 eV, respectively (Figure 4.4 B-C). The indium content from the surface layers (from the surface to approximately 10 nm below the surface) of the nanowires calculated from the area of those peaks is 18 %, which is higher than atomic percentage obtained from TEM-EDS and ICP-MS measurements determining the atomic percentage from the whole structure of the nanowires. This suggests that the dopants were introduced from the surface of the nanowires and the doping did not reach a saturation point. A high-resolution scan from the XPS measurement in the range of 436 eV to 459 eV shown in Figure 4.4 B displays In $3d_{5/2}$ peaks at 444.8 eV. This indicates the presence of In-Se bond[57] and excludes the presence of indium metal in the sample, which would exhibit $3d_{5/2}$ peaks below 444 eV.[58] The TEM, TEM-EDS, ICP-MS, PXRD, and XPS measurements indicates the success of the indium doping reaction.

The effect of indium doping on electronic property of the In(III) doped CdSe nanowires. In order to characterize the electronic property of the CdSe nanowires and In(III) doped CdSe nanowires, nanowire FET devices were fabricated using lithography and dielectrophoretic deposition techniques. First, two metal (Titanium/gold) electrodes with a 2-μm gap (Figure 4.5 A) were fabricated on SiO_2 film (insulator) layer locating on top of heavily p-doped silicon wafer (conductor) via metal deposition process through a photolithography pattern. To fabricate a nanowire FET device, illustrated by a configuration shown in Figure 4.5 B, the intrinsic colloidal CdSe nanowires or In(III) doped CdSe nanowires at various doping times were deposited on the electrodes using a

dielectrophoretic alignment method. This method has been reported to precisely align nanowires on electrodes using electric field between the electrodes supplied from AC or DC bias.[23,59–63] The method demonstrated here uses DC bias to bridge single nanowires between the (Titanium/gold) electrodes to creating a nanowire FET device as illustrated by a representative SEM image of In(III) doped CdSe nanowires bridging between two metal electrodes in Figure 4.6. Transfer characteristics (drain current (I_d) vs. gate bias (V_g)) of nanowire FET devices fabricated from the intrinsic CdSe nanowires (d10 and d11) and In(III) doped CdSe nanowires (d1-d9) are shown in Figure 4.7. From the transfer characteristic, the device exhibiting highest conductivity at 0 gate bias (d8), which is fabricated from 3.8% In doped nanowire sample, show the increase in conductivity by 6 order of magnitude as compared to the device fabricated from the intrinsic CdSe nanowires. Additionally, all In(III) doped CdSe nanowire samples show n-type characteristic, which is typical for indium doped CdSe. This n-type behavior is confirmed by *I-V* measurements at various gate bias. The representative measurement of from d8 is shown in Figure 4.7. All devices fabricated from the doped nanowires exhibit this n-type behavior. Charge carrier mobility and charge carrier density of each doped nanowire sample were calculated from transconductance (dI_d/dV_g) and threshold voltage (V_{th}) extracted from the transfer characteristic collected by a reverse scan Figure 4.6 (solid lines). The transconductance was obtained from a region on a transfer characteristic providing highest slope, and the threshold voltage, the gate voltage at which the device starts to shut down, was obtained by extrapolating the region where the transconductance was collected to zero drain current ($I_d = 0$). The charge carrier mobility and the charge carrier density of each nanowire sample

were calculated using charge in cylinders model[64] explained by eq. 4.1, and 4.2, respectively.

$$\mu = \frac{dI_{\mathrm{d}}}{dV_{\mathrm{g}}}\frac{1}{V_{\mathrm{d}}}\left(F\sum_i \frac{2\pi\epsilon\epsilon_0}{L_i in\left(\frac{4h}{d}\right)}\right)^{-1} \tag{4.1}$$

$$n_e = \frac{V_{\mathrm{th}}\left(\sum_i \frac{2\pi\epsilon\epsilon_0 L_i}{ln\left(\frac{4h}{d}\right)}\right)}{e\cdot\sum_i \pi\left(\frac{d}{2}\right)^2 L_i} \tag{4.2}$$

where V_d is drain voltage, F is a ratio of the total width of the device to the width of the field of view, L is length of single nanowires, d is diameter of the nanowires, h is the thickness of the SiO_2 insulating layer (285 nm), ϵ is relative permittivity of SiO_2 (3.9), ϵ_0 is vacuum permittivity (8.85×10^{-12} C/V·m), and e is electron charge (1.60×10^{-19} C). The charge carrier mobility and charge carrier density of each doped nanowire sample were summarized in Table 4.2. The charge carrier mobility and charge carrier density increase with the increasing indium content in the In(III) CdSe nanowires. This agrees with the results reported by He and coworkers.[5] Furthermore, the doping efficiency of 3.8% In and 1.9% In sample were calculated to be 0.059 and 0.026 %, respectively, using eq. 4.3

$$doping\ efficiency = \frac{number\ of\ charge\ carrier}{number\ of\ dopants} \times 100\% \tag{4.3}$$

The data from *I-V* measurements of a representative device (d8) at different gate voltages is shown in Figure 4.8. Figure 4.8 A indicates the increase in drain current in the range of drained voltage measured with increasing gate voltage. This confirms an n-type behavior of the nanowire FET device. The data in log scale (Figure 4.8 B) indicates Schottky contact between the metal electrodes and the nanowires bridging between the electrodes. This suggests that the nanowires have higher original fermi level as compared to that of the metal electrode.

4.4 CONCLUSIONS

In summary, we demonstrate the doping of indium into colloidal CdSe nanowires via sequential nanocrystal diffusion doping and cation exchange mechanism for the first time. This doping approach allows for controlling indium concentration in the dope nanowires, and thus the electronic transport property of the nanowires. The doping concentration was simply controlled by the ratio of reactants used in the doping reaction. The practical approach for nanowire FET device fabrication from the colloidal doped nanowires were demonstrated. The doping increases the conductivity of the nanowires by up to 6 order of magnitudes as well as provide carrier concentration as high as approximately 10^{17} cm^{-3}. Controlling electronic property of semiconductors is crucial to enable their practical application. This novel doping approach will certainly aid in optimizing electronic property of CdSe nanowires for practical use.

Table 4.1 Summary of XPS data of the In(III) doped CdSe nanowires from 3.8 atomic % indium sample.

Element	Peak	Binding Energy (eV)[a]	Raw Area (CPS)[b]	Relative Atomic Sensitivity[c]	Atomic Percentage[d]
In	In $3d_{5/2}$	444.8	3447.3	7.265	2.04
	In $3d_{3/2}$	452.3			
Cd	Cd $3d_{5/2}$	405.0	6993.1	6.623	4.53
	Cd $3d_{3/2}$	411.8			
Se	Se 3d	53.9	979.6	0.853	4.92

[a]Binding energy is extracted from Gaussian-Lorentzian fit of the data using XPSPEAK 4.1 software.
[b]Raw peak area is obtained from signal above background using XPSPEAK 4.1 software.
[c]Relative atomic sensitivity is provided by XPSPEAK 4.1 software.
[d]Atomic percentage is calculated using XPSPEAK 4.1 software. Numbers do not add to 100% because of contributions from carbon and oxygen signals (not shown).

Table 4.2 Summary of data extracted from transfer characteristic measurements.

InCdSe sample	device	dI_d/dV_g (10^{-6}C/V·s)	Charge carrier mobility, μ_e (cm^2/V·s)	$\mu_{e,avg}$ [a] (cm^2/V·s)	V_{th}	Charger carrier density, n_e (10^{17}cm^{-3})	$n_{e,avg}$ [a] (10^{17}cm^{-3})	Doping efficiency, charge carrier/dopant (%)
1.3% In	d4	0.12	0.0107	0.0179 ± 0.095	1.17	n/a	n/a	n/a
	d5	0.14	0.0287		4.50	n/a		
	d6	0.041	0.0144		4.39	n/a		
1.9% In	d1	0.35	0.114	0.179 ± 0.063	-1.51	2.43	1.86 ± 1.25	0.026
	d2	0.53	0.183		-3.21	2.74		
	d3	0.80	0.240		-0.888	0.43		
3.8 % In	d7	0.34	0.0721	0.334 ± 0.278 [b]	-4.70	10.40	8.32 ± 3.30	0.059
	d8	3.0	0.531		-2.30	4.52		
	d9	1.1	0.138		-7.00	10.00		

[a] Uncertainty represents standard deviation

[b] the average value excludes the charge carrier mobility from d7

Note: charger carrier density values of 1.3% In sample cannot be obtained via this method used for nanowire FET due to the positive threshold voltage (V_{th}).

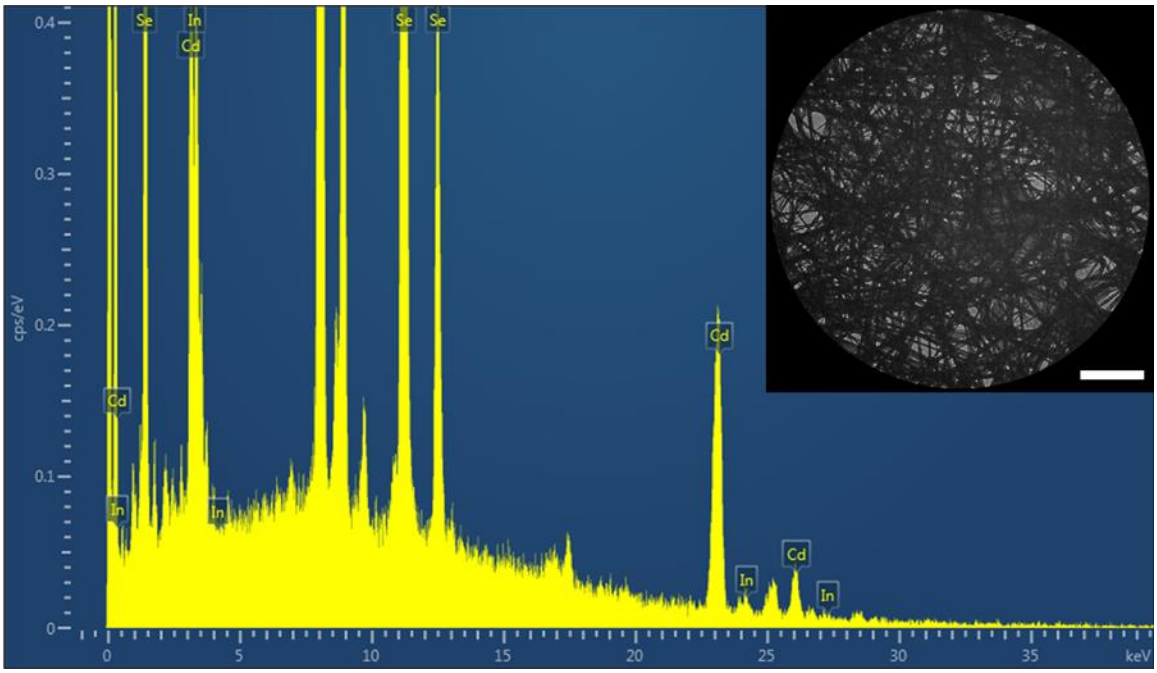

Figure 4.1 A representative EDS spectrum of the In(III) doped CdSe nanowires from the indium doping reaction using 2 to 1 equivalent ratio of TBPSe to CdSe. Inset: the TEM image of the spot where EDS spectrum is measured. Scale bar is 1 μm.

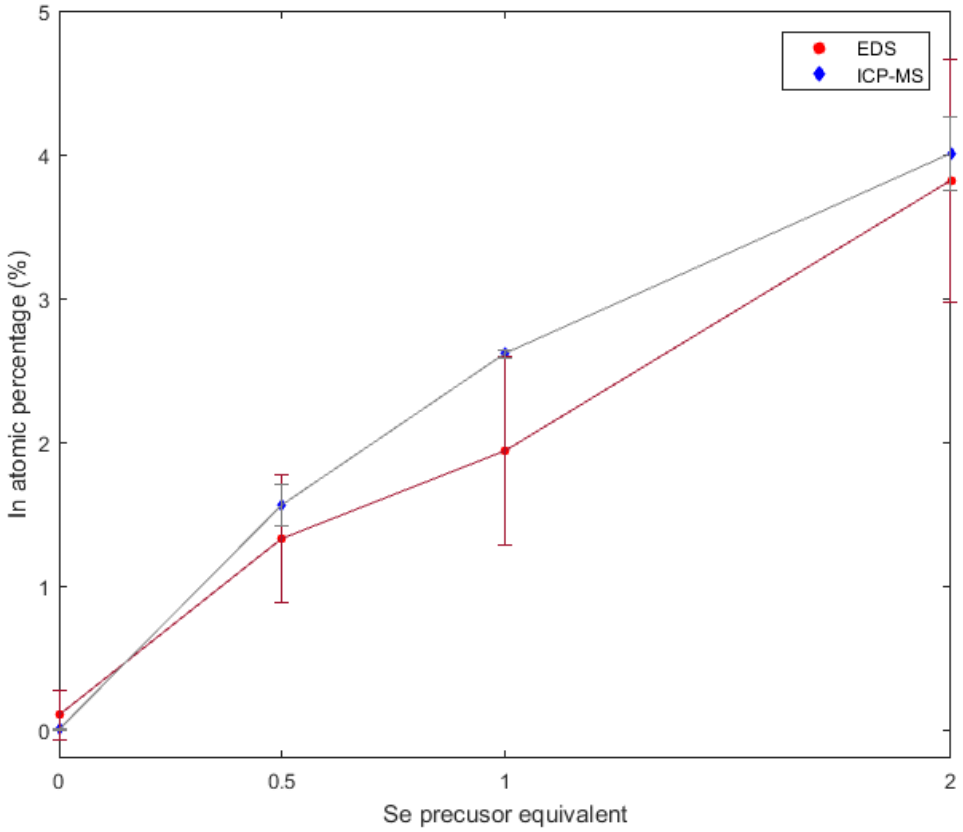

Figure 4.2 Indium atomic percentage of In(III) doped CdSe nanowire samples prepared from the doping reactions containing selenium precursor at various equivalent ratios of TBPSe (selenium precursor) to CdSe obtained from TEM-EDS (red circles) and ICP-MS (blue circles) measurements. The solid lines are guides to the eyes. The error bars represent sample standard deviations of the data.

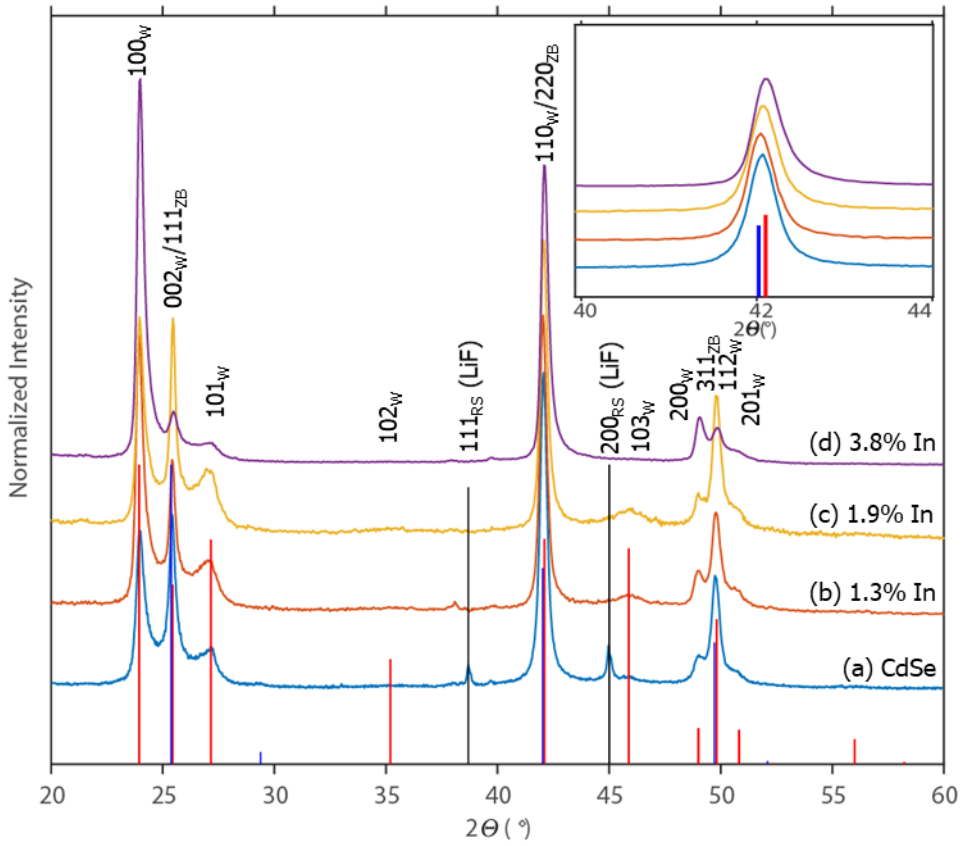

Figure 4.3 PXRD patterns of (a) colloidal CdSe nanowires, (b) In(III)CdSe nanowires with 1.3 at. % indium, (c) In(III)CdSe nanowires with 1.9 at. % indium, and (d) In(III)CdSe nanowires with 3.8 at. % indium. Stick patterns of wurtzite phase of CdSe (red), zincblende phase of CdSe (blue), and LiF (black) are presented for comparison. The measurement was conducted on a zero-background stage leading to a shift of a PXRD pattern, thus LiF was added to the samples to provide reference peaks. PXRD patterns of the In(III) doped CdSe samples were measured with and without mixing LiF into the samples. The PXRD patterns of the In(III) doped CdSe samples shown here are measured without LiF, and displacements were made to align the patterns to match PXRD patterns of the samples measured with LiF added into the samples, so LiF peaks do not show in PXRD of In(III) doped CdSe samples.

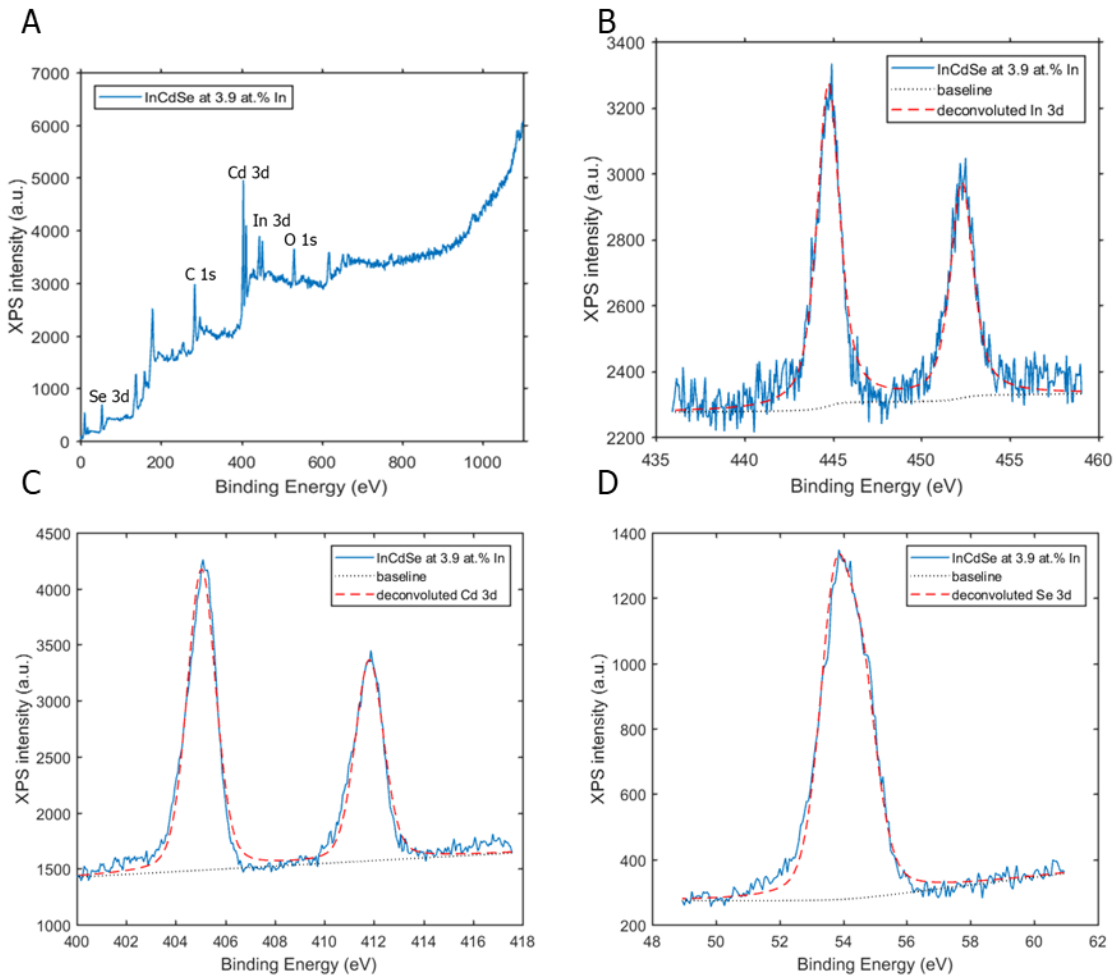

Figure 4.4 XPS spectra of In(III) doped CdSe nanowires with 3.8 atomic % In: (A) survey scan and (B-D) high resolution core level spectra. Peak deconvolutions in panel B, C, and, D show the presence of In 3d, Cd 3d, and Se 3d peaks, respectively.

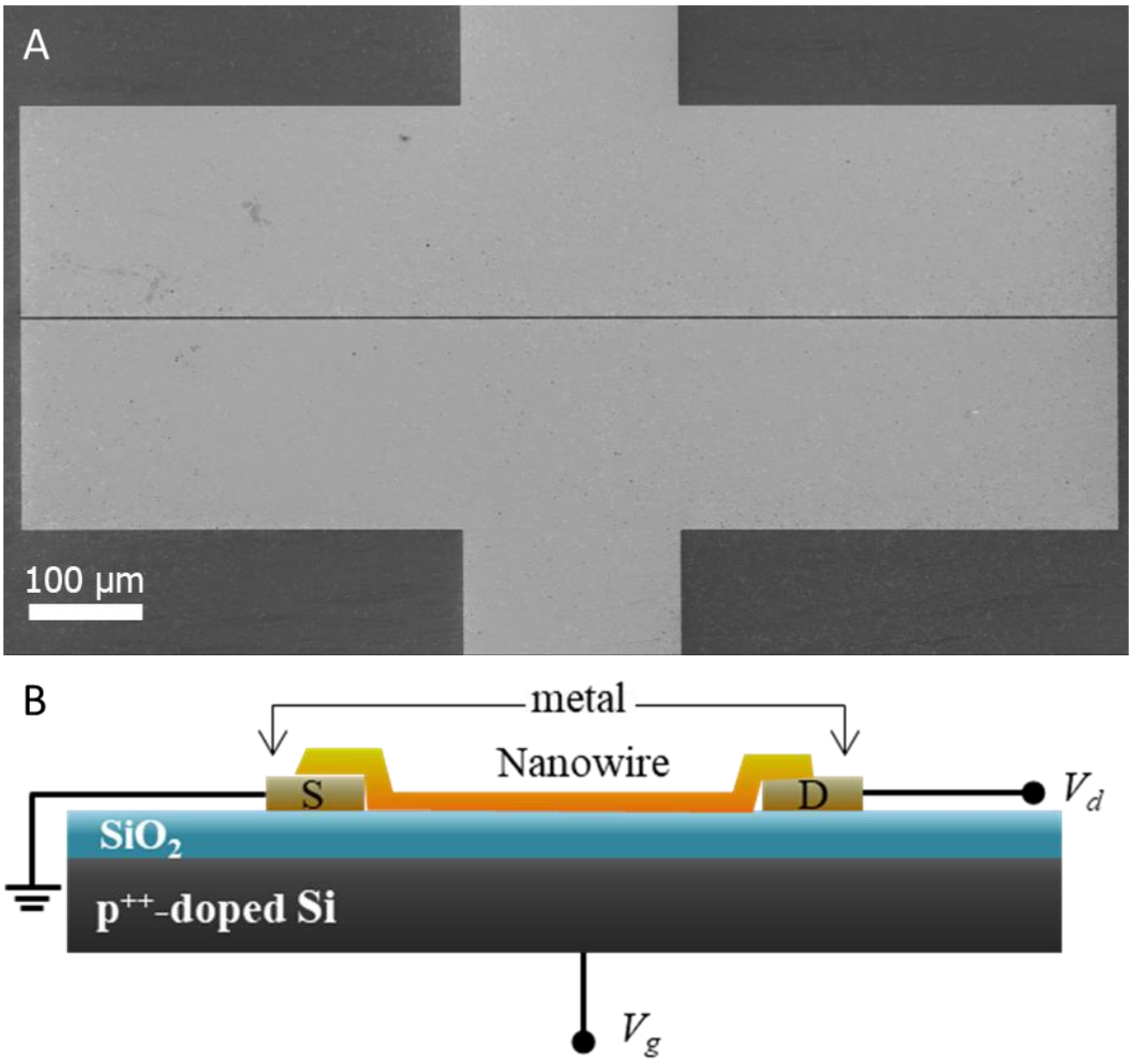

Figure 4.5 Nanowire FET device. (A) an SEM image of a top-view of a representative nanowire FET device (B) a diagram of nanowire FET device.

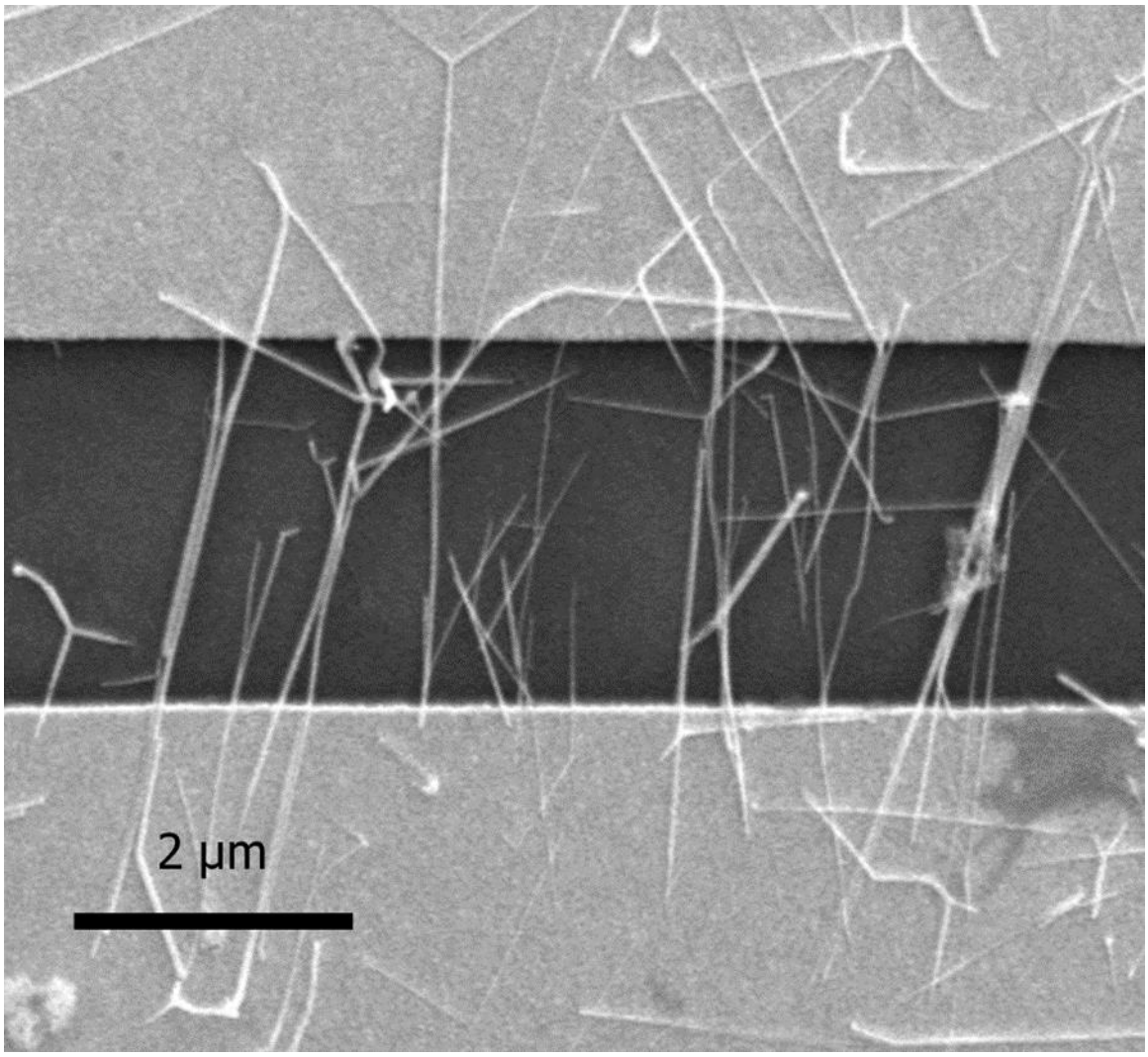

Figure 4.6 An SEM image of nanowires bridging between metal electrodes of a nanowire FET device.

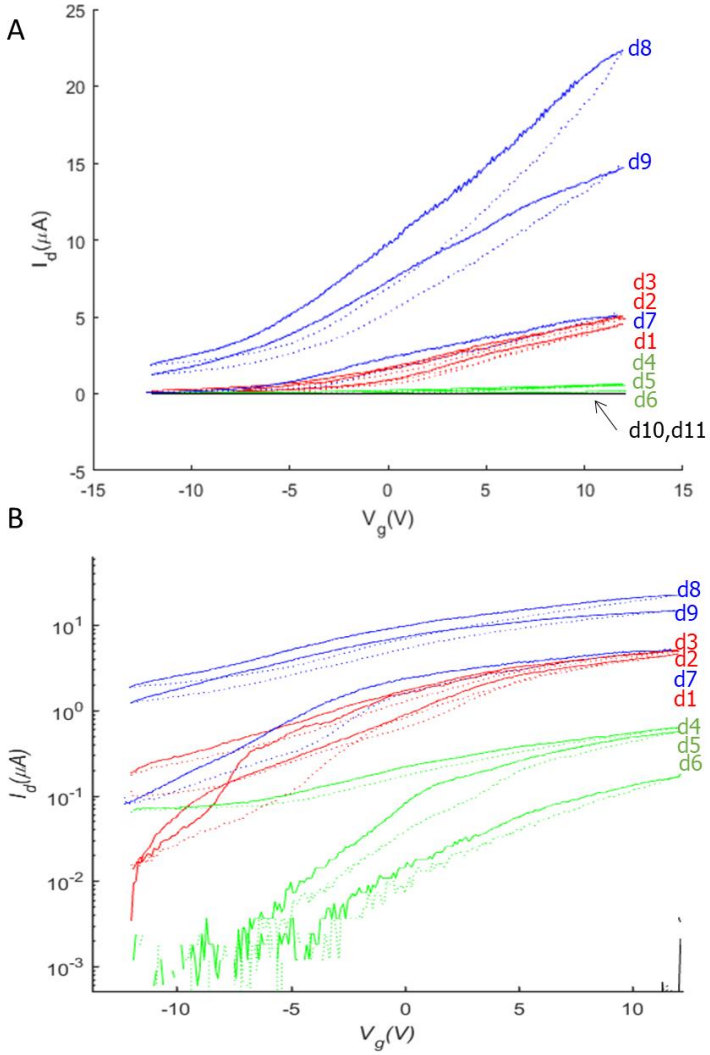

Figure 4.7 Comparison of transfer characteristics under dark at V_d = 4 V of nanowire FET devices (d) made from In(III)CdSe nanowires with 3.9 at. % indium (blue), In(III)CdSe nanowires with 1.8 at. % indium (red), In(III)CdSe nanowires with 1.3 at. % indium (green), and CdSe nanowires (black). Panel A and B shows the transfer characteristics in linear scale and log scale, respectively. Solid lines represents reverse scans and dash lines represents forward scans. Device numbers are labeled as d1-d11.

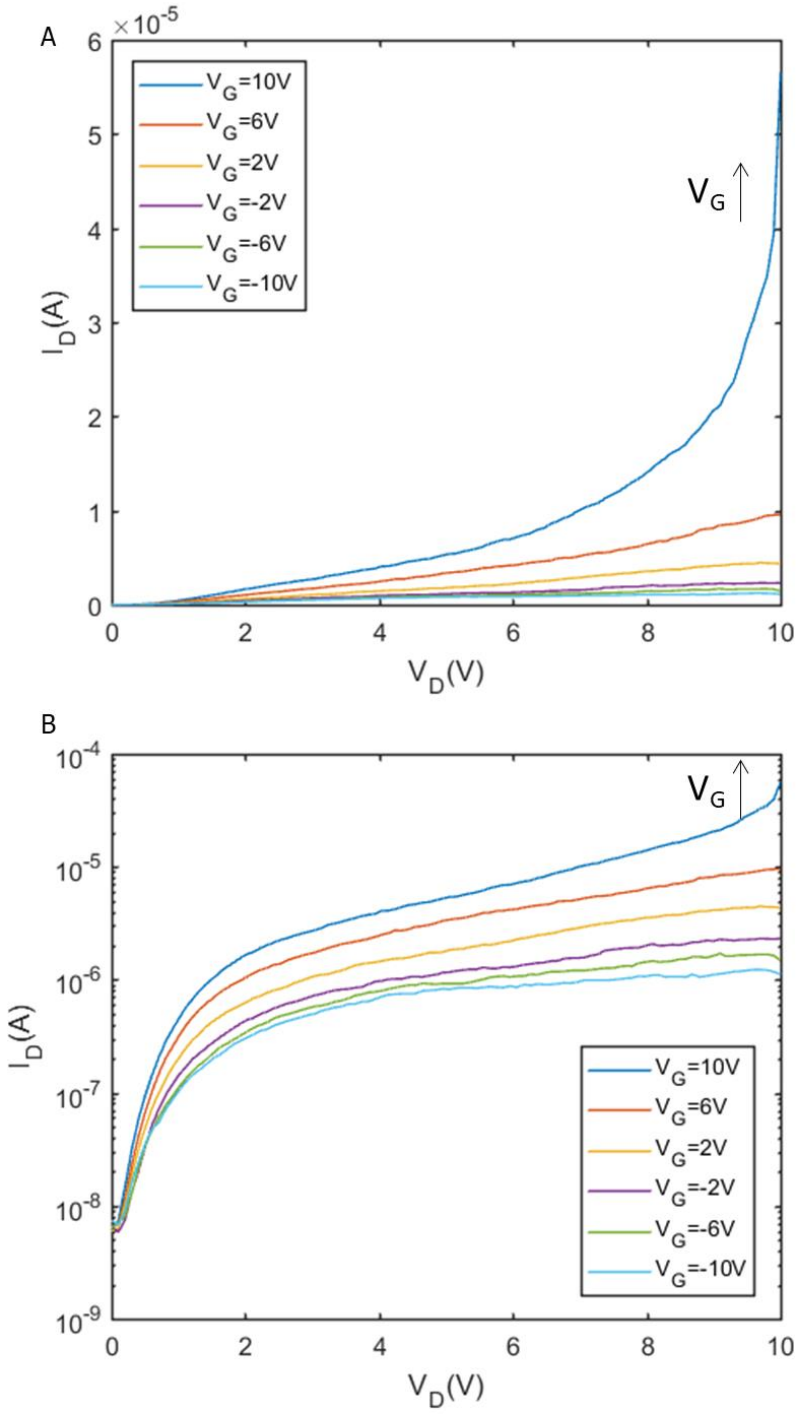

Figure 4.8 Gate-dependent I-V measurements of nanowire FET device d8 under dark: (A) in normal scale (B) in log scale.

CHAPTER 5

AN EFFORT TO CONTROL ELECTRONIC PROPERTY OF CDSE NANOWIRES VIA PHOTOCHEMICAL DOPING

5.1 INTRODUCTION

As mention in previous chapters, electronic doping is a crucial step to improve electronic properties of semiconductors which enable semiconductors for practical applications. Conventionally, electronic doping is done by introducing impurity atoms, so called dopants into an intrinsic semiconductor lattice. This approach has been successfully used for bulk semiconductors. However, in nanoscale semiconductors, doping via this approach is still be immature. It has been limited to semiconductor nanostructures in only some compositions and forms. Additionally, semiconductor nanostructure doping via this traditional method usually requires complicated procedures. Although there has been a lot of improvement in terms of synthetic procedures and electronic device fabrications, semiconductor nanowires also have these same problems in doping as other semiconductor nanostructures. Alternative method for doping in semiconductor nanowires will certainly promote semiconductor nanowires for practical uses in many applications. In nanomaterials, including quantum dot[12,45,65–69] and graphene.[70,71] photochemical doping has successfully been used to add delocalized electrons to their conduction bands, which can lead to an increase in conductivities of those materials. This process contains two steps (Figure 1A). First, materials are illuminated by light exciting electrons from a valence band

to a conduction band of a semiconductor, which generates delocalized electrons in the conduction band and holes in the valence band. Then electrons are added to the valence band at the surface of the material by electron donating molecules. This prevents the delocalized electrons from relaxing to the valence band resulting in an n-type semiconductor. Though QDs and semiconductor nanowires has similarities in terms of morphology (e.g. nanoscale diameter and high surface-to-volume ratio) and chemical compositions, this technique has never been used in semiconductor nanowires. This chapter demonstrates the potential of photochemical doping as a novel approach to dope semiconductor nanowires.

5.2 PROPOSING EXPERIMENTS

Probing photochemical doping via spectroscopic techniques. Colloidal CdSe nanowires suspended in toluene/THF solvent with Na[Et_3BH], the redox indicator, and [Bu_4N][PF_6] supporting electrolyte to test photochemical doping of CdSe nanowires in solution. In particular, a 405-nm LED will be used to excite the sample in a cuvette under inert atmosphere, while the UV-vis spectrum (to monitor the redox indicator) will be recorded on an orthogonal light path (Figure 5.1). Initially, electrons left in the conduction band will transfer to the redox indicator, but as the Fermi level reaches the band edge, both will be populated at equilibrium. This is the key observation indicating success. Then indicator/nanowire sample will be titrated with ferrocenium to determine the number of electrons evolved. By comparison to mass or ICP-MS measurements of the quantity of nanowires, *n*-type carrier density in cm^{-3} can be estimated. We may also be able to perform electrochemical monitoring of the Fermi level. Near-infrared absorbance at the start and

end of the photochemical doping step will be used to monitor for signatures of free carriers though the resonance due to greater delocalization of carriers in the nanowires.

Probing photochemical doping via electronic measurement. Nanowire FET devices will be fabricated from colloidal CdSe nanowires using the method described in chapter 4. The nanowire FET devices will be immersed in a solution of $Li[Et_3BH]$ in THF under the illumination of a 405-nm LED. After the nanowire FET device is cleaned with clean THF and dried, its transfer characteristic will be measured.

Fabrication of nanowire diode via spatially selective photochemical doping. Electrolytes and/or hole scavengers, $Li[Et_3BH]$, will be embedded in a polymeric solid or gel to facilitate local control and the formation of modulation-doped devices. co-dissolve both $Li[Et_3BH]$ (or an alternative borohydride) and a supporting electrolyte with a compatible polymer and cast the mixture on top of bottom-contacted CdSe nanowires. The conductance will be monitored as the electrolyte gate – contacted from the top or with a metal side-electrode on the surface of the chip – is swept to locate the threshold voltage for *n*-type conduction. Then, illumination will be provided to stimulate photochemical doping and the gate sweep subsequently repeated: the electrolyte gate threshold voltage should decrease to a value below zero indicating *n*-type conduction. If a large enough shift in the threshold voltage is observed, then one can envision a scenario where most of the chip is brought via the electrolyte gate to *p*-type conduction, but a selected area of the device, such as the channel close to one contact, is photochemical doped into *n*-type conduction. In this case, a *p*-*n* junction would be formed along the axis of the nanowire that should display rectifying conductivity. This can be explored using a lithographic pattern similar to the one in Figure 5.2 where numerous D-S electrode pairs could share the same electrolyte gate,

but could be differently photochemically doped using a localized light source. Scanning photocurrent microscope with a continuously-variable field aperture (probe size) that will be used to locally photochemically dope at high intensity, and then to identify the p-n junction by recording a photocurrent map at reverse bias. Some of these more advanced measurements would require a hermetic seal, such as cover glass, to be glued in place over the active area of the device so that it could be removed from the glovebox.

5.3 EXPERIMENTAL SECTION

Chemicals. Lithium triethylborohydride (1 M in THF) was obtained from BEANTOWN CHEMICAL. Tetrahydrofuran (THF) were dried over activated alumina.

Electrode fabrication. Devices were fabricated on a heavily p-doped Si wafer with 285 nm thermally grown SiO_2 obtained from Addison Engineering, Inc. First, the Si wafer was rinsed thoroughly with acetone, isopropyl alcohol, and DI water, and then immediately dried with a nitrogen stream. The wafer was then heated at 180 ºC for 5 min to remove water on the SiO_2 surface. Metal contacts on the SiO_2 surface were defined by photolithography and electron-beam evaporation of titanium/gold (30 nm/70 nm) at 3×10^6 torr.

Nanowire FET device fabrication. First, a nanowire solution was prepared by mixing a stock solution of nanowires suspended in toluene (1-5 mg/mL) and ODE at a 2:1 (v/v) ratio. Then the nanowires were deposited to bridge between two metal electrodes via dielectrophoretic alignment in a nitrogen atmosphere glovebox; the nanowire solution was dropped between the electrodes on the device fabricated by the method explained above under a DC electric field (2.5×10^6 V/m) between the electrodes, and then the electric field was kept constant for 5 min. After that, the device was rinsed with toluene, and dried by

wicking the remaining toluene. The device was left in the glovebox at least 10 min before electronic measurements.

Electronic characterization. All measurements were performed in a nitrogen glovebox under dark. Transfer characteristics were collected using the following instruments. Gate biases were swept linearly at 0.18 V/s (intrinsic sample) or 4 V/s (doped sample), and a constant drain voltage was supplied by a DC power supply (Keithley 2636A SourceMeter). Drain current was also collected by Keithley 2636A SourceMeter.

Photochemical doping. The following procedures were done in a nitrogen glovebox. First, 1 mM Lithium triethylborohydride solution in THF was prepared. Nanowire FET device was immersed in the Lithium triethylborohydride solution for 2 min under ambient illumination. The nanowire FET device was then rinsed with THF and left to dry before it electronic property was measured.

5.4 PRELIMINARY RESULTS AND DISCUSSION

Figure 5.3 indicates the change in electronic transport properties after the photochemical doping was performed on the nanowire FET device made of intrinsic NWs. The doped nanowires is n-type. Furthermore, transconductance (dI_d/dV_g) is significantly increased from 27 pA/V to 630 pA/V after doping indicating that charge carrier mobility of the nanowires increases after the doping. Finally, the threshold voltage (V_{th}) of the nanowires reduces from 0.40 to 0.22 V indicating an increase in charge carrier density in the nanowires after the doping. The transconductance and threshold voltage were calculated using the same method explained in chapter 4. These results suggest that photochemical doping can be used to control electronic transport properties of

semiconductor NWs, but additional measurements are necessary to confirm and characterize the extent and lifetime of photochemical doping that can be achieved.

5.5 CONCLUSIONS

This project is significant because it will provide an alternative way to prepare colloidal doped semiconductor nanowires needed for application and a semiconductor nanowire system having extra free electrons without perturbation by impurities, which is needed for a variety of experiments. An alternative way of fabricating nanowire diode will also be achieved.

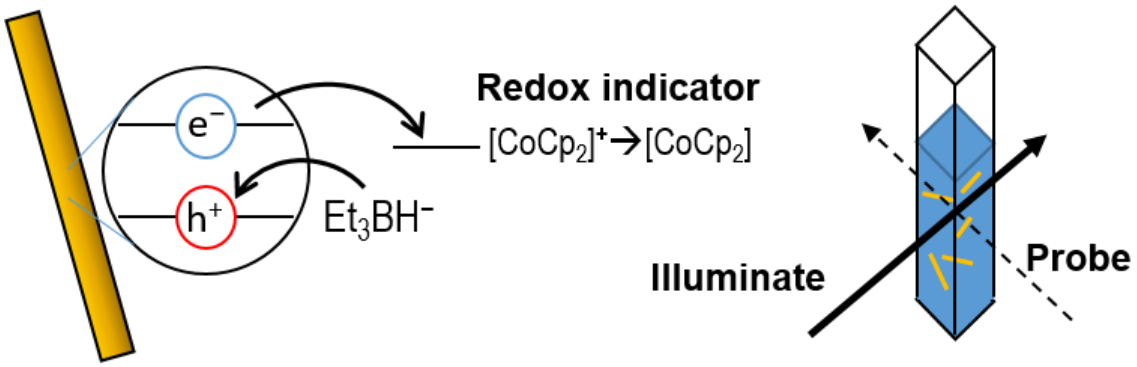

Figure 5.1 Photochemical doping occurs on excitation of the nanowire due to rapid quenching of the hole, leaving an electron in the conduction band. The extra electron can equilibrate with a cobaltocenium redox indicator (cross reaction between borohydride and cobaltocenium can be tested and is minimal in absence of excitation).

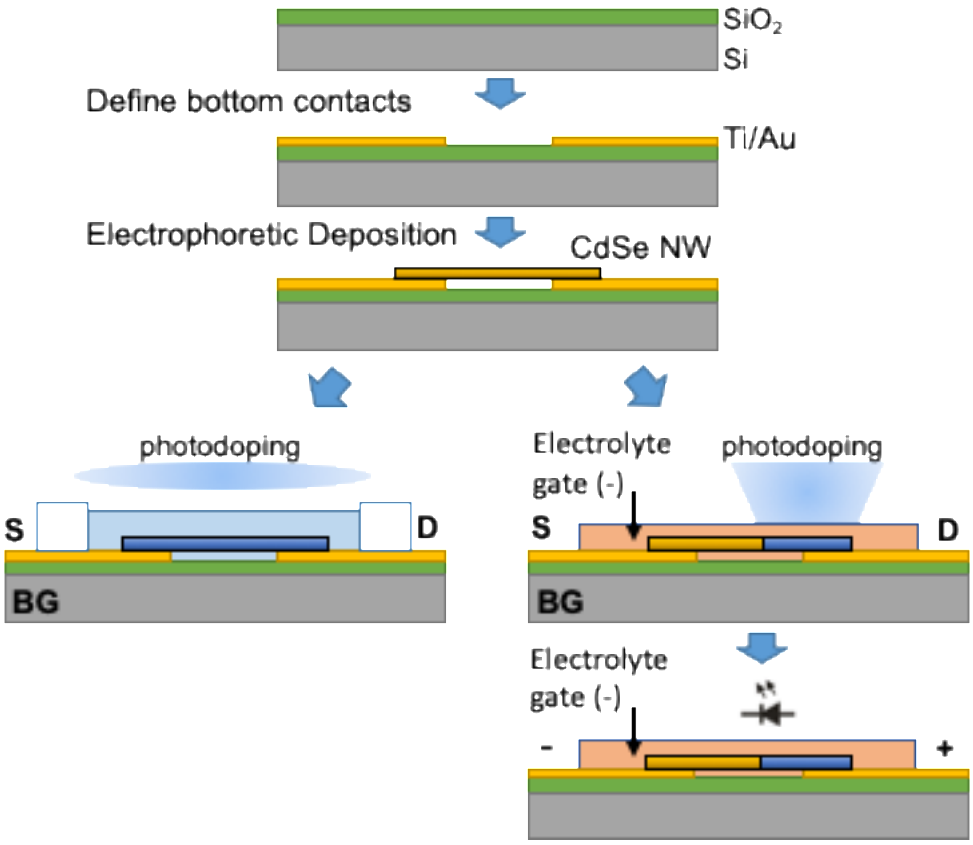

Figure 5.2 Formation of bottom-contacted nanowire FETs and subsequent photochemical doping steps for probing photochemical doping via electronic and fabrication of nanowire diode via spatially selective photochemical doping measurements

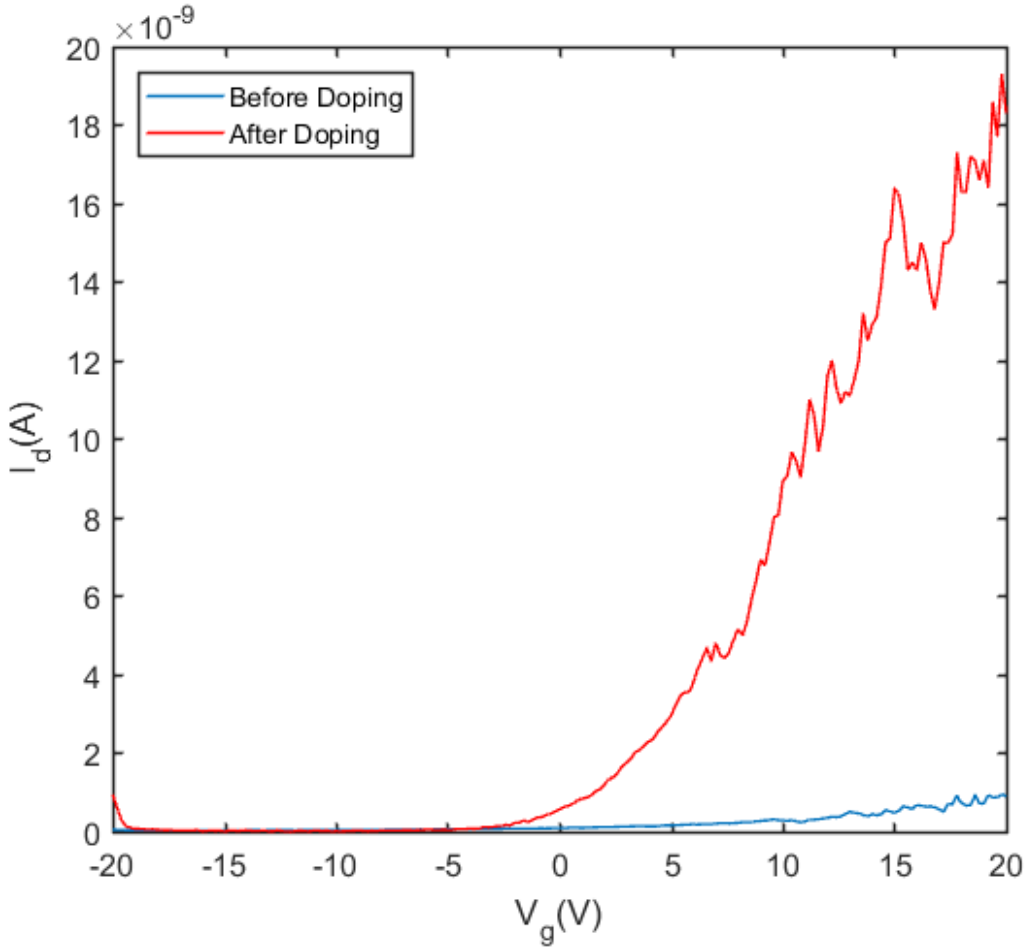

Figure 5.3 Comparison of transfer characteristics under dark at V_d = 5 V of nanowire FET devices before (blue solid), and after photochemical doping was being performed on the nanowires (red solid).

REFERENCES

(1) Yang, P.; Yan, R.; Fardy, M. Semiconductor Nanowire: What's Next? *Nano Lett.* **2010**, *10* (5), 1529–1536. https://doi.org/10.1021/nl100665r.

(2) Dasgupta, N. P.; Sun, J.; Liu, C.; Brittman, S.; Andrews, S. C.; Lim, J.; Gao, H.; Yan, R.; Yang, P. 25th Anniversary Article: Semiconductor Nanowires – Synthesis, Characterization, and Applications. *Adv. Mater.* **2014**, *26* (14), 2137–2184. https://doi.org/10.1002/adma.201305929.

(3) Chen, C.-C.; Hsu, Y.-J.; Lin, Y.-F.; Lu, S.-Y. Superparamagnetism Found in Diluted Magnetic Semiconductor Nanowires: Mn-Doped CdSe. *J. Phys. Chem. C* **2008**, *112* (46), 17964–17968. https://doi.org/10.1021/jp807032q.

(4) Li, Z.; Cheng, L.; Sun, Q.; Zhu, Z.; Riley, M. J.; Aljada, M.; Cheng, Z.; Wang, X.; Hanson, G. R.; Qiao, S.; et al. Diluted Magnetic Semiconductor Nanowires Prepared by the Solution–Liquid–Solid Method. *Angew. Chem. Int. Ed.* **2010**, *49* (15), 2777–2781. https://doi.org/10.1002/anie.200907021.

(5) He, Z.; Jie, J.; Zhang, W.; Zhang, W.; Luo, L.; Fan, X.; Yuan, G.; Bello, I.; Lee, S.-T. Tuning Electrical and Photoelectrical Properties of CdSe Nanowires via Indium Doping. *Small* **2009**, *5* (3), 345–350. https://doi.org/10.1002/smll.200801006.

(6) Radovanovic, P. V.; Barrelet, C. J.; Gradečak, S.; Qian, F.; Lieber, C. M. General Synthesis of Manganese-Doped II−VI and III−V Semiconductor Nanowires. *Nano Lett.* **2005**, *5* (7), 1407–1411. https://doi.org/10.1021/nl050747t.

(7) Cai, J.; Jie, J.; Jiang, P.; Wu, D.; Xie, C.; Wu, C.; Wang, Z.; Yu, Y.; Wang, L.; Zhang, X.; et al. Tuning the Electrical Transport Properties of N-Type CdS Nanowires via Ga Doping and Their Nano-Optoelectronic Applications. *Phys. Chem. Chem. Phys.* **2011**, *13* (32), 14663–14667. https://doi.org/10.1039/C1CP21104H.

(8) Hobbs, R. G.; Petkov, N.; Holmes, J. D. Semiconductor Nanowire Fabrication by Bottom-Up and Top-Down Paradigms. *Chem. Mater.* **2012**, *24* (11), 1975–1991. https://doi.org/10.1021/cm300570n.

(9) Wang, F.; Dong, A.; Buhro, W. E. Solution–Liquid–Solid Synthesis, Properties, and Applications of One-Dimensional Colloidal Semiconductor Nanorods and Nanowires. *Chem. Rev.* **2016**, *116* (18), 10888–10933. https://doi.org/10.1021/acs.chemrev.5b00701.

(10) Beaulac, R.; Archer, P. I.; Ochsenbein, S. T.; Gamelin, D. R. Mn^{2+}-Doped CdSe Quantum Dots: New Inorganic Materials for Spin-Electronics and Spin-Photonics. *Adv. Funct. Mater.* **2008**, *18* (24), 3873–3891. https://doi.org/10.1002/adfm.200801016.

(11) Vlaskin, V. A.; Barrows, C. J.; Erickson, C. S.; Gamelin, D. R. Nanocrystal Diffusion Doping. *J. Am. Chem. Soc.* **2013**, *135* (38), 14380–14389. https://doi.org/10.1021/ja4072207.

(12) Rinehart, J. D.; Schimpf, A. M.; Weaver, A. L.; Cohn, A. W.; Gamelin, D. R. Photochemical Electronic Doping of Colloidal CdSe Nanocrystals. *J. Am. Chem. Soc.* **2013**, *135* (50), 18782–18785. https://doi.org/10.1021/ja410825c.

(13) Wang, F.; Buhro, W. E. An Easy Shortcut Synthesis of Size-Controlled Bismuth Nanoparticles and Their Use in the SLS Growth of High-Quality Colloidal Cadmium Selenide Quantum Wires. *Small* **2010**, *6* (4), 573–581. https://doi.org/10.1002/smll.200902077.

(14) Wang, F.; Dong, A.; Sun, J.; Tang, R.; Yu, H.; Buhro, W. E. Solution−Liquid−Solid Growth of Semiconductor Nanowires. *Inorg. Chem.* **2006**, *45* (19), 7511–7521. https://doi.org/10.1021/ic060498r.

(15) Buhro, W. E. In the Flow: A Finely Controlled Approach to Catalyzed Nanowire Growth. *NPG Asia Mater.* **2014**, *6* (2), e83. https://doi.org/10.1038/am.2013.77.

(16) Dorn, A.; Wong, C. R.; Bawendi, M. G. Electrically Controlled Catalytic Nanowire Growth from Solution. *Adv. Mater.* **2009**, *21* (34), 3479–3482. https://doi.org/10.1002/adma.200900086.

(17) Dorn, A.; Allen, P. M.; Bawendi, M. G. Electrically Controlling and Monitoring InP Nanowire Growth from Solution. *ACS Nano* **2009**, *3* (10), 3260–3265. https://doi.org/10.1021/nn900820h.

(18) Dorn, A.; Allen, P. M.; Harris, D. K.; Bawendi, M. G. In Situ Electrical Monitoring of Cation Exchange in Nanowires. *Nano Lett.* **2010**, *10* (10), 3948–3951. https://doi.org/10.1021/nl102560b.

(19) Puthussery, J.; Kosel, T. H.; Kuno, M. Facile Synthesis and Size Control of II–VI Nanowires Using Bismuth Salts. *Small* **2009**, *5* (10), 1112–1116. https://doi.org/10.1002/smll.200801838.

(20) Wang, F.; Tang, R.; Kao, J. L.-F.; Dingman, S. D.; Buhro, W. E. Spectroscopic Identification of Tri-n-Octylphosphine Oxide (TOPO) Impurities and Elucidation of Their Roles in Cadmium Selenide Quantum-Wire Growth. *J. Am. Chem. Soc.* **2009**, *131* (13), 4983–4994. https://doi.org/10.1021/ja900191n.

(21) Kuno, M. An Overview of Solution-Based Semiconductor Nanowires : Synthesis and Optical Studies. *Phys. Chem. Chem. Phys.* **2008**, *10* (5), 620–639. https://doi.org/10.1039/B708296G.

(22) Reim, N.; Littig, A.; Behn, D.; Mews, A. Controlled Electrodeposition of Bismuth Nanocatalysts for the Solution–Liquid–Solid Synthesis of CdSe Nanowires on Transparent Conductive Substrates. *J. Am. Chem. Soc.* **2013**, *135* (49), 18520–18527. https://doi.org/10.1021/ja408265s.

(23) Kim, D. K.; Fafarman, A. T.; Diroll, B. T.; Chan, S. H.; Gordon, T. R.; Murray, C. B.; Kagan, C. R. Solution-Based Stoichiometric Control over Charge Transport in Nanocrystalline CdSe Devices. *ACS Nano* **2013**, *7* (10), 8760–8770. https://doi.org/10.1021/nn403132x.

(24) Ouyang, L.; Maher, K. N.; Yu, C. L.; McCarty, J.; Park, H. Catalyst-Assisted Solution−Liquid−Solid Synthesis of CdS/CdSe Nanorod Heterostructures. *J. Am. Chem. Soc.* **2007**, *129* (1), 133–138. https://doi.org/10.1021/ja066243u.

(25) Yarema, M.; Kovalenko, M. V.; Hesser, G.; Talapin, D. V.; Heiss, W. Highly Monodisperse Bismuth Nanoparticles and Their Three-Dimensional Superlattices. *J. Am. Chem. Soc.* **2010**, *132* (43), 15158–15159. https://doi.org/10.1021/ja107458s.

(26) Carmalt, C. J.; Compton, N. A.; Errington, R. J.; Fisher, G. A.; Moenandar, I.; Norman, N. C.; Whitmire, K. H. Homoleptic Bismuth Amides. In *Inorganic Syntheses*; John Wiley & Sons, Ltd, 2007; pp 98–101. https://doi.org/10.1002/9780470132623.ch15.

(27) Tomashyk, V.; Feychuk, P.; Shcherbak, L. *Ternary Alloys Based on II-VI Semiconductor Compounds*, 1st ed.; CRC Press, 2013.

(28) Dietl, T.; Ohno, H. Dilute Ferromagnetic Semiconductors: Physics and Spintronic Structures. *Rev. Mod. Phys.* **2014**, *86* (1), 187–251. https://doi.org/10.1103/RevModPhys.86.187.

(29) Stowell, C. A.; Wiacek, R. J.; Saunders, A. E.; Korgel, B. A. Synthesis and Characterization of Dilute Magnetic Semiconductor Manganese-Doped Indium Arsenide Nanocrystals. *Nano Lett.* **2003**, *3* (10), 1441–1447. https://doi.org/10.1021/nl034419+.

(30) Djerdj, I.; Garnweitner, G.; Arčon, D.; Pregelj, M.; Jagličić, Z.; Niederberger, M. Diluted Magnetic Semiconductors: Mn/Co-Doped ZnO Nanorods as Case Study. *J. Mater. Chem.* **2008**, *18* (43), 5208–5217. https://doi.org/10.1039/B808361D.

(31) Chang, Y. Q.; Wang, D. B.; Luo, X. H.; Xu, X. Y.; Chen, X. H.; Li, L.; Chen, C. P.; Wang, R. M.; Xu, J.; Yu, D. P. Synthesis, Optical, and Magnetic Properties of Diluted Magnetic Semiconductor $Zn_{1-x}Mn_xO$ Nanowires via Vapor Phase Growth. *Appl. Phys. Lett.* **2003**, *83* (19), 4020–4022. https://doi.org/10.1063/1.1625788.

(32) Yu, H.; Li, J.; Loomis, R. A.; Gibbons, P. C.; Wang; Buhro, W. E. Cadmium Selenide Quantum Wires and the Transition from 3D to 2D Confinement. *J. Am. Chem. Soc.* **2003**, *125* (52), 16168–16169. https://doi.org/10.1021/ja037971+.

(33) Barrows, C. J.; Chakraborty, P.; Kornowske, L. M.; Gamelin, D. R. Tuning Equilibrium Compositions in Colloidal $Cd_{1-X}Mn_xSe$ Nanocrystals Using Diffusion Doping and Cation Exchange. *ACS Nano* **2016**, *10* (1), 910–918. https://doi.org/10.1021/acsnano.5b07389.

(34) Crank, J.; Crank, E. P. J. *The Mathematics of Diffusion*; Clarendon Press, 1979.

(35) Biesinger, M. C.; Payne, B. P.; Grosvenor, A. P.; Lau, L. W. M.; Gerson, A. R.; Smart, R. St. C. Resolving Surface Chemical States in XPS Analysis of First Row

Transition Metals, Oxides and Hydroxides: Cr, Mn, Fe, Co and Ni. *Appl. Surf. Sci.* **2011**, *257* (7), 2717–2730. https://doi.org/10.1016/j.apsusc.2010.10.051.

(36) Chen, D.-X.; Sanchez, A.; Taboada, E.; Roig, A.; Sun, N.; Gu, H.-C. Size Determination of Superparamagnetic Nanoparticles from Magnetization Curve. *J. Appl. Phys.* **2009**, *105* (8), 083924. https://doi.org/10.1063/1.3117512.

(37) Magana, D.; Perera, S. C.; Harter, A. G.; Dalal, N. S.; Strouse, G. F. Switching-on Superparamagnetism in Mn/CdSe Quantum Dots. *J. Am. Chem. Soc.* **2006**, *128* (9), 2931–2939. https://doi.org/10.1021/ja055785t.

(38) Fonseca, F. C.; Goya, G. F.; Jardim, R. F.; Muccillo, R.; Carreño, N. L. V.; Longo, E.; Leite, E. R. Superparamagnetism and Magnetic Properties of Ni Nanoparticles Embedded in SiO_2. *Phys. Rev. B* **2002**, *66* (10), 104406. https://doi.org/10.1103/PhysRevB.66.104406.

(39) Mukherjee, S.; Pal, A. K.; Bhattacharya, S.; Raittila, J. Magnetism of Mn_2O_3 Nanocrystals Dispersed in a Silica Matrix: Size Effects and Phase Transformations. *Phys. Rev. B* **2006**, *74* (10), 104413. https://doi.org/10.1103/PhysRevB.74.104413.

(40) Nam, K. M.; Kim, Y.-I.; Jo, Y.; Lee, S. M.; Kim, B. G.; Choi, R.; Choi, S.-I.; Song, H.; Park, J. T. New Crystal Structure: Synthesis and Characterization of Hexagonal Wurtzite MnO. *J. Am. Chem. Soc.* **2012**, *134* (20), 8392–8395. https://doi.org/10.1021/ja302440y.

(41) Zheng, M.; Zhang, H.; Gong, X.; Xu, R.; Xiao, Y.; Dong, H.; Liu, X.; Liu, Y. A Simple Additive-Free Approach for the Synthesis of Uniform Manganese Monoxide Nanorods with Large Specific Surface Area. *Nanoscale Res. Lett.* **2013**, *8* (1), 166. https://doi.org/10.1186/1556-276X-8-166.

(42) Knauf, R. R.; Lennox, J. C.; Dempsey, J. L. Quantifying Ligand Exchange Reactions at CdSe Nanocrystal Surfaces. *Chem. Mater.* **2016**, *28* (13), 4762–4770. https://doi.org/10.1021/acs.chemmater.6b01827.

(43) Kittilstved, K. R.; Gamelin, D. R. Activation of High-TC Ferromagnetism in Mn^{2+}-Doped ZnO Using Amines. *J. Am. Chem. Soc.* **2005**, *127* (15), 5292–5293. https://doi.org/10.1021/ja050723o.

(44) Sahu, A.; Kang, M. S.; Kompch, A.; Notthoff, C.; Wills, A. W.; Deng, D.; Winterer, M.; Frisbie, C. D.; Norris, D. J. Electronic Impurity Doping in CdSe Nanocrystals. *Nano Lett.* **2012**, *12* (5), 2587–2594. https://doi.org/10.1021/nl300880g.

(45) Schimpf, A. M.; Knowles, K. E.; Carroll, G. M.; Gamelin, D. R. Electronic Doping and Redox-Potential Tuning in Colloidal Semiconductor Nanocrystals. *Acc. Chem. Res.* **2015**, *48* (7), 1929–1937. https://doi.org/10.1021/acs.accounts.5b00181.

(46) LaPierre, R. R.; Robson, M.; Azizur-Rahman, K. M.; Kuyanov, P. A Review of III–V Nanowire Infrared Photodetectors and Sensors. *J. Phys. Appl. Phys.* **2017**, *50* (12), 123001. https://doi.org/10.1088/1361-6463/aa5ab3.

(47) Liu, S.; Han, C.; Tang, Z.-R.; Xu, Y.-J. Heterostructured Semiconductor Nanowire Arrays for Artificial Photosynthesis. *Mater. Horiz.* **2016**, *3* (4), 270–282. https://doi.org/10.1039/C6MH00063K.

(48) Briseno, A. L.; Holcombe, T. W.; Boukai, A. I.; Garnett, E. C.; Shelton, S. W.; Fréchet, J. J. M.; Yang, P. Oligo- and Polythiophene/ZnO Hybrid Nanowire Solar Cells. *Nano Lett.* **2009**, *10* (1), 334–340. https://doi.org/10.1021/nl9036752.

(49) Huang, R.; Wang, R.; Zhuge, J.; Liu, C.; Yu, T.; Zhang, L.; Huang, X.; Ai, Y.; Zou, J.; Liu, Y.; et al. Characterization and Analysis of Gate-All-around Si Nanowire Transistors

for Extreme Scaling. In *2011 IEEE Custom Integrated Circuits Conference (CICC)*; 2011; pp 1–8. https://doi.org/10.1109/CICC.2011.6055334.

(50) Roy, S.; Tuinenga, C.; Fungura, F.; Dagtepe, P.; Chikan, V.; Jasinski, J. Progress toward Producing N-Type CdSe Quantum Dots: Tin and Indium Doped CdSe Quantum Dots. *J. Phys. Chem. C* **2009**, *113* (30), 13008–13015. https://doi.org/10.1021/jp8113946.

(51) Raut, V. S.; Lokhande, C. D.; Killedar, V. V. Synthesis and Studies on Effect of Indium Doping on Physical Properties of Electrodeposited CdSe Thin Films. *J. Mater. Sci. Mater. Electron.* **2017**, *28* (4), 3140–3150. https://doi.org/10.1007/s10854-016-5902-6.

(52) Scilla, G. J.; Luo, F. C. Indium Diffusion in Cadmium Selenide Thin-film Transistors with Indium-gold Contacts. *Appl. Phys. Lett.* **1983**, *42* (6), 538–540. https://doi.org/10.1063/1.93997.

(53) Straus, D. B.; Goodwin, E. D.; Gaulding, E. A.; Muramoto, S.; Murray, C. B.; Kagan, C. R. Increased Carrier Mobility and Lifetime in CdSe Quantum Dot Thin Films through Surface Trap Passivation and Doping. *J. Phys. Chem. Lett.* **2015**, *6* (22), 4605–4609. https://doi.org/10.1021/acs.jpclett.5b02251.

(54) Yadav, A. A.; Barote, M. A.; Chavan, T. V.; Masumdar, E. U. Influence of Indium Doping on the Properties of Spray Deposited $CdS_{0.2}Se_{0.8}$ Thin Films. *J. Alloys Compd.* **2011**, *509* (3), 916–921. https://doi.org/10.1016/j.jallcom.2010.09.130.

(55) Basheer, M. G. S. A.; Rajni, K. S.; Vidhya, V. S.; Swaminathan, V.; Thayumanavan, A.; Murali, K. R.; Jayachandran, M. Structural, Optical, Electrical and Luminescence Properties of Electron Beam Evaporated CdSe:In Films. *Cryst. Res. Technol.* **2011**, *46* (3), 261–266. https://doi.org/10.1002/crat.201000546.

(56) Chakraborty, P.; Jin, Y.; Barrows, C. J.; Dunham, S. T.; Gamelin, D. R. Kinetics of Isovalent (Cd^{2+}) and Aliovalent (In^{3+}) Cation Exchange in $Cd_{1-X}Mn_xSe$ Nanocrystals. *J. Am. Chem. Soc.* **2016**, *138* (39), 12885–12893. https://doi.org/10.1021/jacs.6b05949.

(57) Brojerdi, G.; Tyuliev, G.; Fargues, D.; Eddrief, M.; Balkanski, M. Ion Beam Modification of InSe Surfaces. *Surf. Interface Anal.* **1997**, *25* (2), 111–118. https://doi.org/10.1002/(SICI)1096-9918(199702)25:2<111::AID-SIA215>3.0.CO;2-W.

(58) Moulder, J. F. *Handbook of X-Ray Photoelectron Spectroscopy: A Reference Book of Standard Spectra for Identification and Interpretation of XPS Data*; Physical Electronics Division, Perkin-Elmer Corporation, 1992.

(59) Freer, E. M.; Grachev, O.; Duan, X.; Martin, S.; Stumbo, D. P. High-Yield Self-Limiting Single-Nanowire Assembly with Dielectrophoresis. *Nat. Nanotechnol.* **2010**, *5* (7), 525–530. https://doi.org/10.1038/nnano.2010.106.

(60) Raychaudhuri, S.; Dayeh, S. A.; Wang, D.; Yu, E. T. Precise Semiconductor Nanowire Placement Through Dielectrophoresis. *Nano Lett.* **2009**, *9* (6), 2260–2266. https://doi.org/10.1021/nl900423g.

(61) Liu, Y.; Chung, J.-H.; Liu, W. K.; Ruoff, R. S. Dielectrophoretic Assembly of Nanowires. *J. Phys. Chem. B* **2006**, *110* (29), 14098–14106. https://doi.org/10.1021/jp061367e.

(62) Wang, X.; Chen, K.; Liu, L.; Xiang, N.; Ni, Z. Dielectrophoresis-Based Multi-Step Nanowire Assembly on a Flexible Superstrate. *Nanotechnology* **2017**, *29* (2), 025301. https://doi.org/10.1088/1361-6528/aa9a22.

(63) Talapin, D. V.; Black, C. T.; Kagan, C. R.; Shevchenko, E. V.; Afzali, A.; Murray, C. B. Alignment, Electronic Properties, Doping, and On-Chip Growth of Colloidal PbSe

Nanowires. *J. Phys. Chem. C* **2007**, *111* (35), 13244–13249. https://doi.org/10.1021/jp074156y.

(64) Huang, Y.; Duan, X.; Cui, Y.; Lieber, C. M. Gallium Nitride Nanowire Nanodevices. *Nano Lett.* **2002**, *2* (2), 101–104. https://doi.org/10.1021/nl015667d.

(65) Tsui, E. Y.; Carroll, G. M.; Miller, B.; Marchioro, A.; Gamelin, D. R. Extremely Slow Spontaneous Electron Trapping in Photodoped N-Type CdSe Nanocrystals. *Chem. Mater.* **2017**, *29* (8), 3754–3762. https://doi.org/10.1021/acs.chemmater.7b00839.

(66) Aguirre, A. D.; Vinegoni, C.; Sebas, M.; Weissleder, R. Intravital Imaging of Cardiac Function at the Single-Cell Level. *Proc. Natl. Acad. Sci.* **2014**, *111* (31), 11257–11262. https://doi.org/10.1073/pnas.1401316111.

(67) Carroll, G. M.; Brozek, C. K.; Hartstein, K. H.; Tsui, E. Y.; Gamelin, D. R. Potentiometric Measurements of Semiconductor Nanocrystal Redox Potentials. *J. Am. Chem. Soc.* **2016**, *138* (13), 4310–4313. https://doi.org/10.1021/jacs.6b00936.

(68) Schimpf, A. M.; Gunthardt, C. E.; Rinehart, J. D.; Mayer, J. M.; Gamelin, D. R. Controlling Carrier Densities in Photochemically Reduced Colloidal ZnO Nanocrystals: Size Dependence and Role of the Hole Quencher. *J. Am. Chem. Soc.* **2013**, *135* (44), 16569–16577. https://doi.org/10.1021/ja408030u.

(69) Schimpf, A. M.; Ochsenbein, S. T.; Buonsanti, R.; Milliron, D. J.; Gamelin, D. R. Comparison of Extra Electrons in Colloidal N-Type Al^{3+}-Doped and Photochemically Reduced ZnO Nanocrystals. *Chem. Commun.* **2012**, *48* (75), 9352–9354. https://doi.org/10.1039/C2CC34635D.

(70) Wang, H. I.; Braatz, M.-L.; Richter, N.; Tielrooij, K.-J.; Mics, Z.; Lu, H.; Weber, N.-E.; Müllen, K.; Turchinovich, D.; Kläui, M.; et al. Reversible Photochemical Control

of Doping Levels in Supported Graphene. *J. Phys. Chem. C* **2017**, *121* (7), 4083–4091. https://doi.org/10.1021/acs.jpcc.7b00347.

(71) Li, X.; Tang, T.; Li, M.; He, X. Nitrogen-Doped Graphene Films from Simple Photochemical Doping for n-Type Field-Effect Transistors. *Appl. Phys. Lett.* **2015**, *106* (1), 013110. https://doi.org/10.1063/1.4905342.